

Information-based Transductive Active Learning

Jonas Hübotter¹ Bhavya Sukhija¹ Lenart Treven¹ Yarden As¹ Andreas Krause¹

Abstract

We generalize active learning to address real-world settings where sampling is restricted to an accessible region of the domain, while prediction targets may lie outside this region. To this end, we propose **ITL**, short for *information-based transductive learning*, an approach which samples adaptively to maximize the information gained about specified prediction targets. We show, under general regularity assumptions, that **ITL** converges uniformly to the smallest possible uncertainty obtainable from the accessible data. We demonstrate **ITL** in two key applications: Few-shot fine-tuning of large neural networks and safe Bayesian optimization, and in both cases, **ITL** significantly outperforms the state-of-the-art.

1. Introduction

Machine learning, at its core, is about designing systems that can extract knowledge or patterns from data. One part of this challenge is determining not just how to learn given observed data but deciding what data to obtain next, given the information already available. More formally, provided a stochastic process $\{f(\mathbf{x})\}_{\mathbf{x} \in \mathcal{X}}$ over a domain \mathcal{X} : *How can we learn f sample-efficiently from (noisy) observations?* This problem is widely studied in *active learning* and *experimental design* (Chaloner & Verdinelli, 1995; Settles, 2009).

Active learning methods commonly aim to learn f globally, i.e., across the entire domain \mathcal{X} . However, in many real-world problems, **(i)** the domain \mathcal{X} is so large that learning f globally is hopeless or **(ii)** agents have limited information and cannot access the entire domain \mathcal{X} (e.g., due to restricted access or to act safely). Thus, global learning is often not desirable or even possible. Instead, intelligent systems are typically required to act in a more *directed* manner and *extrapolate* beyond their limited information. This work formalizes the above two aspects of active learning, which have remained largely unaddressed by prior work. We provide a comprehensive overview of related work in Section 6.

¹ETH Zurich, Switzerland. Correspondence to: Jonas Hübotter <jonas.huebotter@inf.ethz.ch>.

Preprint. Under review.

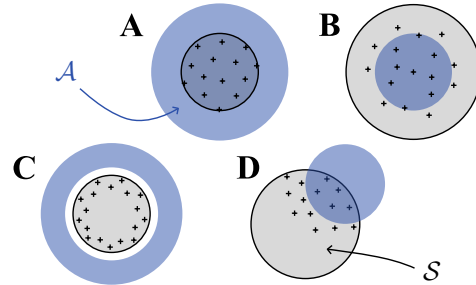


Figure 1. Instances of transductive active learning where the target space \mathcal{A} is shown in blue and the sample space \mathcal{S} is shown in gray. The points denote plausible observations within \mathcal{S} to “learn” \mathcal{A} . In (A), the target space contains “everything” within \mathcal{S} as well as points *outside* \mathcal{S} . In (B, C, D), one makes observations *directed* towards learning about a particular target. Prior work on active learning has focused on the instance $\mathcal{X} = \mathcal{A} = \mathcal{S}$.

Directed “transductive” learning We consider the problem of *transductive active learning*, where given two arbitrary subsets of the domain \mathcal{X} ; a *target space* $\mathcal{A} \subseteq \mathcal{X}$, and a *sample space* $\mathcal{S} \subseteq \mathcal{X}$, we study the question:

*How can we learn f within \mathcal{A}
by actively sampling observations within \mathcal{S} ?*

This problem is ubiquitous in real-world applications such as safe Bayesian optimization, where \mathcal{S} is a set of safe parameters and \mathcal{A} might represent parameters outside \mathcal{S} whose safety we want to infer. Fine-tuning of neural networks is another example, where the target space represents the test distribution $\mathcal{P}_{\mathcal{A}}$ over which we want to minimize risk, and the sample space represents the train distribution $\mathcal{P}_{\mathcal{S}}$ from which we can sample data points to fit or fine-tune our model. Figure 1 visualizes some instances of transductive active learning. Whereas most prior work has focused on the instance $\mathcal{X} = \mathcal{A} = \mathcal{S}$, transductive active learning generalizes to other instances such as (A), (B), (C), and (D).

Contributions Our main contributions are:

- We propose an intuitive information-based decision rule, **ITL**, which adheres to the principle (†) of selecting points in \mathcal{S} to minimize the “posterior uncertainty” about points in \mathcal{A} .
- To the best of our knowledge, we are the first to give rates for the uniform convergence of uncertainty over

the target space \mathcal{A} to the smallest attainable value, given samples from the sample space \mathcal{S} (Theorems 3.2 and 3.3).

- We apply the transductive active learning framework to batch-wise *active few-shot fine-tuning of large neural networks* and to *safe Bayesian optimization*. We empirically show, in both cases, that **ITL** outperforms the state-of-the-art.

The remaining paper is structured as follows: Section 2 discusses the problem setting and Section 3 introduces **ITL** as well as our main theoretical contributions. The two key applications to fine-tuning neural networks and safe Bayesian optimization are in Sections 4 and 5. We discuss related works and limitations in Sections 6 and 7.

2. Problem Setting

We assume that the target space $|\mathcal{A}|$ and sample space $|\mathcal{S}|$ are finite.¹ Assume f is a stochastic process and denote the marginal random variables $f(\mathbf{x})$ by $f_{\mathbf{x}}$, and joint random vectors $\{f(\mathbf{x})\}_{\mathbf{x} \in X}$ for some $X \subseteq \mathcal{X}$, $|X| < \infty$ by f_X . Let \mathbf{y}_X denote the noisy observations of f_X , $\{\mathbf{y}_{\mathbf{x}} = f_{\mathbf{x}} + \varepsilon_{\mathbf{x}}\}_{\mathbf{x} \in X}$, where $\varepsilon_{\mathbf{x}}$ is independent noise.² We assume that any such f and \mathbf{y} have a joint density $p(\mathbf{f}, \mathbf{y})$.

We study the “adaptive” setting, where in round n the agent selects a point $\mathbf{x}_n \in \mathcal{S}$ and observes $y_n = y_{\mathbf{x}_n}$. The agent’s choice of \mathbf{x}_n may depend on the outcome of prior observations $\mathcal{D}_{n-1} \stackrel{\text{def}}{=} \{(\mathbf{x}_i, y_i)\}_{i < n}$.

Background on information theory We briefly recap several important concepts from information theory, of which we provide formal definitions in Appendix A. The (differential) entropy $H[f]$ is one possible measure of uncertainty about f and the conditional entropy $H[f | \mathbf{y}]$ is the (expected) posterior uncertainty about f after observing \mathbf{y} . The information gain $I(f; \mathbf{y}) = H[f] - H[f | \mathbf{y}]$ measures the (expected) reduction in uncertainty about f due to \mathbf{y} .

2.1. Measures of Learning Complexity

In transductive active learning, two measures play a crucial role in expressing the complexity of a learning problem specified by the target space \mathcal{A} and sample space \mathcal{S} . We introduce these two in the following.

Definition 2.1 (Information capacity). The maximum information gain about \mathcal{A} from n observations within \mathcal{S} is

$$\gamma_n(\mathcal{A}; \mathcal{S}) \stackrel{\text{def}}{=} \max_{\substack{X \subseteq \mathcal{S} \\ |X| \leq n}} I(f_{\mathcal{A}}; \mathbf{y}_X).$$

¹Infinite domains can be addressed via discretization arguments as often done in the Bayesian optimization literature.

² X may be a multiset, in which case repeated occurrence of \mathbf{x} corresponds to repeated independent observations of $y_{\mathbf{x}}$.

The information capacity measures the amount of information about $f_{\mathcal{A}}$ that is accessible from within \mathcal{S} . This measure has been used previously (e.g., by Srinivas et al., 2009; Chowdhury & Gopalan, 2017; Vakili et al., 2021), in the setting where $\mathcal{X} = \mathcal{A} = \mathcal{S}$, taking the form of $\gamma_n \stackrel{\text{def}}{=} \gamma_n(\mathcal{X}) \stackrel{\text{def}}{=} \gamma_n(\mathcal{X}, \mathcal{X})$. We remark that $\gamma_n(\mathcal{A}; \mathcal{S}) \leq \gamma_n(\mathcal{S})$ holds uniformly for all \mathcal{A} , \mathcal{S} , and n . Generally, $\gamma_n(\mathcal{A}; \mathcal{S})$ can be substantially smaller if the target space is a sparse subset of the sample space.

Example 2.2. Consider the example where f is a stochastic process of three random variables X, Y, Z where X and Y are Bernoulli ($p = \frac{1}{2}$), and Z is the XOR of X and Y . Suppose that observations are exact (i.e., $\varepsilon_n = 0$), that the target space \mathcal{A} comprises the output variable Z while the sample space \mathcal{S} comprises the input variables X and Y . Observing any single X or Y yields no information about Z : $I(Z; X) = I(Z; Y) = 0$, however, observing both inputs jointly perfectly determines Z : $I(Z; X, Y) = 1$. Thus, $\gamma_n(\mathcal{A}; \mathcal{S}) = 1$ if $n \geq 2$ and $\gamma_n(\mathcal{A}; \mathcal{S}) = 0$ else.

Learning about Z in examples of this kind is difficult for agents that make decisions greedily, since the next action (observing X or Y) yields no signal about its long-term usefulness. We call a sequence of observations, such as $\{X, Y\}$, *synergistic* since its combined information value is larger than the individual values. The prevalence of synergies is not captured by the information capacity $\gamma_n(\mathcal{A}; \mathcal{S})$ since it measures only the joint information gain of n samples within \mathcal{S} . Instead, the prevalence of synergies is captured by the sequence $\Gamma_n \stackrel{\text{def}}{=} \max_{\mathbf{x} \in \mathcal{S}} I(f_{\mathcal{A}}; \mathbf{y}_{\mathbf{x}} | \mathcal{D}_n)$, which measures the maximum information gain of y_{n+1} . If $\Gamma_n > \Gamma_{n-1}$ at any round n , this indicates a synergy. We propose to measure the additional complexity due to synergies by the following key object.

Definition 2.3 (Task complexity). For $n \geq 1$, assuming $\Gamma_i > 0$ for all $1 \leq i \leq n$, we define the *task complexity* as

$$\alpha_n(\mathcal{A}; \mathcal{S}) \stackrel{\text{def}}{=} \max_{i \in \{0, \dots, n-1\}} \frac{\Gamma_{n-1}}{\Gamma_i}.$$

Note that $\alpha_n(\mathcal{A}; \mathcal{S})$ is large only if the information gain of y_n is larger than that of a previous observation y_i . Intuitively, if $\alpha_n(\mathcal{A}; \mathcal{S})$ is large, the agent had to discover the *implicit* intermediate observations y_1, \dots, y_{n-1} that lead to downstream synergies. We formalize the intimate connections of the task complexity to synergies and submodularity in Appendix C. In the global transductive active learning problem considered in most prior works, where $\mathcal{S} \subseteq \mathcal{A}$ and f is a Gaussian process, it holds that $\gamma_n(\mathcal{A}; \mathcal{S}) = \gamma_n(\mathcal{X})$ and $\alpha_n(\mathcal{A}; \mathcal{S}) = 1$ since all learning targets appear *explicitly* in \mathcal{S} (cf. Appendix C). Note that generally, $\alpha_n(\mathcal{A}; \mathcal{S})$ can be computed online by keeping track of the smallest Γ_i during previous rounds i . In the following section, we propose the **ITL** decision rule, and show that the information capacity γ and the task complexity α govern its learning progress.

3. Information-based Transductive Learning

We propose **ITL**, which greedily maximizes the information gain at each round n between the prediction targets $f_{\mathcal{A}}$ and the next observation $y_{\mathbf{x}}$ conditioned on the prior observations \mathcal{D}_{n-1} . Formally,

$$\mathbf{x}_n = \arg \max_{\mathbf{x} \in \mathcal{S}} I(f_{\mathcal{A}}; y_{\mathbf{x}} \mid \mathcal{D}_{n-1}). \quad (\text{ITL})$$

ITL can also be interpreted as minimizing the “posterior uncertainty” among points in \mathcal{A} as measured by entropy:

$$\mathbf{x}_n = \arg \min_{\mathbf{x} \in \mathcal{S}} H[f_{\mathcal{A}} \mid \mathcal{D}_{n-1}, y_{\mathbf{x}}].$$

This simple decision rule generalizes several widely used algorithms which we discuss in more detail in Section 6. Most prominently, in the global learning setting where $\mathcal{S} \subseteq \mathcal{A}$, **ITL** reduces to $\mathbf{x}_n = \arg \max_{\mathbf{x} \in \mathcal{S}} I(f_{\mathcal{A}}; y_{\mathbf{x}} \mid \mathcal{D}_{n-1})$, i.e., is “undirected” (cf. Appendix D.2). While the convergence properties for this special instance of **ITL** have been studied extensively, we give convergence guarantees for the more general case of transductive active learning.

3.1. Gaussian Process Setting

When $f \sim \mathcal{GP}(\mu, k)$ is a Gaussian process (GP, Williams & Rasmussen (2006)) with known mean function μ and kernel k , and the noise $\varepsilon_{\mathbf{x}}$ is mutually independent and zero-mean Gaussian with known variance $\rho^2(\mathbf{x}) > 0$, the **ITL** objective has a closed form expression:

$$I(f_{\mathcal{A}}; y_{\mathbf{x}} \mid \mathcal{D}_{n-1}) = \frac{1}{2} \log \left(\frac{\text{Var}[y_{\mathbf{x}} \mid \mathcal{D}_{n-1}]}{\text{Var}[y_{\mathbf{x}} \mid f_{\mathcal{A}}, \mathcal{D}_{n-1}]} \right). \quad (1)$$

We first show that the step-wise uncertainty reduction is governed by the two sources of complexity from Section 2: the information capacity γ and the task complexity α .

Theorem 3.1 (Bound of uncertainty reduction for **ITL**). *Assume that f is a GP and that the noise $\varepsilon_{\mathbf{x}}$ is mutually independent and zero-mean Gaussian. Then, for any $n \geq 1$, if **ITL** generated the sequence $\{\mathbf{x}_i\}_{i=1}^n$,*

$$\Gamma_{n-1} \leq \alpha_n(\mathcal{A}; \mathcal{S}) \frac{\gamma_n(\mathcal{A}; \mathcal{S})}{n}. \quad (2)$$

We provide a formal proof of Theorem 3.1 in Appendix D.1. Theorem 3.1 suggests that designing a target space \mathcal{A} that is both goal-directed (i.e., has small γ) and explicit (i.e., has small α) is important for efficient learning. The information capacity γ_n is sublinear in n for a rich class of GPs, with rates summarized in Table 3 of the appendix (Srinivas et al., 2009; Vakili et al., 2021). If $|\mathcal{A}| < \infty$ then $\gamma_n(\mathcal{A}; \mathcal{S}) \leq \mathcal{O}(|\mathcal{A}| \log n)$ is a loose upper bound by simple reduction to an $|\mathcal{A}|$ -dimensional linear bandit.

Convergence to irreducible uncertainty So far, our discussion was centered around analyzing the role of the target space \mathcal{A} in facilitating *directed* learning. An orthogonal contribution of this work is to study *extrapolation* from the sample space \mathcal{S} to points $\mathbf{x} \in \mathcal{A} \setminus \mathcal{S}$. To this end, we derive bounds on the marginal posterior variance $\sigma_n^2(\mathbf{x}) \stackrel{\text{def}}{=} \text{Var}[f(\mathbf{x}) \mid \mathcal{D}_n]$ for points in \mathcal{A} . These bounds depend on the instance of transductive active learning (i.e., \mathcal{A} and \mathcal{S}) and might be of independent interest for active learning. For **ITL**, they imply uniform convergence of the variance for a rich class of GPs. To the best of our knowledge, we are the first to derive such bounds.

We define the *irreducible uncertainty* as the variance of $f(\mathbf{x})$ provided complete knowledge of f in \mathcal{S} , i.e.,

$$\eta^2(\mathbf{x}; \mathcal{S}) \stackrel{\text{def}}{=} \text{Var}[f_{\mathbf{x}} \mid f_{\mathcal{S}}].$$

As the name suggests, $\eta^2(\mathbf{x}; \mathcal{S})$ represents the smallest uncertainty one can hope to achieve from observing only within \mathcal{S} . For all $\mathbf{x} \in \mathcal{S}$, it is easy to see that $\eta^2(\mathbf{x}; \mathcal{S}) = 0$. However, the irreducible uncertainty of $\mathbf{x} \notin \mathcal{S}$ may be (and typically is!) strictly positive.

Theorem 3.2 (Bound on marginal variance). *Assume that $f \sim \mathcal{GP}(\mu, k)$ with known mean function μ and kernel k , the noise $\varepsilon_{\mathbf{x}}$ is mutually independent and zero-mean Gaussian with known variance $\rho^2(\mathbf{x}) > 0$, and γ_n is sublinear in n . Then for any $n \geq 0$, $\epsilon > 0$, and $\mathbf{x} \in \mathcal{A}$, there exists a constant C_{ϵ} independent of n such that*

$$\sigma_n^2(\mathbf{x}) \leq \underbrace{\eta^2(\mathbf{x}; \mathcal{S})}_{\text{irreducible}} + \underbrace{\nu_{n,\epsilon}^2}_{\text{reducible}} + \epsilon \quad (3)$$

where $\nu_{n,\epsilon}^2 \stackrel{\text{def}}{=} C_{\epsilon} \Gamma_n \tilde{\alpha}_{n,\epsilon}$ denotes the reducible uncertainty, and $\tilde{\alpha}_{n,\epsilon}$ is closely related to the task complexity (cf. Appendix D.3.1).³ Moreover, if $\mathbf{x} \in \mathcal{A} \cap \mathcal{S}$, there exists a constant C independent of n such that

$$\sigma_n^2(\mathbf{x}) \leq C \Gamma_n.$$

Intuitively, Equation (3) of Theorem 3.2 can be understood as bounding an epistemic “generalization gap” (Wainwright, 2019) of the learner. We provide a formal proof of Theorem 3.2 in Appendix D.3. To better understand the implications of Theorem 3.2, suppose for ease of notation that $\alpha_n, \tilde{\alpha}_{n,\epsilon} \leq 1$. By choosing, e.g., $\epsilon = c \sqrt{\gamma_n/n}$ we have $C_{\epsilon} \leq c' \sqrt{n \gamma_n}$ with constants c and c' (cf. Appendix D.3.2), which implies together with Theorem 3.1 that $\nu_{n,\epsilon}^2 + \epsilon \leq c' \sqrt{\gamma_n^3/n}$. For **ITL**, this guarantees that the reducible uncertainty converges, e.g., for Gaussian and smooth Matérn kernels.

3.2. Agnostic Setting

The result from the GP setting translates also to the agnostic setting, where the “ground truth” f^* may be any sufficiently

³In the special case where $\mathcal{S} \subseteq \mathcal{A}$, $\tilde{\alpha}_{n,\epsilon} \leq 1$.

regular fixed function on \mathcal{X} .⁴ In this case, we use the model f from Section 3.1 as a (misspecified) model of f^* , and we denote by $\mu_n(\mathbf{x}) \stackrel{\text{def}}{=} \mathbb{E}[f(\mathbf{x}) \mid \mathcal{D}_n]$ the posterior mean of f . W.l.o.g. we assume in the following result that the prior variance is bounded, i.e., $\text{Var}[f(\mathbf{x})] \leq 1$.⁵

Theorem 3.3 (Bound on approximation error, following Abbasi-Yadkori (2013); Chowdhury & Gopalan (2017)). *Pick any $\delta \in (0, 1)$ and $\epsilon > 0$. Assume that f^* lies in the reproducing kernel Hilbert space $\mathcal{H}_k(\mathcal{X})$ of the kernel k with norm $\|f^*\|_k < \infty$, the noise ε_n is conditionally ρ -sub-Gaussian, and γ_n is sublinear in n . Let $\beta_n(\delta) = \|f^*\|_k + \rho\sqrt{2(\gamma_n + 1 + \log(1/\delta))}$. Then for any $n \geq 0$ and $\mathbf{x} \in \mathcal{A}$ jointly with probability at least $1 - \delta$,*

$$|f^*(\mathbf{x}) - \mu_n(\mathbf{x})| \leq \beta_n(\delta) \left[\underbrace{\eta(\mathbf{x}; \mathcal{S})}_{\text{irreducible}} + \underbrace{\nu_{n, \epsilon^2}}_{\text{reducible}} + \epsilon \right]$$

where the reducible uncertainty ν_{n, ϵ^2} is with respect to the misspecified GP-model from Section 3.1.

We provide a formal proof of Theorem 3.3 in Appendix D.4. Similar to the GP setting, the result from Theorem 3.1 can be used to show convergence of **ITL** for a rich class of functions. Theorem 3.3 generalizes confidence bounds of prior works to the extrapolation setting, where some prediction targets $\mathbf{x} \in \mathcal{A}$ lie outside the sample space \mathcal{S} . For prediction targets $\mathbf{x} \in \mathcal{A} \cap \mathcal{S}$, the irreducible uncertainty vanishes and we recover previous results.

3.3. Experiments in the Gaussian Process Setting

Before demonstrating **ITL** on GPs to develop more intuition, we discuss some alternative interpretations of the fundamental learning principle (†).

Alternative decision rules **ITL** represents the posterior uncertainty via the entropy $H[f_{\mathcal{A}} \mid \mathcal{D}_n]$. We study the analogous decision rule which measures posterior uncertainty instead by the total variance $\text{tr} \text{Var}[f_{\mathcal{A}} \mid \mathcal{D}_n]$,

$$\mathbf{x}_n = \arg \min_{\mathbf{x} \in \mathcal{S}} \text{tr} \text{Var}[f_{\mathcal{A}} \mid \mathcal{D}_{n-1}, y_{\mathbf{x}}]. \quad (\text{VTL})$$

For **VTL**, we derive novel bounds analogous to Theorems 3.1 and 3.2 in Appendix E.2. Without deriving theoretical guarantees, **VTL** has previously been proposed in a transductive active learning setting by Seo et al. (2000). We also study the correlation-based decision rule,

$$\mathbf{x}_n = \arg \max_{\mathbf{x} \in \mathcal{S}} \sum_{\mathbf{x}' \in \mathcal{A}} \text{Cor}[f_{\mathbf{x}}, f_{\mathbf{x}'} \mid \mathcal{D}_{n-1}] \quad (\text{CTL})$$

which we show to be a tight approximation of **VTL** (cf. Appendix E.3). Unlike **VTL** and **CTL**, **ITL** takes into account the mutual dependence between points in \mathcal{A} .

⁴Here $f^*(\mathbf{x})$ denotes the mean observation $y_{\mathbf{x}} = f^*(\mathbf{x}) + \epsilon_{\mathbf{x}}$

⁵The results can be generalized to kernels with $\text{Var}[f(\mathbf{x})] \leq c$ (Chowdhury & Gopalan, 2017).

How does the smoothness of f affect **ITL?** We contrast two “extreme” kernels: the *Gaussian kernel* $k(\mathbf{x}, \mathbf{x}') = \exp(-\|\mathbf{x} - \mathbf{x}'\|_2^2/2)$ and the *Laplace kernel* $k(\mathbf{x}, \mathbf{x}') = \exp(-\|\mathbf{x} - \mathbf{x}'\|_1)$. In the mean-squared sense, the Gaussian kernel yields a smooth process f whereas the Laplace kernel yields a continuous but non-differentiable f (Williams & Rasmussen, 2006). Figure 2 (A) shows how **ITL** adapts to the smoothness of f : Under the “smooth” Gaussian kernel, points outside \mathcal{A} provide higher-order information. In contrast, under the “rough” Laplace kernel and if $\mathcal{A} \subseteq \mathcal{S}$, points outside \mathcal{A} do not provide any additional information, and therefore are not sampled by **ITL**. If, however, $\mathcal{A} \not\subseteq \mathcal{S}$, information “leaks” \mathcal{A} even under a Laplace kernel prior. That is, even for non-smooth functions, the point with most information need not be in \mathcal{A} .

Does **ITL outperform uncertainty sampling?** Uncertainty sampling (UNSA, Lewis & Catlett (1994)) is one of the most popular active learning methods. UNSA selects points \mathbf{x} with high *prior* uncertainty: $\mathbf{x}_n = \arg \max_{\mathbf{x} \in \mathcal{S}} \sigma_{n-1}^2(\mathbf{x})$. This is in stark contrast to **ITL** and **VTL** which select points \mathbf{x} that minimize *posterior* (epistemic) uncertainty about \mathcal{A} . It can be seen that UNSA is the special “undirected” case of **ITL** when $\mathcal{S} \subseteq \mathcal{A}$ and observation noise is homoscedastic (cf. Appendix D.2).

We compare UNSA to **ITL**, **VTL**, and **CTL** in Figure 2 (B). We observe that **ITL** outperforms UNSA which also samples points that are not informative about \mathcal{A} . Further, **ITL** outperforms “local” UNSA (constrained to $\mathcal{A} \cap \mathcal{S}$) which neglects all information provided by points outside \mathcal{A} .⁶ We include ablations in Appendix H where we, in particular, observe that the advantage of **ITL** over UNSA increases as the volume of prediction targets shrinks in comparison to the size of domain. In Appendix H, we additionally study the reduction of the total variance of $f_{\mathcal{A}}$ (as opposed to the entropy of $f_{\mathcal{A}}$) where, predictably, **VTL** has an advantage over **ITL**.

4. Few-Shot Fine-Tuning of Neural Networks

The “directed” learning problem also appears in the context of fine-tuning large neural networks (NNs) to downstream tasks. Consider a supervised learning problem, where the function f maps inputs $\mathbf{x} \in \mathcal{X}$ to outputs $y \in \mathcal{Y}$. We have access to noisy samples from a train data distribution $\mathcal{P}_{\mathcal{S}}$ on \mathcal{X} , and we would like to learn f such that our estimate minimizes a given risk measure, such as classification error, with respect to a test distribution $\mathcal{P}_{\mathcal{A}}$ on \mathcal{X} . The goal is to actively and efficiently sample from $\mathcal{P}_{\mathcal{S}}$ to minimize risk with respect to $\mathcal{P}_{\mathcal{A}}$. In this setting, $\mathcal{P}_{\mathcal{A}}$ and $\mathcal{P}_{\mathcal{S}}$ are akin to \mathcal{A} and \mathcal{S} , respectively.⁷

⁶If $\mathcal{A} \not\subseteq \mathcal{S}$ then “local” UNSA does *not* converge to the irreducible uncertainty.

⁷The setting with target distributions $\mathcal{P}_{\mathcal{A}}$ can be reduced to considering target sets \mathcal{A} , cf. Appendix F.

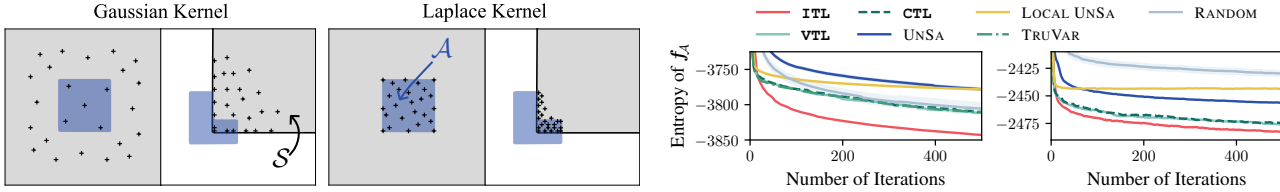


Figure 2. (A): The left figure depicts initial 25 samples of **ITL** under a Gaussian kernel with lengthscale 1 (left) and a Laplace kernel with lengthscale 10 (right). Shown in gray is the sample space \mathcal{S} and shown in blue is the target space \mathcal{A} . In three of the four examples, points outside the target space provide useful information. (B): The right figure depicts the entropy of f_A under the Gaussian kernel for the two instances of \mathcal{A} and \mathcal{S} from (A). The **TRUVAR** baseline only applies when $\mathcal{A} \subseteq \mathcal{S}$ (cf. Section 6). Uncertainty bands correspond to one standard error over 10 random seeds. Plots of the average marginal variance within \mathcal{A} can be found in Appendix H.

Despite the remarkable successes of large NNs across various fields, such as image classification and natural language processing, their performance can deteriorate when faced with slight variations between the source domain \mathcal{P}_S and target domain \mathcal{P}_A (Recht et al., 2019; Hendrycks & Dietterich, 2019; Koh et al., 2021; Lee et al., 2022). Additionally, training large NNs requires large amounts of (labeled) data, which is often expensive or even impossible to obtain, and furthermore, training on such large datasets requires prohibitive computational resources. Fine-tuning a large pre-trained model on a (small) dataset from the target domain is a cost- and computation-effective approach to address the distribution shift between source and target domains. While previous work has studied the effectiveness of various training procedures for fine-tuning (Howard & Ruder, 2018; Kornblith et al., 2019; Shen et al., 2021; Lee et al., 2022; Silva-Rodríguez et al., 2023), the problem of obtaining a good dataset for fine-tuning has received less attention. Accordingly, we show in this section that **ITL** can efficiently learn f using only *few* examples from \mathcal{P}_A .

From neural networks to stochastic processes The approximation of NNs $f(\cdot; \theta)$ as linear functions in a latent embedding space,

$$f(\mathbf{x}; \theta) \approx \boldsymbol{\beta}^\top \phi_\theta(\mathbf{x}), \quad (4)$$

with weights $\boldsymbol{\beta} \in \mathbb{R}^p$ and embeddings $\phi_\theta : \mathcal{X} \rightarrow \mathbb{R}^p$ has been studied by a rich line of prior work. Common choices of embeddings include last-layer embeddings (Devlin et al., 2019; Holzmüller et al., 2023), neural tangent embeddings arising from neural tangent kernels (Jacot et al., 2018) which are motivated by their relationship to the training and fine-tuning of ultra-wide NNs (Arora et al., 2019; Lee et al., 2019; Khan et al., 2019; He et al., 2020; Malladi et al., 2023), and loss gradient embeddings (Ash et al., 2020). We provide a comprehensive overview of embeddings in Appendix I.2. Now, supposing the prior $\boldsymbol{\beta} \sim \mathcal{N}(\mathbf{0}, \boldsymbol{\Sigma})$, often with $\boldsymbol{\Sigma} = \mathbf{I}$ (Khan et al., 2019; He et al., 2020; Antorán et al., 2022; Wei et al., 2022), the approximation of f from Equation (4) is a Gaussian process with kernel $k(\mathbf{x}, \mathbf{x}') = \phi_\theta(\mathbf{x})^\top \boldsymbol{\Sigma} \phi_\theta(\mathbf{x}')$. The covariance matrix $\boldsymbol{\Sigma}$ quantifies uncertainty about the weights $\boldsymbol{\beta}$, and we study approximations in Appendix I.3. In

our experiments, we use this Gaussian approximation with loss gradient embeddings⁸ and $\boldsymbol{\Sigma} = \mathbf{I}$ to evaluate the **ITL** decision rule, and select inputs for labeling and training f . Notably, the approximation of Equation (4) is only used to guide the active data selection, and not for inference.

Whereas prior work has studied the generalization error when using the posterior mean of $\boldsymbol{\beta}$ for prediction at a test point (Wei et al., 2022), our results from Section 3 bound the epistemic posterior uncertainty about this prediction given that the model is trained using data selected by **ITL**.

Batch selection via conditional embeddings Efficient labeling and training necessitates a batch-wise selection of inputs. The selection of a batch of size $b > 1$ can be seen as an individual *non-adaptive* active learning problem, and significant recent work has shown that batch diversity is crucial in this setting (Ash et al., 2020; Zanette et al., 2021; Holzmüller et al., 2023; Pacchiano et al., 2024). A batch-wise selection strategy is formalized by the following non-adaptive transductive active learning problem:

$$B_n = \arg \max_{\substack{B \subseteq \mathcal{S}, |B|=b}} I(f_A; y_B \mid \mathcal{D}_{n-1}). \quad (5)$$

This problem is NP-hard (Krause & Golovin, 2014; Golovin & Krause, 2011), and **ITL** optimizes it greedily:

$$\mathbf{x}_{n,i} = \arg \max_{\mathbf{x} \in \mathcal{S}} I(f_A; y_{\mathbf{x}} \mid \mathcal{D}_{n-1}, \mathbf{y}_{\mathbf{x}_{n,1:i-1}}). \quad (6)$$

We show in Appendix B that the approximation error of $B'_n = \mathbf{x}_{n,1:b}$ can be bounded in terms of the submodularity ratio of **ITL** (Das & Kempe, 2018) which is related to the task complexity. The batch B_n , and therefore also B'_n , is diverse and informative by design. We discuss an efficient iterative implementation of Equation (6) and an ablation in Appendix I.4. Prior work has shown that the greedy solution B'_n is also competitive with a fully sequential “batchless” decision rule (Chen & Krause, 2013; Esfandiari et al., 2021).⁹

⁸We observe essentially the same performance with neural tangent embeddings, cf. Appendix I.2.

⁹They prove this for the case where Equation (5) is submodular, but their results readily generalize to “approximate” submodularity.

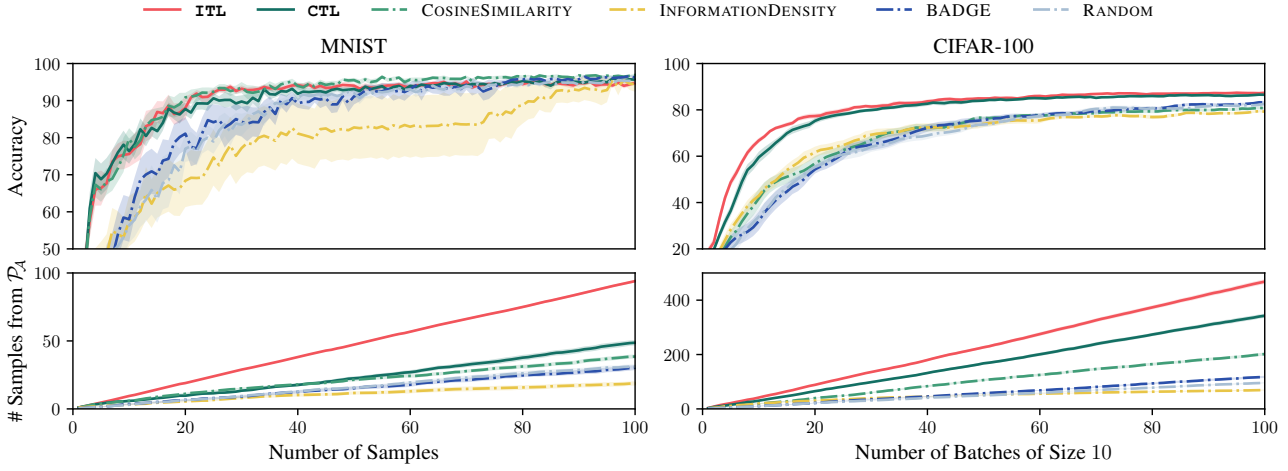


Figure 3. Few-shot training of NNs on MNIST (left) and CIFAR-100 (right). RANDOM selects each observation uniformly at random from \mathcal{P}_S . The batch size is 1 for MNIST and 10 for CIFAR-100. Uncertainty bands correspond to one standard error over 10 random seeds. We see that **ITL** significantly outperforms the state-of-the-art, and in particular, retrieves substantially more samples from the support of \mathcal{P}_A than competing methods. See Appendix I for details and additional experiments.

4.1. Experiments with Neural Networks

As testbeds, we evaluate the performance of **ITL** on two image classification tasks: MNIST (LeCun et al., 1998) and CIFAR-100 (Krizhevsky et al., 2009). In both cases, we take \mathcal{P}_S to be the data distribution, and we consider the task of learning the digits 3, 6, and 9 (MNIST) or the first 10 categories of CIFAR-100 via *few-shot* training of NNs.¹⁰

Architectures For MNIST, we train a simple convolutional neural network with ReLU activations, three convolutional layers with max-pooling, and two fully-connected layers. For CIFAR-100, we fine-tune an EfficientNet-B0 (Tan & Le, 2019) pre-trained on ImageNet (Deng et al., 2009), augmented by a final fully-connected layer. We train the NNs using the cross-entropy loss and the ADAM optimizer (Kingma & Ba, 2014).

Results **ITL** and **CTL** consistently and significantly outperform RANDOM, various widely used “undirected” heuristics such as BADGE (Ash et al., 2020),¹¹ and other “directed” heuristics such as COSINESIMILARITY and INFORMATIONDENSITY (Settles & Craven, 2008). In fact, the COSINESIMILARITY with \mathcal{A} using embeddings ϕ (cf. Appendix I.5), specializes **CTL** when $\Sigma = \mathbf{I}$ and the batch size is 1. Our results are summarized in Figure 3.

Improved data retrieval Both **ITL** and **CTL** use the learned embeddings to observe points similar to \mathcal{P}_A , and in particular, obtain more samples from the support of \mathcal{P}_A than

¹⁰That is, we restrict \mathcal{P}_A to the support of points with labels $\{3, 6, 9\}$ (MNIST) or labels $\{0, \dots, 9\}$ (CIFAR-100) and train a neural network using few examples drawn from \mathcal{P}_S .

¹¹We show in Appendix I.5 that **ITL** and **CTL** also substantially outperform a wide selection of other “undirected” heuristics.

RANDOM sampling of \mathcal{P}_S . We observe empirically that **ITL** obtains samples from \mathcal{P}_A at more than twice the rate of COSINESIMILARITY, which translates to a significant improvement in accuracy in more difficult learning tasks, while requiring fewer (labeled) samples from \mathcal{P}_S . This phenomenon manifests for both MNIST and CIFAR-100, as well as imbalanced data distributions \mathcal{P}_S or imbalanced reference samples from \mathcal{P}_A (cf. Appendix I.6). The improvement in accuracy appears to increase in the large-data regime, where the learning tasks become more difficult. Akin to the previously identified scaling trend with size of the pre-training dataset (Tamkin et al., 2022), this suggests a potential scaling trend where the improvement of **ITL** over random batch selection grows as models are fine-tuned on a larger pool of data.

Substantial prior work has studied data retrieval, e.g., in vector databases, using approximate nearest neighbor search (Johnson et al., 2019; Guo et al., 2020; Aumüller et al., 2020) where cosine similarity is a standard metric. Following the link between cosine similarity and **CTL**, **ITL** can be seen as a generalization of cosine similarity-based retrieval to batch and query sizes larger than one. Few-shot fine-tuning can be implemented also for sequences of *different* tasks (Vinyals et al., 2016), and as such task-driven few-shot fine-tuning can be seen as a form of “memory recall” akin to associative memory (Hopfield, 1982).

5. Safe Bayesian Optimization

Another practical problem that can be cast as “directed” learning is safe Bayesian optimization (Safe BO, Sui et al. (2015); Berkenkamp et al. (2021)) which has applications in natural science (Cooper & Netoff, 2022) and robotics (Wischniewski et al., 2019; Sukhija et al., 2023; Widmer et al.,

2023). Safe BO solves the following optimization problem

$$\max_{\mathbf{x} \in \mathcal{S}^*} f^*(\mathbf{x}) \quad \text{where} \quad \mathcal{S}^* = \{\mathbf{x} \in \mathcal{X} \mid g^*(\mathbf{x}) \geq 0\} \quad (7)$$

which can be generalized to multiple constraints. The functions f^* and g^* , and hence also the “safe set” \mathcal{S}^* , are unknown and have to be actively learned from data. However, it is crucial that the data collection does not violate the constraint, i.e., $\mathbf{x}_n \in \mathcal{S}^*, \forall n \geq 1$.

ITL for safe Bayesian optimization In the agnostic setting from Section 3.2, GPs f and g can be used as well-calibrated models of the ground truths f^* and g^* , and we denote lower- and upper-confidence bounds by $l_n^f(\mathbf{x}), l_n^g(\mathbf{x})$ and $u_n^f(\mathbf{x}), u_n^g(\mathbf{x})$, respectively. These confidence bounds induce a *pessimistic* safe set $\mathcal{S}_n \stackrel{\text{def}}{=} \{\mathbf{x} \mid l_n^g(\mathbf{x}) \geq 0\}$ and an *optimistic* safe set $\widehat{\mathcal{S}}_n \stackrel{\text{def}}{=} \{\mathbf{x} \mid u_n^g(\mathbf{x}) \geq 0\}$ which satisfy $\mathcal{S}_n \subseteq \mathcal{S}^* \subseteq \widehat{\mathcal{S}}_n$ with high probability at all times. Similarly, the set of *potential maximizers*

$$\mathcal{A}_n \stackrel{\text{def}}{=} \{\mathbf{x} \in \widehat{\mathcal{S}}_n \mid u_n^f(\mathbf{x}) \geq \max_{\mathbf{x}' \in \mathcal{S}_n} l_n^f(\mathbf{x}')\} \quad (8)$$

contains the solution to Equation (7) at all times with high probability.

The (simple) regret $r_n(\mathcal{S}) \stackrel{\text{def}}{=} \max_{\mathbf{x} \in \mathcal{S}} f^*(\mathbf{x}) - f^*(\widehat{\mathbf{x}}_n)$ with $\widehat{\mathbf{x}}_n \stackrel{\text{def}}{=} \arg \max_{\mathbf{x} \in \mathcal{S}_n} l_n^f(\mathbf{x})$ measures the worst-case performance of a decision rule. To achieve small regret, one faces an *exploration-expansion* dilemma wherein one needs to explore points that are known-to-be-safe, i.e., lie in the estimated safe set \mathcal{S}_n , and might be optimal, while at the same time discovering new safe points by “expanding” \mathcal{S}_n . Accordingly, a natural choice for the target space for Safe BO is \mathcal{A}_n since it captures both exploration and expansion *simultaneously* because it restricts learning to all potentially optimal points that might be safe. Furthermore, to prevent constraint violation, the sample space is restricted to the pessimistic safe set \mathcal{S}_n . In Safe BO, both the target space and sample space change with each round n , and we generalize our theoretical results from Section 3 in Appendix D to this setting.

Theorem 5.1 (Convergence to safe optimum). *Pick any $\epsilon > 0$, $\delta \in (0, 1)$. Assume that f^* lies in the reproducing kernel Hilbert space $\mathcal{H}_k(\mathcal{X})$ of the kernel k , and that the noise ε_n is conditionally ρ -sub-Gaussian. Then, we have with probability at least $1 - \delta$,*

Safety: for all $n \geq 1$, $\mathbf{x}_n \in \mathcal{S}^$.*

Moreover, assume $\mathcal{S}_0 \neq \emptyset$ and denote with \mathcal{R} the largest reachable safe set starting from \mathcal{S}_0 . Then, the convergence of reducible uncertainty implies that there exists $n^ > 0$ such that with probability at least $1 - \delta$,*

Optimality: for all $n \geq n^$, $r_n(\mathcal{R}) \leq \epsilon$.*

We provide a formal proof in Appendix D.5. In Section 3, we outline settings where the reducible uncertainty con-

verges. This is the case for a very general class of functions, and for such instances Theorem 5.1 guarantees optimality in the largest reachable safe set \mathcal{R} . \mathcal{R} represents the largest set any safe learning algorithm can explore without violating the safety constraints (with high probability) during learning (cf. Definition D.13). Our guarantees are similar to those of other Safe BO algorithms (Berkenkamp et al., 2021) but require fewer assumptions. We obtain Theorem 5.1 from a more general result (Theorem D.17) which can be specialized to yield “free” convergence guarantees for problems other than Bayesian optimization, such as level set estimation, by choosing an appropriate target space.

5.1. Experiments on Safe Bayesian Optimization

We evaluate two synthetic experiments for a 1d and 2d parameter space, respectively (cf. Appendix J.4 for details), which demonstrate the various shortcomings of existing Safe BO baselines. Additionally, as third experiment, we safely tune the controller of a quadcopter.

Safe controller tuning for a quadcopter We consider the dynamical system of a quadcopter with unknown dynamics; $\mathbf{s}_{t+1} = \mathbf{T}(\mathbf{s}_t, \mathbf{u}_t)$ where $\mathbf{u}_t \in \mathbb{R}^{d_u}$ is the control signal and $\mathbf{s}_t \in \mathbb{R}^{d_s}$ is the state at time t . The inputs \mathbf{u}_t are calculated through a deterministic function of the state $\pi : \mathcal{S} \rightarrow \mathcal{U}$ which we call the policy. The policy is parameterized via parameters $\mathbf{x} \in \mathcal{X}$, e.g., PID controller gains, such that $\mathbf{u}_t = \pi_{\mathbf{x}}(\mathbf{s}_t)$. The goal is to find the optimal parameters with respect to an unknown objective f^* while satisfying some unknown constraint(s) $g^*(\mathbf{x}) \geq 0$, e.g., the quadcopter does not fall on the ground. This is a typical Safe BO problem which is widely applied for safe controller learning in robotics (Berkenkamp et al., 2021; Baumann et al., 2021; Widmer et al., 2023). We discuss additional details in Appendix J.4.

Baselines We provide a detailed discussion of baselines in Appendix J.2 and give a brief overview here. The most widely used method for Safe BO is SAFE OPT (Sui et al., 2015; Berkenkamp et al., 2021) which keeps track of separate candidate sets for expansion and exploration and uses UNSA to pick one of the candidates in each round. Treating expansion and exploration separately, sampling is directed towards expansion in *all* directions — even those that are known to be suboptimal. The safe set is expanded based on a Lipschitz constant of g^* , which is assumed to be known. In most real-world settings, this constant is unknown and has to be estimated using the GP. This estimate is generally conservative and results in suboptimal performance. To this end, Berkenkamp et al. (2016) proposed HEURISTIC SAFE OPT which relies solely on the confidence intervals of g to expand the safe set, but lacks convergence guarantees.

Recently, Bottero et al. (2022) proposed ISE which queries parameters from \mathcal{S}_n that yield the most “information” about

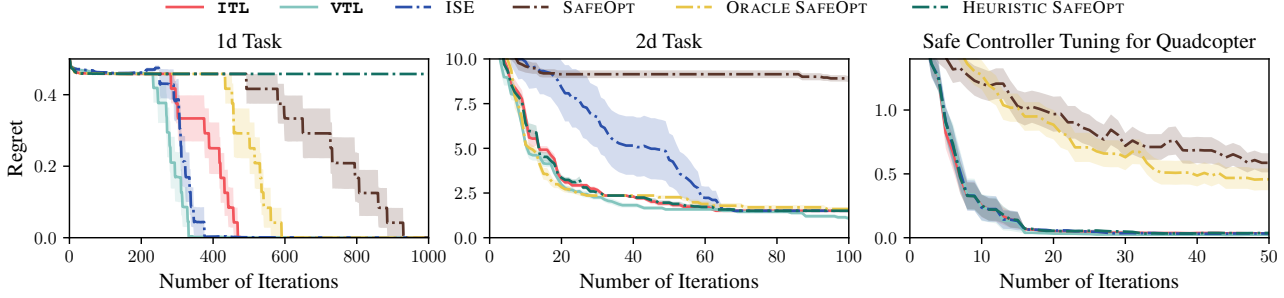


Figure 4. We compare **ITL** and **VTL** to **ORACLE SAFEOPT**, which has oracle knowledge of the Lipschitz constants, **SAFEOPT**, where the Lipschitz constants are estimated from the GP, as well as **HEURISTIC SAFEOPT** and **ISE**. We compare against additional baselines in Appendix J.1. The regret is evaluated with respect to the ground truth objective f^* and constraint g^* , and averaged over 10 (in synthetic experiments) and 25 (in the quadcopter experiment) random seeds.

the safety of another parameter in \mathcal{X} . Hence, **ISE** focuses solely on the expansion of the safe set \mathcal{S}_n and does not take into account the objective f . In practice, this can lead to significantly worse performance on the simplest of problems (cf. Figure 4). In contrast, **ITL** balances expansion of and exploration within the safe set. Furthermore, **ISE** does not have known convergence guarantees of the kind of Theorem 5.1. In parallel independent work, Bottero et al. (2024) proposed a combination of **ISE** and max-value entropy search (Wang & Jegelka, 2017) for which they derive a similar guarantee to Theorem 5.1.¹² Similar to **SAFEOPT**, their method aims to expand the safe set in all directions including those that are known to be suboptimal. In contrast, **ITL** directs expansion only towards potentially optimal regions.

Results In all our experiments, summarized in Figure 4, we observe that **ITL** (and **VTL**) systematically perform well, i.e., better or on par with our baselines. Moreover, in the 1d task and quadcopter experiment, we observe that **SAFEOPT** and even **ORACLE SAFEOPT** converge significantly slower than **ITL** to the safe optima. We believe this is due to their conservative Lipschitz-continuity/global smoothness-based expansion, as opposed to **ITL**’s expansion, which adapts to the local smoothness of the constraints. **HEURISTIC SAFEOPT** does not efficiently expand the safe set due to its heuristic which only considers single-step expansion, and which leads to its failure in the 1d task. **VTL** has a slight advantage over **ITL**, which we attribute to the fact that **VTL** minimizes marginal variances (as opposed to entropy), and the safe set is likewise expanded based on marginal variances. While **ITL** and **VTL** do not violate constraints, we observe that other methods that do not explicitly enforce safety such as EIC (Gardner et al., 2014) lead to constraint violation (cf. Appendix J.4.2).

Stochastic target space Alternatively to the target space \mathcal{A}_n which comprises all potentially optimal points,

¹²We provide an empirical evaluation in Appendix J.2.4.

we evaluate the stochastic target space

$$\mathcal{P}_{\mathcal{A}_n}(\cdot) = \mathbb{P}(\arg \max_{\mathbf{x} \in \mathcal{X}: g(\mathbf{x}) \geq 0} f(\mathbf{x}) = \cdot \mid \mathcal{D}_n) \quad (9)$$

which effectively weights points in \mathcal{A}_n according to how likely they are to be the safe optimum. Samples from $\mathcal{P}_{\mathcal{A}_n}$ can be obtained efficiently via Thompson sampling (Russo et al., 2018). Whether **ITL** with \mathcal{A}_n or $\mathcal{P}_{\mathcal{A}_n}$ performs better is task-dependent, and we include a detailed discussion in Appendix J.1.

6. Related Work

Several works have previously found entropy-based decision rules to be useful for global active learning (Krause & Guestrin, 2007; Guo & Greiner, 2007; Krause et al., 2008) and semi-supervised learning (Grandvalet & Bengio, 2004). The variance-based **VTL** has previously been proposed by Yu et al. (2006) in the special case of global active learning without proving theoretical guarantees. Shoham & Avron (2023) recently analyzed experimental designs for global one-shot learning in overparameterized models.

Substantial work on active learning has studied entropy-based criteria in *parameter-space*, most notably BALD (Houlsby et al., 2011; Kirsch et al., 2019), which selects actions $\mathbf{x}_n = \arg \max_{\mathbf{x} \in \mathcal{X}} I(\theta; y_{\mathbf{x}} \mid \mathcal{D}_{n-1})$, where θ is the random parameter vector of a parametric model (e.g., obtained via Bayesian deep learning). Such methods are inherently “undirected” in the sense that they do not facilitate learning on specific prediction targets. In contrast, **ITL** operates in *output-space* where it is straightforward to specify prediction targets, and which is computationally easier.

More recently, “directed” active learning methods have been proposed for the problem of determining the optimum of an unknown function, also known as best-arm identification (Audibert et al., 2010) or pure exploration bandits (Bubeck et al., 2009). Entropy search methods (Hennig & Schuler, 2012; Hernández-Lobato et al., 2014) are widely

used and select $\mathbf{x}_n = \arg \max_{\mathbf{x} \in \mathcal{X}} I(\mathbf{x}^*; y_{\mathbf{x}} | \mathcal{D}_{n-1})$ in *input-space* where $\mathbf{x}^* = \arg \max_{\mathbf{x}} f_{\mathbf{x}}$. Similarly to **ITL**, *output-space* entropy search methods (Hoffman & Ghahramani, 2015; Wang & Jegelka, 2017), which select $\mathbf{x}_n = \arg \max_{\mathbf{x} \in \mathcal{X}} I(f^*; y_{\mathbf{x}} | \mathcal{D}_{n-1})$ with $f^* = \max_{\mathbf{x}} f_{\mathbf{x}}$, are more computationally tractable. In fact, output-space entropy search is a special case of **ITL** with the stochastic target space $\mathcal{P}_{\mathcal{A}_n}$ from Equation (9) (cf. Appendix J.1). Bogunovic et al. (2016) analyze TRUVAR in the context of Bayesian optimization and level set estimation. TRUVAR is akin to **VTL** with a similar notion of “target space”, but their algorithm and analysis rely on a threshold scheme which requires that $\mathcal{A} \subseteq \mathcal{S}$. Fiez et al. (2019) introduce the *transductive linear bandit* problem, which is a special case of transductive active learning limited to a linear function class and with the objective of determining the maximum within an initial candidate set.¹³

We subsequently discuss more loosely related works. The general principle of non-active “transductive learning” was introduced by Vapnik (2006). The notion of “target” from transductive active learning is akin to the notion of “task” in curriculum learning (Bengio et al., 2009; Graves et al., 2017; Soviany et al., 2022). The study of settings where the irreducible uncertainty is zero is related to the study of estimability in experimental design (Graybill, 1961; Mutny & Krause, 2022). In feature selection, selecting features that maximize information gain with respect to a to-be-predicted label is a standard approach (Peng et al., 2005; Vergara & Estévez, 2014; Beraha et al., 2019) which is akin to **ITL** (cf. Appendix E). Transductive active learning is complimentary to other learning methodologies, such as semi-supervised learning (Gao et al., 2020), self-supervised learning (Shwartz-Ziv & LeCun, 2023; Balestriero et al., 2023), and meta-learning (Kaddour et al., 2020; Rothfuss et al., 2023).

7. Limitations

Better models In this work, we focus solely on sequential decision-making *given* some model, rather than asking how one should construct such a model so that it is representative of the ground truth. Learning stochastic models and approximations thereof have been the subject of much recent work (Blundell et al., 2015; Maddox et al., 2019; Daxberger et al., 2021; Antorán et al., 2022; Lin et al., 2023). Specifically, **ITL** benefits if the model f captures the right “correlations” between points and if its “uncertainty” about the prediction at a specific point is accurate.¹⁴

¹³The transductive bandit problem can be solved analogously to Safe BO, by maintaining a set of potential maximizers \mathcal{A}_n .

¹⁴For example, the application to NNs from Section 4 relies on embeddings being trained to capture the distribution shift.

Efficient computation of **ITL with large \mathcal{A}** Naïve computation of the **ITL** decision rule for m points within \mathcal{S} takes $\mathcal{O}(|\mathcal{A}|^3 + m)$ time and $\mathcal{O}(|\mathcal{A}|^2)$ space (cf. Appendix G) which is prohibitive for large $|\mathcal{A}|$. A practical solution for large \mathcal{A} is to subsample \mathcal{A} (such as in Section 4 and Equation (9)) within each round, and we provide a formal analysis of this approach in Appendix F and demonstrate its effectiveness for Safe BO in Appendix J.1.¹⁵

8. Conclusion

We investigated the generalization of active learning to settings with concrete prediction targets and/or with limited information due to constrained sample spaces. This provides a flexible framework, applicable also to other domains than were discussed (such as recommender systems, molecular design, robotics, etc.) by varying the choice of target space and sample space. Further, we proved novel generalization bounds which may be of independent interest for active learning. Finally, we demonstrated two broad applications where **ITL** substantially outperforms the state-of-the-art: fine-tuning neural networks and safely optimizing unknown constrained functions.

Broader Impact

This paper presents work whose goal is to advance the field of Machine Learning. There are many potential societal consequences of our work, none which we feel must be specifically highlighted here.

Acknowledgements

Many thanks to Armin Lederer, Johannes Kirschner, Jonas Rothfuss, Lars Loch, Manish Prajapat, Nicolas Emmenegger, Parnian Kassraie, and Scott Sussex for their insightful feedback on different versions of this manuscript, as well as Anton Baumann for helpful discussions.

This project was supported in part by the European Research Council (ERC) under the European Union’s Horizon 2020 research and Innovation Program Grant agreement no. 815943, the Swiss National Science Foundation under NCCR Automation, grant agreement 51NF40 180545, and by a grant of the Hasler foundation (grant no. 21039). Jonas Hübotter was supported in part by the German Academic Scholarship Foundation (Studienstiftung).

References

Abbasi-Yadkori, Y. *Online learning for linearly parametrized control problems*. PhD thesis, University

¹⁵In our NN experiments, we subsample \mathcal{A} to a small set with size equal to the number of classes; cf. Appendix I.1.

of Alberta, 2013.

Antorán, J., Janz, D., Allingham, J. U., Daxberger, E., Barban, R. R., Nalisnick, E., and Hernández-Lobato, J. M. Adapting the linearised laplace model evidence for modern deep learning. In *International Conference on Machine Learning*, pp. 796–821. PMLR, 2022.

Arora, S., Du, S. S., Hu, W., Li, Z., Salakhutdinov, R. R., and Wang, R. On exact computation with an infinitely wide neural net. *NeurIPS*, 32, 2019.

Arthur, D., Vassilvitskii, S., et al. k-means++: The advantages of careful seeding. In *SODA*, volume 7, 2007.

Ash, J., Goel, S., Krishnamurthy, A., and Kakade, S. Gone fishing: Neural active learning with fisher embeddings. *NeurIPS*, 34, 2021.

Ash, J. T., Zhang, C., Krishnamurthy, A., Langford, J., and Agarwal, A. Deep batch active learning by diverse, uncertain gradient lower bounds. *ICLR*, 2020.

Audibert, J.-Y., Bubeck, S., and Munos, R. Best arm identification in multi-armed bandits. In *COLT*, 2010.

Aumüller, M., Bernhardsson, E., and Faithfull, A. Ann-benchmarks: A benchmarking tool for approximate nearest neighbor algorithms. *Information Systems*, 87, 2020.

Balestrieri, R., Ibrahim, M., Sobal, V., Morcos, A., Shekhar, S., Goldstein, T., Bordes, F., Bardes, A., Mialon, G., Tian, Y., et al. A cookbook of self-supervised learning. *arXiv preprint arXiv:2304.12210*, 2023.

Barrett, A. B. Exploration of synergistic and redundant information sharing in static and dynamical gaussian systems. *Physical Review E*, 91(5), 2015.

Baumann, D., Marco, A., Turchetta, M., and Trimpe, S. Gosafe: Globally optimal safe robot learning. In *ICRA*, 2021.

Bengio, Y., Louradour, J., Collobert, R., and Weston, J. Curriculum learning. In *ICML*, volume 26, 2009.

Beraha, M., Metelli, A. M., Papini, M., Tirinzoni, A., and Restelli, M. Feature selection via mutual information: New theoretical insights. In *IJCNN*, 2019.

Berkenkamp, F., Schoellig, A. P., and Krause, A. Safe controller optimization for quadrotors with gaussian processes. In *ICRA*, 2016.

Berkenkamp, F., Krause, A., and Schoellig, A. P. Bayesian optimization with safety constraints: safe and automatic parameter tuning in robotics. *Machine Learning*, 2021.

Blundell, C., Cornebise, J., Kavukcuoglu, K., and Wierstra, D. Weight uncertainty in neural network. In *ICML*, 2015.

Bogunovic, I., Scarlett, J., Krause, A., and Cevher, V. Truncated variance reduction: A unified approach to bayesian optimization and level-set estimation. *NeurIPS*, 29, 2016.

Bottero, A., Luis, C., Vinogradsk, J., Berkenkamp, F., and Peters, J. R. Information-theoretic safe exploration with gaussian processes. *NeurIPS*, 35, 2022.

Bottero, A. G., Luis, C. E., Vinogradsk, J., Berkenkamp, F., and Peters, J. Information-theoretic safe bayesian optimization. *arXiv preprint arXiv:2402.15347*, 2024.

Bubeck, S., Munos, R., and Stoltz, G. Pure exploration in multi-armed bandits problems. In *ALT*, volume 20, 2009.

Chaloner, K. and Verdinelli, I. Bayesian experimental design: A review. *Statistical Science*, 1995.

Chandra, B. Quadrotor simulation, 2023. URL <https://github.com/Bharath2/Quadrotor-Simulation>.

Chen, Y. and Krause, A. Near-optimal batch mode active learning and adaptive submodular optimization. In *ICML*, 2013.

Chowdhury, S. R. and Gopalan, A. On kernelized multi-armed bandits. In *ICML*, 2017.

Cohn, D. Neural network exploration using optimal experiment design. *Advances in neural information processing systems*, 6, 1993.

Coleman, C., Chou, E., Katz-Samuels, J., Culatana, S., Bailis, P., Berg, A. C., Nowak, R., Sumbaly, R., Zaharia, M., and Yalniz, I. Z. Similarity search for efficient active learning and search of rare concepts. In *AAAI*, volume 36, 2022.

Cooper, S. E. and Netoff, T. I. Multidimensional bayesian estimation for deep brain stimulation using the safeopt algorithm. *medRxiv*, 2022.

Cover, T. M. *Elements of information theory*. John Wiley & Sons, 1999.

Das, A. and Kempe, D. Algorithms for subset selection in linear regression. In *STOC*, volume 40, 2008.

Das, A. and Kempe, D. Approximate submodularity and its applications: Subset selection, sparse approximation and dictionary selection. *JMLR*, 19(1), 2018.

Daxberger, E., Kristiadi, A., Immer, A., Eschenhagen, R., Bauer, M., and Hennig, P. Laplace redux-effortless bayesian deep learning. *NeurIPS*, 34, 2021.

Deng, J., Dong, W., Socher, R., Li, L.-J., Li, K., and Fei-Fei, L. Imagenet: A large-scale hierarchical image database. In *CVPR*, 2009.

Devlin, J., Chang, M.-W., Lee, K., and Toutanova, K. BERT: Pre-training of deep bidirectional transformers for language understanding. In *NAACL*, 2019.

Emmenegger, N., Mutný, M., and Krause, A. Likelihood ratio confidence sets for sequential decision making. *NeurIPS*, 37, 2023.

Esfandiari, H., Karbasi, A., and Mirrokni, V. Adaptivity in adaptive submodularity. In *COLT*, 2021.

Fiez, T., Jain, L., Jamieson, K. G., and Ratliff, L. Sequential experimental design for transductive linear bandits. *NeurIPS*, 32, 2019.

Gao, M., Zhang, Z., Yu, G., Arik, S. Ö., Davis, L. S., and Pfister, T. Consistency-based semi-supervised active learning: Towards minimizing labeling cost. In *ECCV*, 2020.

Gardner, J. R., Kusner, M. J., Xu, Z. E., Weinberger, K. Q., and Cunningham, J. P. Bayesian optimization with inequality constraints. In *ICML*, volume 2014, 2014.

Geifman, Y. and El-Yaniv, R. Deep active learning over the long tail. *arXiv preprint arXiv:1711.00941*, 2017.

Golovin, D. and Krause, A. Adaptive submodularity: Theory and applications in active learning and stochastic optimization. *JAIR*, 42, 2011.

Grandvalet, Y. and Bengio, Y. Semi-supervised learning by entropy minimization. *NeurIPS*, 17, 2004.

Graves, A., Bellemare, M. G., Menick, J., Munos, R., and Kavukcuoglu, K. Automated curriculum learning for neural networks. In *ICML*, 2017.

Graybill, F. A. *An introduction to linear statistical models*. Literary Licensing, LLC, 1961.

Guo, R., Sun, P., Lindgren, E., Geng, Q., Simcha, D., Chern, F., and Kumar, S. Accelerating large-scale inference with anisotropic vector quantization. In *ICML*, 2020.

Guo, Y. and Greiner, R. Optimistic active-learning using mutual information. In *IJCAI*, volume 7, 2007.

He, B., Lakshminarayanan, B., and Teh, Y. W. Bayesian deep ensembles via the neural tangent kernel. *NeurIPS*, 33, 2020.

Hendrycks, D. and Dietterich, T. Benchmarking neural network robustness to common corruptions and perturbations. *ICLR*, 2019.

Hendrycks, D. and Gimpel, K. A baseline for detecting misclassified and out-of-distribution examples in neural networks. *ICLR*, 2017.

Hennig, P. and Schuler, C. J. Entropy search for information-efficient global optimization. *JMLR*, 13(6), 2012.

Hernández-Lobato, J. M., Hoffman, M. W., and Ghahramani, Z. Predictive entropy search for efficient global optimization of black-box functions. *NeurIPS*, 27, 2014.

Hoffman, M. W. and Ghahramani, Z. Output-space predictive entropy search for flexible global optimization. In *NeurIPS workshop on Bayesian Optimization*, 2015.

Holzmüller, D., Zaverkin, V., Kästner, J., and Steinwart, I. A framework and benchmark for deep batch active learning for regression. *JMLR*, 24(164), 2023.

Hopfield, J. J. Neural networks and physical systems with emergent collective computational abilities. *Proceedings of the national academy of sciences*, 79(8), 1982.

Houlsby, N., Huszár, F., Ghahramani, Z., and Lengyel, M. Bayesian active learning for classification and preference learning. *CoRR*, 2011.

Howard, J. and Ruder, S. Universal language model fine-tuning for text classification. In *ACL*, 2018.

Hübotter, J., Sukhija, B., Treven, L., As, Y., and Krause, A. Active few-shot fine-tuning. *arXiv preprint arXiv:2402.15441*, 2024.

Jacot, A., Gabriel, F., and Hongler, C. Neural tangent kernel: Convergence and generalization in neural networks. *NeurIPS*, 31, 2018.

Johnson, J., Douze, M., and Jégou, H. Billion-scale similarity search with gpus. *IEEE Transactions on Big Data*, 7(3), 2019.

Kaddour, J., Sæmundsson, S., et al. Probabilistic active meta-learning. *NeurIPS*, 33, 2020.

Kassraie, P. and Krause, A. Neural contextual bandits without regret. In *AISTATS*, 2022.

Khan, M. E. E., Immer, A., Abedi, E., and Korzepa, M. Approximate inference turns deep networks into gaussian processes. *NeurIPS*, 32, 2019.

Khanna, R., Elenberg, E., Dimakis, A., Negahban, S., and Ghosh, J. Scalable greedy feature selection via weak submodularity. In *AISTATS*, 2017.

Kingma, D. P. and Ba, J. Adam: A method for stochastic optimization. In *ICLR*, 2014.

Kirsch, A., Van Amersfoort, J., and Gal, Y. Batchbald: Efficient and diverse batch acquisition for deep bayesian active learning. *NeurIPS*, 32, 2019.

Kirschner, J., Mutny, M., Hiller, N., Ischebeck, R., and Krause, A. Adaptive and safe bayesian optimization in high dimensions via one-dimensional subspaces. In *ICML*, 2019.

Koh, P. W., Sagawa, S., Marklund, H., Xie, S. M., Zhang, M., Balsubramani, A., Hu, W., Yasunaga, M., Phillips, R. L., Gao, I., et al. Wilds: A benchmark of in-the-wild distribution shifts. In *ICML*, 2021.

Kornblith, S., Shlens, J., and Le, Q. V. Do better imagenet models transfer better? In *CVPR*, 2019.

Krause, A. and Golovin, D. Submodular function maximization. *Tractability*, 3, 2014.

Krause, A. and Guestrin, C. Nonmyopic active learning of gaussian processes: an exploration-exploitation approach. In *ICML*, volume 24, 2007.

Krause, A., Singh, A., and Guestrin, C. Near-optimal sensor placements in gaussian processes: Theory, efficient algorithms and empirical studies. *JMLR*, 9(2), 2008.

Krizhevsky, A., Hinton, G., et al. Learning multiple layers of features from tiny images. Technical report, University of Toronto, 2009.

LeCun, Y., Cortes, C., and Burges, C. J. The mnist database of handwritten digits. <http://yann.lecun.com/exdb/mnist/>, 1998.

Lee, J., Bahri, Y., Novak, R., Schoenholz, S. S., Pennington, J., and Sohl-Dickstein, J. Deep neural networks as gaussian processes. *ICLR*, 2018.

Lee, J., Xiao, L., Schoenholz, S., Bahri, Y., Novak, R., Sohl-Dickstein, J., and Pennington, J. Wide neural networks of any depth evolve as linear models under gradient descent. *NeurIPS*, 32, 2019.

Lee, Y., Chen, A. S., Tajwar, F., Kumar, A., Yao, H., Liang, P., and Finn, C. Surgical fine-tuning improves adaptation to distribution shifts. *NeurIPS workshop on Distribution Shifts*, 2022.

Lewis, D. and Gale, W. A sequential algorithm for training text classifiers. In *SIGIR*, 1994.

Lewis, D. D. and Catlett, J. Heterogeneous uncertainty sampling for supervised learning. In *Machine learning proceedings 1994*. Elsevier, 1994.

Lin, J. A., Antorán, J., Padhy, S., Janz, D., Hernández-Lobato, J. M., and Terenin, A. Sampling from gaussian process posteriors using stochastic gradient descent. *NeurIPS*, 37, 2023.

Maddox, W. J., Izmailov, P., Garipov, T., Vetrov, D. P., and Wilson, A. G. A simple baseline for bayesian uncertainty in deep learning. *NeurIPS*, 32, 2019.

Malladi, S., Wettig, A., Yu, D., Chen, D., and Arora, S. A kernel-based view of language model fine-tuning. In *ICML*, 2023.

Martens, J. and Grosse, R. Optimizing neural networks with kronecker-factored approximate curvature. In *ICML*, 2015.

Murphy, K. P. *Probabilistic machine learning: Advanced topics*. MIT Press, 2023.

Mutny, M. and Krause, A. Experimental design for linear functionals in reproducing kernel hilbert spaces. *NeurIPS*, 35, 2022.

Nemhauser, G. L., Wolsey, L. A., and Fisher, M. L. An analysis of approximations for maximizing submodular set functions—i. *Mathematical programming*, 14, 1978.

Ostrovsky, R., Rabani, Y., Schulman, L. J., and Swamy, C. The effectiveness of lloyd-type methods for the k-means problem. *JACM*, 2013.

Pacchiano, A., Lee, J. N., and Brunskill, E. Experiment planning with function approximation. *NeurIPS*, 37, 2024.

Peng, H., Long, F., and Ding, C. Feature selection based on mutual information criteria of max-dependency, max-relevance, and min-redundancy. *IEEE Transactions on pattern analysis and machine intelligence*, 27(8), 2005.

Rahimi, A. and Recht, B. Random features for large-scale kernel machines. *NeurIPS*, 20, 2007.

Recht, B., Roelofs, R., Schmidt, L., and Shankar, V. Do imagenet classifiers generalize to imagenet? In *ICML*, 2019.

Rothfuss, J., Koenig, C., Rupenyan, A., and Krause, A. Meta-learning priors for safe bayesian optimization. In *COLT*, 2023.

Russo, D. J., Van Roy, B., Kazerouni, A., Osband, I., Wen, Z., et al. A tutorial on thompson sampling. *Foundations and Trends® in Machine Learning*, 11(1), 2018.

Scheffer, T., Decomain, C., and Wrobel, S. Active hidden markov models for information extraction. In *IDA*, 2001.

Schreiter, J., Nguyen-Tuong, D., Eberts, M., Bischoff, B., Markert, H., and Toussaint, M. Safe exploration for active learning with gaussian processes. In *ECML PKDD*, 2015.

Sener, O. and Savarese, S. Active learning for convolutional neural networks: A core-set approach. *ICLR*, 2017.

Seo, S., Wallat, M., Graepel, T., and Obermayer, K. Gaussian process regression: Active data selection and test point rejection. In *Mustererkennung 2000*. Springer, 2000.

Settles, B. Active learning literature survey. Technical report, University of Wisconsin-Madison Department of Computer Sciences, 2009.

Settles, B. and Craven, M. An analysis of active learning strategies for sequence labeling tasks. In *EMNLP*, 2008.

Shen, Z., Liu, Z., Qin, J., Savvides, M., and Cheng, K.-T. Partial is better than all: revisiting fine-tuning strategy for few-shot learning. In *AAAI*, volume 35, 2021.

Shoham, N. and Avron, H. Experimental design for overparameterized learning with application to single shot deep active learning. *IEEE Transactions on Pattern Analysis and Machine Intelligence*, 2023.

Shwartz-Ziv, R. and LeCun, Y. To compress or not to compress—self-supervised learning and information theory: A review. *arXiv preprint arXiv:2304.09355*, 2023.

Silva-Rodríguez, J., Dolz, J., and Ayed, I. B. Towards foundation models and few-shot parameter-efficient finetuning for volumetric organ segmentation. In *MICCAI*, 2023.

Soviany, P., Ionescu, R. T., Rota, P., and Sebe, N. Curriculum learning: A survey. *IJCV*, 2022.

Srinivas, N., Krause, A., Kakade, S. M., and Seeger, M. Gaussian process optimization in the bandit setting: No regret and experimental design. In *ICML*, volume 27, 2009.

Sui, Y., Gotovos, A., Burdick, J., and Krause, A. Safe exploration for optimization with gaussian processes. In *ICML*, 2015.

Sukhija, B., Turchetta, M., Lindner, D., Krause, A., Trimpe, S., and Baumann, D. Gosafeopt: Scalable safe exploration for global optimization of dynamical systems. *Artificial Intelligence*, 2023.

Tamkin, A., Nguyen, D., Deshpande, S., Mu, J., and Goodman, N. Active learning helps pretrained models learn the intended task. *NeurIPS*, 35, 2022.

Tan, M. and Le, Q. Efficientnet: Rethinking model scaling for convolutional neural networks. In *ICML*, 2019.

Tu, S., Frostig, R., Singh, S., and Sindhwani, V. JAX: A python library for differentiable optimal control on accelerators, 2023. URL <http://github.com/google/trajax>.

Turchetta, M., Berkenkamp, F., and Krause, A. Safe exploration for interactive machine learning. *NeurIPS*, 32, 2019.

Vakili, S., Khezeli, K., and Picheny, V. On information gain and regret bounds in gaussian process bandits. In *AISTATS*, 2021.

Vapnik, V. *Estimation of dependences based on empirical data*. Springer Science & Business Media, 2006.

Vergara, J. R. and Estévez, P. A. A review of feature selection methods based on mutual information. *Neural computing and applications*, 24, 2014.

Vinyals, O., Blundell, C., Lillicrap, T., Wierstra, D., et al. Matching networks for one shot learning. *NeurIPS*, 29, 2016.

Wainwright, M. J. *High-dimensional statistics: A non-asymptotic viewpoint*, volume 48. Cambridge university press, 2019.

Wang, Z. and Jegelka, S. Max-value entropy search for efficient bayesian optimization. In *ICML*, 2017.

Wei, A., Hu, W., and Steinhardt, J. More than a toy: Random matrix models predict how real-world neural representations generalize. In *ICML*, 2022.

Widmer, D., Kang, D., Sukhija, B., Hübotter, J., Krause, A., and Coros, S. Tuning legged locomotion controllers via safe bayesian optimization. *CORL*, 2023.

Wilks, S. S. Certain generalizations in the analysis of variance. *Biometrika*, 1932.

Williams, C. K. and Rasmussen, C. E. *Gaussian processes for machine learning*, volume 2. MIT press Cambridge, MA, 2006.

Wischnewski, A., Betz, J., and Lohmann, B. A model-free algorithm to safely approach the handling limit of an autonomous racecar. In *ICCVE*, 2019.

Yu, H. and Kim, S. Passive sampling for regression. In *ICDM*, 2010.

Yu, K., Bi, J., and Tresp, V. Active learning via transductive experimental design. In *ICML*, volume 23, 2006.

Zanette, A., Dong, K., Lee, J. N., and Brunskill, E. Design of experiments for stochastic contextual linear bandits. *NeurIPS*, 34, 2021.

Appendices

A general principle of “transductive learning” was already formulated by the famous computer scientist Vladimir Vapnik in the 20th century. Vapnik proposes the following “imperative for a complex world”:

When solving a problem of interest, do not solve a more general problem as an intermediate step. Try to get the answer that you really need but not a more general one.

– Vapnik (2006)

These appendices provide additional background, proofs, experiment details, and ablation studies.

Contents

A Background	15	F Subsampling Target Spaces	26
A.1 Information Theory	15	F.1 Stochastic Target Spaces	26
A.2 Gaussian Processes	15		
B Non-adaptivity and Submodularity Ratio	15	G Computational Complexity	26
C Task Complexity and Submodularity Ratio Measure Downstream Synergies	16	H Additional GP Experiments & Details	26
C.1 The Information Ratio	16	I Additional NN Experiments & Details	27
C.2 The Relationship to the Submodularity Ratio	16	I.1 Experiment Details	28
C.3 The Relationship to the Task Complexity	16	I.2 Embeddings and Kernels	28
C.4 The Information Ratio is Strictly Positive in the Gaussian Case	16	I.3 Towards Uncertainty Quantification in Latent Space	29
D Proofs	17	I.4 Batch Selection via Conditional Embeddings	30
D.1 Proof of Theorem 3.1	17	I.5 Baselines	30
D.2 Undirected Case of ITL	17	I.6 Additional experiments	32
D.3 Proof of Theorem 3.2	17	I.7 Ablation study of noise standard deviation ρ	34
D.4 Proof of Theorem 3.3	20		
D.5 Proof of Theorem 5.1	20	J Additional Safe BO Experiments & Details	37
D.6 Useful Facts and Inequalities	23	J.1 Subsampling \mathcal{A} via Thompson Sampling	37
E Interpretations & Approximations of Principle	23	J.2 Detailed Comparison with Prior Works	37
(\dagger)	23	J.3 Jumping Past Local Barriers	40
E.1 Interpretations of ITL	24	J.4 Experiment Details	41
E.2 Variance-based Transductive Learning	24		
E.3 Correlation-based Transductive Learning	25		

A. Background

A.1. Information Theory

Throughout this work, \log denotes the natural logarithm. Given random vectors \mathbf{x} and \mathbf{y} , we denote by

$$\begin{aligned} H[\mathbf{x}] &\stackrel{\text{def}}{=} \mathbb{E}_{p(\mathbf{x})}[-\log p(\mathbf{x})], \\ H[\mathbf{x} \mid \mathbf{y}] &\stackrel{\text{def}}{=} \mathbb{E}_{p(\mathbf{x}, \mathbf{y})}[-\log p(\mathbf{x} \mid \mathbf{y})], \quad \text{and} \\ I(\mathbf{x}; \mathbf{y}) &\stackrel{\text{def}}{=} H[\mathbf{x}] - H[\mathbf{x} \mid \mathbf{y}] \end{aligned}$$

the (differential) entropy, conditional entropy, and information gain, respectively (Cover, 1999).¹⁶

The *multivariate information gain* (Murphy, 2023) between random vectors $\mathbf{x}, \mathbf{y}, \mathbf{z}$ is given by

$$I(\mathbf{x}; \mathbf{y}; \mathbf{z}) \stackrel{\text{def}}{=} I(\mathbf{x}; \mathbf{y}) - I(\mathbf{x}; \mathbf{y} \mid \mathbf{z}) \quad (10)$$

$$= I(\mathbf{x}; \mathbf{y}) + I(\mathbf{x}; \mathbf{z}) - I(\mathbf{x}; \mathbf{y}, \mathbf{z}). \quad (11)$$

When $I(\mathbf{x}; \mathbf{y}; \mathbf{z}) \neq 0$ it is said that \mathbf{y} and \mathbf{z} *interact* regarding their information about \mathbf{x} . If the interaction is positive, it is said that the information of \mathbf{z} about \mathbf{x} is *redundant* given \mathbf{y} . Conversely, if the interaction is negative, it is said that the information of \mathbf{z} about \mathbf{x} is *synergistic* with \mathbf{y} . The notion of synergy is akin to the frequentist notion of “suppressor variables” in linear regression (Das & Kempe, 2008).

A.2. Gaussian Processes

The stochastic process f is a Gaussian process (GP, Williams & Rasmussen (2006)), denoted $f \sim \mathcal{GP}(\mu, k)$, with mean function μ and kernel k if for any finite subset $X = \{\mathbf{x}_1, \dots, \mathbf{x}_n\} \subseteq \mathcal{X}$, $\mathbf{f}_X \sim \mathcal{N}(\boldsymbol{\mu}_X, \mathbf{K}_{XX})$ is jointly Gaussian with mean vector $\boldsymbol{\mu}_X(i) = \mu(\mathbf{x}_i)$ and covariance matrix $\mathbf{K}_{XX}(i, j) = k(\mathbf{x}_i, \mathbf{x}_j)$.

In the following, we formalize the assumptions from the GP setting (cf. Section 3.1).

Assumption A.1 (Gaussian prior). We assume that $f \sim \mathcal{GP}(\mu, k)$ with known mean function μ and kernel k .

Assumption A.2 (Gaussian noise). We assume that the noise $\varepsilon_{\mathbf{x}}$ is mutually independent and zero-mean Gaussian with known variance $\rho^2(\mathbf{x}) > 0$. We write $\mathbf{P}_X = \text{diag}\{\rho^2(\mathbf{x}_1), \dots, \rho^2(\mathbf{x}_n)\}$.

Under Assumptions A.1 and A.2, the posterior distribution of f after observing points X is $\mathcal{GP}(\boldsymbol{\mu}_n, k_n)$ with

$$\begin{aligned} \boldsymbol{\mu}_n(\mathbf{x}) &= \mu(\mathbf{x}) + \mathbf{K}_{\mathbf{x}X}(\mathbf{K}_{XX} + \mathbf{P}_X)^{-1}(\mathbf{y}_X - \boldsymbol{\mu}_X), \\ k_n(\mathbf{x}, \mathbf{x}') &= k(\mathbf{x}, \mathbf{x}') - \mathbf{K}_{\mathbf{x}X}(\mathbf{K}_{XX} + \mathbf{P}_X)^{-1}\mathbf{K}_{X\mathbf{x}'}, \\ \sigma_n^2(\mathbf{x}) &= k_n(\mathbf{x}, \mathbf{x}). \end{aligned}$$

¹⁶One has to be careful to ensure that $I(\mathbf{x}; \mathbf{y})$ exists, i.e., $|I(\mathbf{x}; \mathbf{y})| < \infty$. We will assume that this is the case throughout this work. When \mathbf{x} and \mathbf{y} are jointly Gaussian, this is satisfied when the noise variance ρ^2 is positive.

For Gaussian random vectors \mathbf{f} and \mathbf{y} , the entropy is $H[\mathbf{f}] = \frac{n}{2} \log(2\pi e) + \frac{1}{2} \log |\text{Var}[\mathbf{f}]|$, the information gain is $I(\mathbf{f}; \mathbf{y}) = \frac{1}{2}(\log |\text{Var}[\mathbf{y}]| - \log |\text{Var}[\mathbf{y} \mid \mathbf{f}]|)$, and

$$\gamma_n = \max_{\substack{X \subseteq \mathcal{X} \\ |X| \leq n}} \frac{1}{2} \log |\mathbf{I} + \mathbf{P}_X^{-1} \mathbf{K}_{XX}|.$$

B. Non-adaptivity and Submodularity Ratio

Recall the non-adaptive optimization problem

$$B_{n,k} = \arg \max_{\substack{B \subseteq \mathcal{S} \\ |B|=k}} I(\mathbf{f}_A; \mathbf{y}_B \mid \mathcal{D}_{n-1})$$

from Equation (5), and denote by $B'_{n,k} = \mathbf{x}_{n,1:k}$ the greedy approximation from Equation (6). Note that the objective function

$$\begin{aligned} F_n(B) &\stackrel{\text{def}}{=} I(\mathbf{f}_A; \mathbf{y}_B \mid \mathcal{D}_{n-1}) \\ &= H[\mathbf{f}_A \mid \mathcal{D}_{n-1}] - H[\mathbf{f}_A \mid \mathcal{D}_{n-1}, \mathbf{y}_B] \end{aligned}$$

is non-negative and monotone,¹⁷ since conditional entropy is monotone (which is also called the “information never hurts” principle).

Let $\Delta_n(\mathbf{x} \mid B) \stackrel{\text{def}}{=} \Delta_n(\{\mathbf{x}\} \mid B) \stackrel{\text{def}}{=} F_n(B \cup \{\mathbf{x}\}) - F(B)$ denote the *marginal gain* of $\mathbf{x} \in \mathcal{S}$ given $B \subseteq \mathcal{S}$ which simplifies to

$$\begin{aligned} \Delta_n(\mathbf{x} \mid B) &= I(\mathbf{f}_A; \mathbf{y}_B, y_{\mathbf{x}} \mid \mathcal{D}_{n-1}) - I(\mathbf{f}_A; \mathbf{y}_B \mid \mathcal{D}_{n-1}) \\ &= H[\mathbf{f}_A \mid \mathcal{D}_{n-1}, \mathbf{y}_B] - H[\mathbf{f}_A \mid \mathcal{D}_{n-1}, \mathbf{y}_B, y_{\mathbf{x}}] \\ &= I(\mathbf{f}_A; y_{\mathbf{x}} \mid \mathcal{D}_{n-1}, \mathbf{y}_B) \end{aligned}$$

and which is precisely the objective function of **ITL** from Equation (6).

Batch selection via conditional embeddings approximates $B_{n,k}$ Building upon the theory of maximizing monotone submodular functions (Nemhauser et al., 1978; Krause & Golovin, 2014), Das & Kempe (2018) study greedy maximization under “approximate” submodularity:

Definition B.1 (Submodularity ratio of **ITL**). Das & Kempe (2018) define the *submodularity ratio* of F_n up to cardinality $k \geq 1$ as

$$\kappa_n(k) \stackrel{\text{def}}{=} \min_{\substack{B \subseteq B'_{n,k} \\ X \subseteq \mathcal{S}: |X| \leq k \\ B \cap X = \emptyset}} \frac{\sum_{\mathbf{x} \in X} \Delta_n(\mathbf{x} \mid B)}{\Delta_n(X \mid B)}, \quad (12)$$

where they define $\frac{0}{0} \equiv 1$.

¹⁷Formally, $F_n(B) \geq 0$ and $F_n(B') \leq F_n(B)$ for any $B' \subseteq B \subseteq \mathcal{S}$.

As a special case of theorem 6 from Das & Kempe (2018), applying that F_n is non-negative and monotone, we obtain the following result.

Theorem B.2 (Efficiency of batch selection via conditional embeddings). *For any $n, k \geq 1$, the greedy solution $B'_{n,k}$ provides a $(1 - e^{-\kappa_n(k)})$ -approximation of $B_{n,k}$.*

If $\mathcal{S} \subseteq \mathcal{A}$, it is well known (e.g., Srinivas et al., 2009) that F_n is submodular, which implies that $\kappa_n(k) \geq 1$ for all $k \geq 1$.

C. Task Complexity and Submodularity Ratio Measure Downstream Synergies

Both $\kappa_n(k)$ and the task complexity $\alpha_n(\mathcal{A}; \mathcal{S})$ are ratios of information gains, which as we will see in this section can be seen as natural measures of “redundancy” and “synergy”.

C.1. The Information Ratio

We will study a multiplicative interpretation of the multivariate information gain (cf. Equation (11)), which we call the *information ratio* of $X \subseteq \mathcal{S}, |X| < \infty$:

$$\bar{\kappa}(X) \stackrel{\text{def}}{=} \frac{\sum_{\mathbf{x} \in X} I(\mathbf{f}_A; y_{\mathbf{x}})}{I(\mathbf{f}_A; \mathbf{y}_X)} \in [0, \infty). \quad (13)$$

Observe that $\bar{\kappa}(X)$ measures the synergy properties of \mathbf{y}_X with respect to \mathbf{f}_A in a multiplicative sense. That is, if $\bar{\kappa}(X) > 1$ then information in \mathbf{y}_X is redundant, whereas if $\bar{\kappa}(X) < 1$ then information in \mathbf{y}_X is synergistic, and if $\bar{\kappa}(X) = 1$ then \mathbf{y}_X do not mutually interact with respect to \mathbf{f}_A . In the degenerate case where $I(\mathbf{f}_A; \mathbf{y}_X) = 0$ (which implies $\sum_{\mathbf{x} \in X} I(\mathbf{f}_A; y_{\mathbf{x}}) = 0$) we therefore let $\bar{\kappa}(X) = 1$.

C.2. The Relationship to the Submodularity Ratio

Let

$$\bar{\kappa}_n(X) \stackrel{\text{def}}{=} \bar{\kappa}(X \mid \mathcal{D}_n) \quad (14)$$

where we write $\bar{\kappa}(X \mid \cdot)$ to denote the conditional information ratio. It is straightforward to see that the submodularity ratio from Equation (12) is an information ratio such that for any $n \geq 1$ and $X \subseteq \mathcal{S}, |X| = k < \infty$,

$$\bar{\kappa}_n(X) \geq \min_{\substack{B \subseteq B'_{n,k} \\ B \cap X = \emptyset}} \bar{\kappa}_n(X \mid B) \geq \kappa_n(k).$$

C.3. The Relationship to the Task Complexity

Whereas $\bar{\kappa}_n$ measures synergy (multiplicatively) based on Equation (11), the task complexity α_n is a multiplicative measure of synergy based on Equation (10). As outlined in Section 2, intuitively, α_n measures downstream synergies between observations and the learning target \mathcal{A} . The

following relates the two measures:

$$\begin{aligned} \bar{\kappa}(\mathbf{x}_{1:n}) &= \frac{\sum_{i=1}^n I(\mathbf{f}_A; y_i)}{I(\mathbf{f}_A; \mathbf{y}_{1:n})} \\ &\stackrel{(i)}{=} \frac{\sum_{i=1}^n I(\mathbf{f}_A; y_i)}{\sum_{i=1}^n I(\mathbf{f}_A; y_i \mid \mathbf{y}_{1:i-1})} \\ &\geq \min_{i \in \{1, \dots, n\}} \frac{I(\mathbf{f}_A; y_i)}{I(\mathbf{f}_A; y_i \mid \mathbf{y}_{1:i-1})} \end{aligned}$$

where (i) follows from the chain rule of information gain.

The special “undirected” case If $\mathcal{S} \subseteq \mathcal{A}$ then mutual information is monotonically decreasing upon conditioning since for any $\mathbf{x} \in \mathcal{S}$ and $X \subseteq \mathcal{S}$, $y_{\mathbf{x}} \perp \mathbf{y}_X \mid \mathbf{f}_A$, which implies $\alpha_n \leq 1$.

C.4. The Information Ratio is Strictly Positive in the Gaussian Case

We prove the following straightforward lower bound to the information ratio.

Lemma C.1. *Let $X \subseteq \mathcal{S}, |X| < \infty$. If \mathbf{f}_A and \mathbf{y}_X are jointly Gaussian then $\bar{\kappa}(X) \geq 0$.*

Proof. We let $X = \{\mathbf{x}_1, \dots, \mathbf{x}_k\}$ and prove lower and upper bound separately. We assume w.l.o.g. that $I(\mathbf{f}_A; \mathbf{y}_X) > 0$ which implies $|\text{Var}[\mathbf{f}_A \mid \mathbf{y}_X]| < |\text{Var}[\mathbf{f}_A]|$. Thus, there exists some i such that \mathbf{f}_A and $y_{\mathbf{x}_i}$ are dependent, so $|\text{Var}[\mathbf{f}_A \mid y_{\mathbf{x}_i}]| < |\text{Var}[\mathbf{f}_A]|$ which implies $I(\mathbf{f}_A; y_{\mathbf{x}_i}) > 0$. We therefore conclude that $\bar{\kappa}(X) > 0$. \square

The following example shows that this lower bound is tight.

Example C.2 (Synergies of Gaussian random variables, inspired by section 3 of Barrett (2015)). Consider the three random variables X , Y , and Z (think $\mathcal{A} = \{X\}$ and $\mathcal{S} = \{Y, Z\}$) which are jointly Gaussian with mean vector $\mathbf{0}$ and covariance matrix

$$\Sigma = \begin{bmatrix} 1 & a & a \\ a & 1 & 0 \\ a & 0 & 1 \end{bmatrix}, \quad \text{for } 2a^2 < 1$$

where the constraint on a is to ensure that Σ is positive definite. Computing the mutual information, we have

$$I(X; Y) = I(X; Z) = -\frac{1}{2} \log(1 - a^2)$$

and $I(X; Y, Z) = -\frac{1}{2} \log(1 - 2a^2)$. Therefore,

$$\frac{I(X; Y) + I(X; Z)}{I(X; Y, Z)} = \frac{\log(1 - 2a^2 + a^4)}{\log(1 - 2a^2)} < 1.$$

Note that

$$\lim_{a \rightarrow \frac{1}{\sqrt{2}}} \frac{\log(1 - 2a^2 + a^4)}{\log(1 - 2a^2)} = 0,$$

and hence — perhaps unintuitively — even if Y and Z are uncorrelated, their information about X may be arbitrarily synergistic.

D. Proofs

We write

- $\sigma^2 \stackrel{\text{def}}{=} \max_{\mathbf{x} \in \mathcal{X}} \sigma_0^2(\mathbf{x})$, and
- $\tilde{\sigma}^2 \stackrel{\text{def}}{=} \max_{\mathbf{x} \in \mathcal{X}} \sigma_0^2(\mathbf{x}) + \rho^2(\mathbf{x})$.

We will where unambiguously abbreviate the task complexity $\alpha_n(\mathcal{A}; \mathcal{S})$ by α_n .

D.1. Proof of Theorem 3.1

Our following analysis allows for changing target spaces \mathcal{A}_n and sample spaces \mathcal{S}_n (cf. Section 5), and to this end, we redefine $\Gamma_n \stackrel{\text{def}}{=} \max_{\mathbf{x} \in \mathcal{S}_n} I(\mathbf{f}_{\mathcal{A}_n}; \mathbf{y}_{\mathbf{x}} \mid \mathcal{D}_n)$. We prove the following more general statement than Theorem 3.1.

Theorem D.1. *Fix any integers $n_1 > n_0 \geq 0$, $\Delta = n_1 - n_0 + 1$ such that for all $i \in \{n_0, \dots, n_1 - 1\}$, $\mathcal{A}_{i+1} \subseteq \mathcal{A}_i$ and $\mathcal{S} \stackrel{\text{def}}{=} \mathcal{S}_{i+1} = \mathcal{S}_i$. Further, assume $|\mathcal{A}_{n_0}| < \infty$. Then, if the sequence $\{\mathbf{x}_{i+1}\}_{i=n_0}^{n_1}$ was generated by **ITL**,*

$$\Gamma_{n_1} \leq \alpha_{n_1}(\mathcal{A}; \mathcal{S}) \frac{\gamma_{\Delta}}{\Delta}. \quad (15)$$

Moreover, if $n_0 = 0$,

$$\Gamma_{n_1} \leq \alpha_{n_1}(\mathcal{A}; \mathcal{S}) \frac{\gamma_{\Delta}(\mathcal{A}_0; \mathcal{S})}{\Delta}. \quad (16)$$

Proof. We have

$$\begin{aligned} \Gamma_{n_1} &= \frac{1}{\Delta} \sum_{i=n_0}^{n_1} \Gamma_{n_1} \\ &\stackrel{(i)}{\leq} \frac{\alpha_{n_1}}{\Delta} \sum_{i=n_0}^{n_1} \Gamma_i \\ &\stackrel{(ii)}{=} \frac{\alpha_{n_1}}{\Delta} \sum_{i=n_0}^{n_1} I(\mathbf{f}_{\mathcal{A}_i}; \mathbf{y}_{\mathbf{x}_{i+1}} \mid \mathcal{D}_i) \\ &\stackrel{(iii)}{\leq} \frac{\alpha_{n_1}}{\Delta} \sum_{i=n_0}^{n_1} I(\mathbf{f}_{\mathcal{A}_{n_0}}; \mathbf{y}_{\mathbf{x}_{i+1}} \mid \mathcal{D}_i) \\ &\stackrel{(iv)}{=} \frac{\alpha_{n_1}}{\Delta} \sum_{i=n_0}^{n_1} I(\mathbf{f}_{\mathcal{A}_{n_0}}; \mathbf{y}_{\mathbf{x}_{i+1}} \mid \mathbf{y}_{\mathbf{x}_{n_0+1:i}}, \mathcal{D}_{n_0}) \\ &\stackrel{(v)}{=} \frac{\alpha_{n_1}}{\Delta} I(\mathbf{f}_{\mathcal{A}_{n_0}}; \mathbf{y}_{\mathbf{x}_{n_0+1:n_1+1}} \mid \mathcal{D}_{n_0}) \\ &\leq \frac{\alpha_{n_1}}{\Delta} \max_{\substack{X \subseteq \mathcal{S} \\ |X|=\Delta}} I(\mathbf{f}_{\mathcal{A}_{n_0}}; \mathbf{y}_X \mid \mathcal{D}_{n_0}) \end{aligned}$$

$$\begin{aligned} &\stackrel{(vi)}{\leq} \frac{\alpha_{n_1}}{\Delta} \max_{\substack{X \subseteq \mathcal{S} \\ |X|=\Delta}} I(\mathbf{f}_X; \mathbf{y}_X \mid \mathcal{D}_{n_0}) \\ &\stackrel{(vii)}{\leq} \frac{\alpha_{n_1}}{\Delta} \max_{\substack{X \subseteq \mathcal{S} \\ |X|=\Delta}} I(\mathbf{f}_X; \mathbf{y}_X) \\ &= \alpha_{n_1} \frac{\gamma_{\Delta}}{\Delta} \end{aligned}$$

where (i) follows from the definition of the task complexity α_{n_1} (cf. Definition 2.3); (ii) uses the objective of **ITL**; (iii) uses $\mathcal{A}_{i+1} \subseteq \mathcal{A}_i$ and monotonicity of information gain; (iv) uses that the posterior variance of Gaussians is independent of the realization and only depends on the *location* of observations; (v) uses the chain rule of information gain; (vi) uses $\mathbf{y}_X \perp \mathbf{f}_{\mathcal{A}_{n_0}} \mid \mathbf{f}_X$ and the data processing inequality. The conditional independence follows from the assumption that the observation noise is independent. Similarly, $\mathbf{y}_X \perp \mathcal{D}_{n_0} \mid \mathbf{f}_X$ which implies (vii).

If $n_0 = 0$, then the bound before line (vi) simplifies to $\alpha_{n_1} \gamma_{\Delta}(\mathcal{A}_0; \mathcal{S}) / \Delta$. \square

Keeping track of the task complexity online In general, the task complexity α_n may be larger than one in the “directed” setting (i.e., when $\mathcal{S} \not\subseteq \mathcal{A}$). However, note that α_n can easily be evaluated online by keeping track of the smallest Γ_i during previous rounds i .

D.2. Undirected Case of **ITL**

We briefly examine the important special case of **ITL** where $\mathcal{S} \subseteq \mathcal{A}$. In this setting, for all $\mathbf{x} \in \mathcal{S}$, the decision rule of **ITL** simplifies to

$$\begin{aligned} I(\mathbf{f}_{\mathcal{A}}; \mathbf{y}_{\mathbf{x}} \mid \mathcal{D}_n) &\stackrel{(i)}{=} I(\mathbf{f}_{\mathcal{A} \setminus \{\mathbf{x}\}}; \mathbf{y}_{\mathbf{x}} \mid \mathbf{f}_{\mathbf{x}}, \mathcal{D}_n) + I(\mathbf{f}_{\mathbf{x}}; \mathbf{y}_{\mathbf{x}} \mid \mathcal{D}_n) \\ &\stackrel{(ii)}{=} I(\mathbf{f}_{\mathbf{x}}; \mathbf{y}_{\mathbf{x}} \mid \mathcal{D}_n) \\ &= H[\mathbf{y}_{\mathbf{x}} \mid \mathcal{D}_n] - H[\varepsilon_{\mathbf{x}}] \end{aligned}$$

where (i) follows from the chain rule of information gain and $\mathbf{x} \in \mathcal{S} \subseteq \mathcal{A}$; and (ii) follows from the conditional independence $\mathbf{f}_{\mathcal{A}} \perp \mathbf{y}_{\mathbf{x}} \mid \mathbf{f}_{\mathbf{x}}$.

If additionally f is a GP then

$$H[\mathbf{y}_{\mathbf{x}} \mid \mathcal{D}_n] - H[\varepsilon_{\mathbf{x}}] = \frac{1}{2} \log \left(1 + \frac{\text{Var}[\mathbf{f}_{\mathbf{x}} \mid \mathcal{D}_n]}{\text{Var}[\varepsilon_{\mathbf{x}}]} \right).$$

Therefore, when $\mathcal{S} \subseteq \mathcal{A}$ and observation noise is homoscedastic, **ITL** is equivalent to uncertainty sampling.

D.3. Proof of Theorem 3.2

We will now prove Theorem 3.2. We first prove the convergence of marginal variance within \mathcal{S} , before proving the convergence outside \mathcal{S} in Appendix D.3.1.

Lemma D.2 (Uniform convergence of marginal variance within \mathcal{S}). For any $n \geq 0$ and $\mathbf{x} \in \mathcal{A} \cap \mathcal{S}$,

$$\sigma_n^2(\mathbf{x}) \leq 2\tilde{\sigma}^2 \cdot \Gamma_n. \quad (17)$$

Proof. We have

$$\begin{aligned} \sigma_n^2(\mathbf{x}) &= \text{Var}[f_{\mathbf{x}} \mid \mathcal{D}_n] - \underbrace{\text{Var}[f_{\mathbf{x}} \mid f_{\mathbf{x}}, \mathcal{D}_n]}_0 \\ &\stackrel{(i)}{=} \text{Var}[y_{\mathbf{x}} \mid \mathcal{D}_n] - \rho^2(\mathbf{x}) \\ &\quad - (\text{Var}[y_{\mathbf{x}} \mid f_{\mathbf{x}}, \mathcal{D}_n] - \rho^2(\mathbf{x})) \\ &= \text{Var}[y_{\mathbf{x}} \mid \mathcal{D}_n] - \text{Var}[y_{\mathbf{x}} \mid f_{\mathbf{x}}, \mathcal{D}_n] \\ &\stackrel{(ii)}{\leq} \tilde{\sigma}^2 \log \left(\frac{\text{Var}[y_{\mathbf{x}} \mid \mathcal{D}_n]}{\text{Var}[y_{\mathbf{x}} \mid f_{\mathbf{x}}, \mathcal{D}_n]} \right) \\ &= 2\tilde{\sigma}^2 \cdot \text{I}(f_{\mathbf{x}}; y_{\mathbf{x}} \mid \mathcal{D}_n) \\ &\stackrel{(iii)}{\leq} 2\tilde{\sigma}^2 \cdot \text{I}(f_{\mathcal{A}}; y_{\mathbf{x}} \mid \mathcal{D}_n) \\ &\stackrel{(iv)}{\leq} 2\tilde{\sigma}^2 \cdot \max_{\mathbf{x}' \in \mathcal{S}} \text{I}(f_{\mathcal{A}}; y_{\mathbf{x}'} \mid \mathcal{D}_n) \\ &= 2\tilde{\sigma}^2 \cdot \Gamma_n \end{aligned}$$

where (i) follows from the noise assumption (cf. Assumption A.2); (ii) follows from Lemma D.20 and using monotonicity of variance; (iii) follows from $\mathbf{x} \in \mathcal{A}$ and monotonicity of information gain; and (iv) follows from $\mathbf{x} \in \mathcal{S}$. \square

D.3.1. CONVERGENCE OUTSIDE \mathcal{S}

We will now show convergence of marginal variance to the irreducible uncertainty for points outside the sample space.

Our proof roughly proceeds as follows: We construct an “approximate Markov boundary” of \mathbf{x} in \mathcal{S} , and show (1) that the size of this Markov boundary is independent of n , and (2) that a small uncertainty reduction within the Markov boundary implies that the marginal variances at the Markov boundary and(!) \mathbf{x} are small.

Definition D.3 (Approximate Markov boundary). For any $\epsilon > 0$, $n \geq 0$, and $\mathbf{x} \in \mathcal{X}$, we denote by $B_{n,\epsilon}(\mathbf{x})$ the smallest (multi-)subset of \mathcal{S} such that

$$\text{Var}[f_{\mathbf{x}} \mid \mathcal{D}_n, \mathbf{y}_{B_{n,\epsilon}(\mathbf{x})}] \leq \eta^2(\mathbf{x}; \mathcal{S}) + \epsilon. \quad (18)$$

We call $B_{n,\epsilon}(\mathbf{x})$ an ϵ -approximate Markov boundary of \mathbf{x} in \mathcal{S} .

Equation (18) is akin to the notion of the smallest Markov blanket in \mathcal{S} of some $\mathbf{x} \in \mathcal{X}$ (called a *Markov boundary*) which is the smallest set $\mathcal{B} \subseteq \mathcal{S}$ such that $f_{\mathbf{x}} \perp \mathbf{f}_{\mathcal{S}} \mid \mathbf{f}_{\mathcal{B}}$.

Lemma D.4 (Existence of an approximate Markov boundary). For any $\epsilon > 0$, let k be the smallest integer satisfying

$$\frac{\gamma_k}{k} \leq \frac{\epsilon \lambda_{\min}(\mathbf{K}_{\mathcal{S}\mathcal{S}})}{2|\mathcal{S}|\sigma^2\tilde{\sigma}^2}. \quad (19)$$

Then, for any $n \geq 0$ and $\mathbf{x} \in \mathcal{X}$, there exists an ϵ -approximate Markov boundary $B_{n,\epsilon}(\mathbf{x})$ of \mathbf{x} in \mathcal{S} with size at most k .

Lemma D.4 shows that for any $\epsilon > 0$ there exists a universal constant b_ϵ such that

$$|B_{n,\epsilon}(\mathbf{x})| \leq b_\epsilon \quad \forall n \geq 0, \mathbf{x} \in \mathcal{X}. \quad (20)$$

We defer the proof of Lemma D.4 to Appendix D.3.3 where we also provide an algorithm to compute $B_{n,\epsilon}(\mathbf{x})$.

Lemma D.5. For any $\epsilon > 0$, $n \geq 0$, and $\mathbf{x} \in \mathcal{X}$,

$$\sigma_n^2(\mathbf{x}) \leq 2\sigma^2 \cdot \text{I}(f_{\mathbf{x}}; \mathbf{y}_{B_{n,\epsilon}(\mathbf{x})} \mid \mathcal{D}_n) + \eta^2(\mathbf{x}; \mathcal{S}) + \epsilon \quad (21)$$

where $B_{n,\epsilon}(\mathbf{x})$ is an ϵ -approximate Markov boundary of \mathbf{x} in \mathcal{S} .

Proof. We have

$$\begin{aligned} \sigma_n^2(\mathbf{x}) &= \text{Var}[f_{\mathbf{x}} \mid \mathcal{D}_n] - \eta^2(\mathbf{x}; \mathcal{S}) + \eta^2(\mathbf{x}; \mathcal{S}) \\ &\stackrel{(i)}{\leq} \text{Var}[f_{\mathbf{x}} \mid \mathcal{D}_n] - \text{Var}[f_{\mathbf{x}} \mid \mathbf{y}_{B_{n,\epsilon}(\mathbf{x})}, \mathcal{D}_n] \\ &\quad + \eta^2(\mathbf{x}; \mathcal{S}) + \epsilon \\ &\stackrel{(ii)}{\leq} \sigma^2 \log \left(\frac{\text{Var}[f_{\mathbf{x}} \mid \mathcal{D}_n]}{\text{Var}[f_{\mathbf{x}} \mid \mathbf{y}_{B_{n,\epsilon}(\mathbf{x})}, \mathcal{D}_n]} \right) \\ &\quad + \eta^2(\mathbf{x}; \mathcal{S}) + \epsilon \\ &= 2\sigma^2 \cdot \text{I}(f_{\mathbf{x}}; \mathbf{y}_{B_{n,\epsilon}(\mathbf{x})} \mid \mathcal{D}_n) + \eta^2(\mathbf{x}; \mathcal{S}) + \epsilon \end{aligned}$$

where (i) follows from the defining property of an ϵ -approximate Markov boundary (cf. Equation (18)); and (ii) follows from Lemma D.20 and using monotonicity of variance. \square

Lemma D.6. For any $\epsilon > 0$, $n \geq 0$, and $\mathbf{x} \in \mathcal{A}$,

$$\text{I}(f_{\mathbf{x}}; \mathbf{y}_{B_{n,\epsilon}(\mathbf{x})} \mid \mathcal{D}_n) \leq \frac{b_\epsilon}{\bar{\kappa}_n(B_{n,\epsilon}(\mathbf{x}))} \Gamma_n \quad (22)$$

where $B_{n,\epsilon}(\mathbf{x})$ is an ϵ -approximate Markov boundary of \mathbf{x} in \mathcal{S} , $|B_{n,\epsilon}(\mathbf{x})| \leq b_\epsilon$, and where $\bar{\kappa}_n(\cdot)$ denotes the information ratio from Equation (14).

We remark that $\bar{\kappa}_n(\cdot) > 0$ as is shown in Lemma C.1, and hence, the right-hand side of the inequality is well-defined.

Proof. We use the abbreviated notation $B = B_{n,\epsilon}(\mathbf{x})$. We have

$$\begin{aligned} \text{I}(f_{\mathbf{x}}; \mathbf{y}_B \mid \mathcal{D}_n) &\stackrel{(i)}{\leq} \text{I}(f_{\mathcal{A}}; \mathbf{y}_B \mid \mathcal{D}_n) \\ &\stackrel{(ii)}{\leq} \frac{1}{\bar{\kappa}_n(b_\epsilon)} \sum_{\tilde{\mathbf{x}} \in B} \text{I}(f_{\mathcal{A}}; y_{\tilde{\mathbf{x}}} \mid \mathcal{D}_n) \\ &\stackrel{(iii)}{\leq} \frac{b_\epsilon}{\bar{\kappa}_n(b_\epsilon)} \max_{\tilde{\mathbf{x}} \in B} \text{I}(f_{\mathcal{A}}; y_{\tilde{\mathbf{x}}} \mid \mathcal{D}_n) \end{aligned}$$

$$\begin{aligned} &\stackrel{(iv)}{\leq} \frac{b_\epsilon}{\bar{\kappa}_{n,b_\epsilon}} \max_{\tilde{\mathbf{x}} \in \mathcal{S}} I(\mathbf{f}_A; y_{\tilde{\mathbf{x}}} \mid \mathcal{D}_n) \\ &= \frac{b_\epsilon}{\bar{\kappa}_{n,b_\epsilon}} \Gamma_n \end{aligned}$$

where (i) follows from monotonicity of mutual information; (ii) follows from the definition of the information ratio $\bar{\kappa}_{n,b_\epsilon}$ (cf. Equation (14)); (iii) follows from $b \leq b_\epsilon$; and (iv) follows from $B \subseteq \mathcal{S}$. \square

Proof of Theorem 3.2. The case where $\mathbf{x} \in \mathcal{A} \cap \mathcal{S}$ is shown by Lemma D.2 with $C = 2\tilde{\sigma}^2$.

To prove the more general result, fix any $\mathbf{x} \in \mathcal{A}$ and $\epsilon > 0$. By Lemma D.4, there exists an ϵ -approximate Markov boundary $B_{n,\epsilon}(\mathbf{x})$ of \mathbf{x} in \mathcal{S} such that $|B_{n,\epsilon}(\mathbf{x})| \leq b_\epsilon$. We have

$$\begin{aligned} \sigma_n^2(\mathbf{x}) &\stackrel{(i)}{\leq} 2\sigma^2 \cdot I(f_{\mathbf{x}}; \mathbf{y}_{B_{n,\epsilon}(\mathbf{x})} \mid \mathcal{D}_n) + \eta^2(\mathbf{x}; \mathcal{S}) + \epsilon \\ &\stackrel{(ii)}{\leq} \frac{2\sigma^2 b_\epsilon}{\bar{\kappa}_n(B_{n,\epsilon}(\mathbf{x}))} \Gamma_n + \eta^2(\mathbf{x}; \mathcal{S}) + \epsilon \end{aligned}$$

where (i) follows from Lemma D.5; and (ii) follows from Lemma D.6.

We let $\tilde{\alpha}_{n,\epsilon} \stackrel{\text{def}}{=} 1/\bar{\kappa}_n(B_{n,\epsilon}(\mathbf{x}))$ which quantifies downstream synergies about \mathcal{A} (between the points in the proxy set $B_{n,\epsilon}(\mathbf{x})$) akin to the task complexity α_n (cf. Appendix C). The result follows by setting $C_\epsilon = 2\sigma^2 b_\epsilon$. \square

We remark that Theorem 3.2 holds irrespectively of the decision rule: the choice of decision rule is absorbed by Γ_n .

D.3.2. EXEMPLARY APPLICATION OF THEOREM 3.2

For ease of notation that $\alpha_n, \tilde{\alpha}_{n,\epsilon} \leq 1$, and further assume that γ_n is sublinear in n . Let $\epsilon = c\sqrt{\frac{\gamma_n}{n}}$ with $c = 2|\mathcal{S}|\sigma^2\tilde{\sigma}^2/\lambda_{\min}(\mathbf{K}_{SS})$. Then, by Equation (19), b_ϵ is the smallest integer satisfying

$$\frac{\gamma_{b_\epsilon}}{b_\epsilon} \leq \sqrt{\frac{\gamma_n}{n}}.$$

Note that b_ϵ depends on n , but can be bounded for instance by $\sqrt{n\gamma_n}$, since

$$\frac{\gamma\sqrt{n\gamma_n}}{\sqrt{n\gamma_n}} \leq \frac{\gamma\sqrt{n^2}}{\sqrt{n\gamma_n}} \leq \frac{\gamma_n}{\sqrt{n\gamma_n}} = \sqrt{\frac{\gamma_n}{n}}.$$

Together with Theorem 3.1 this implies for **ITL** that

$$\begin{aligned} \nu_{n,\epsilon}^2 + \epsilon &\leq 2\sigma^2\sqrt{n\gamma_n}\Gamma_n + c\sqrt{\gamma_n/n} \\ &\leq c'\sqrt{\gamma_n^3/n} \end{aligned}$$

for a constant c' , e.g., $c' = 2\sigma^2 + c$. This guarantees that the reducible uncertainty of **ITL** converges, e.g., for Gaussian and smooth Matérn kernels.

D.3.3. EXISTENCE OF AN APPROXIMATE MARKOV BOUNDARY

We now derive Lemma D.4 which shows the existence of an approximate Markov boundary of \mathbf{x} in \mathcal{S} .

Lemma D.7. *For any $S \subseteq \mathcal{S}$ and $k \geq 0$, there exists $B \subseteq S$ with $|B| = k$ such that for all $\mathbf{x}' \in S$,*

$$\text{Var}[f_{\mathbf{x}'} \mid \mathbf{y}_B] \leq 2\tilde{\sigma}^2 \frac{\gamma_k}{k}. \quad (23)$$

Proof. We choose $B \subseteq S$ greedily using the acquisition function

$$\tilde{\mathbf{x}}_k \stackrel{\text{def}}{=} \arg \max_{\tilde{\mathbf{x}} \in S} I(\mathbf{f}_S; y_{\tilde{\mathbf{x}}} \mid \mathbf{y}_{B_{k-1}})$$

where $B_k = \tilde{\mathbf{x}}_{1:k}$. Note that this is the “undirected” special case of **ITL**, and hence, we have

$$\begin{aligned} \text{Var}[f_{\mathbf{x}'} \mid \mathbf{y}_{B_k}] &\stackrel{(i)}{\leq} 2\tilde{\sigma}^2 \Gamma_k \\ &\stackrel{(ii)}{\leq} 2\tilde{\sigma}^2 \frac{\gamma_k}{k} \end{aligned}$$

where (i) is due to Lemma D.2; and (ii) is due to Theorem 3.1 and $\alpha_k(S; S) \leq 1$. \square

Lemma D.8. *Given any $\epsilon > 0$ and $B \subseteq S \subseteq \mathcal{S}$ with $|S| < \infty$, such that for any $\mathbf{x}' \in S$,*

$$\text{Var}[f_{\mathbf{x}'} \mid \mathbf{y}_B] \leq \frac{\epsilon \lambda_{\min}(\mathbf{K}_{SS})}{|S|\sigma^2}. \quad (24)$$

Then for any $\mathbf{x} \in \mathcal{X}$,

$$\text{Var}[f_{\mathbf{x}} \mid \mathbf{y}_B] \leq \text{Var}[f_{\mathbf{x}} \mid \mathbf{f}_S] + \epsilon. \quad (25)$$

Proof. We will denote the right-hand side of Equation (24) by ϵ' . We have

$$\begin{aligned} &\text{Var}[f_{\mathbf{x}} \mid \mathbf{y}_B] \\ &\stackrel{(i)}{=} \mathbb{E}_{\mathbf{f}_S} [\text{Var}_{f_{\mathbf{x}}} [f_{\mathbf{x}} \mid \mathbf{f}_S, \mathbf{y}_B] \mid \mathbf{y}_B] \\ &\quad + \text{Var}_{\mathbf{f}_S} [\mathbb{E}_{f_{\mathbf{x}}} [f_{\mathbf{x}} \mid \mathbf{f}_S, \mathbf{y}_B] \mid \mathbf{y}_B] \\ &\stackrel{(ii)}{=} \text{Var}_{f_{\mathbf{x}}} [f_{\mathbf{x}} \mid \mathbf{f}_S, \mathbf{y}_B] + \text{Var}_{\mathbf{f}_S} [\mathbb{E}_{f_{\mathbf{x}}} [f_{\mathbf{x}} \mid \mathbf{f}_S, \mathbf{y}_B] \mid \mathbf{y}_B] \\ &\stackrel{(iii)}{=} \underbrace{\text{Var}_{f_{\mathbf{x}}} [f_{\mathbf{x}} \mid \mathbf{f}_S]}_{\text{irreducible uncertainty}} + \underbrace{\text{Var}_{\mathbf{f}_S} [\mathbb{E}_{f_{\mathbf{x}}} [f_{\mathbf{x}} \mid \mathbf{f}_S] \mid \mathbf{y}_B]}_{\text{reducible (epistemic) uncertainty}} \end{aligned}$$

where (i) follows from the law of total variance; (ii) uses that the conditional variance of a Gaussian depends only on the location of observations and not on their value; and (iii) follows from $f_{\mathbf{x}} \perp \mathbf{y}_B \mid \mathbf{f}_S$ since $B \subseteq S$. It remains to bound the reducible uncertainty.

Let $h : \mathbb{R}^d \rightarrow \mathbb{R}$, $\mathbf{f}_S \mapsto \mathbb{E}[f_{\mathbf{x}} \mid \mathbf{f}_S]$ where we write $d \stackrel{\text{def}}{=} |\mathcal{S}|$. Using the formula for the GP posterior mean, we have

$$h(\mathbf{f}_S) = \mathbb{E}[f_{\mathbf{x}}] + \mathbf{z}^\top (\mathbf{f}_S - \mathbb{E}[\mathbf{f}_S])$$

where $\mathbf{z} \stackrel{\text{def}}{=} \mathbf{K}_{SS}^{-1} \mathbf{K}_{S\mathbf{x}}$. Because h is a linear function in \mathbf{f}_S we have for the reducible uncertainty that

$$\begin{aligned} \text{Var}_{\mathbf{f}_S}[h(\mathbf{f}_S) \mid \mathbf{y}_B] &= \mathbf{z}^\top \text{Var}[\mathbf{f}_S \mid \mathbf{y}_B] \mathbf{z} \\ &\stackrel{(i)}{\leq} d \cdot \mathbf{z}^\top \text{diag}\{\text{Var}[\mathbf{f}_S \mid \mathbf{y}_B]\} \mathbf{z} \\ &\stackrel{(ii)}{\leq} \epsilon' d \mathbf{z}^\top \mathbf{z} \\ &= \epsilon' d \mathbf{K}_{\mathbf{x}S} \mathbf{K}_{SS}^{-1} \mathbf{K}_{SS}^{-1} \mathbf{K}_{S\mathbf{x}} \\ &\leq \frac{\epsilon' d}{\lambda_{\min}(\mathbf{K}_{SS})} \mathbf{K}_{\mathbf{x}S} \mathbf{K}_{SS}^{-1} \mathbf{K}_{S\mathbf{x}} \\ &\stackrel{(iii)}{\leq} \frac{\epsilon' d \sigma^2}{\lambda_{\min}(\mathbf{K}_{SS})} \end{aligned}$$

where (i) follows from Lemma D.19; (ii) follows from the assumption that $\text{Var}[f_{\mathbf{x}'} \mid \mathbf{y}_B] \leq \epsilon'$ for all $\mathbf{x}' \in S$; and (iii) follows from

$$\mathbf{K}_{\mathbf{x}S} \mathbf{K}_{SS}^{-1} \mathbf{K}_{S\mathbf{x}} \leq \mathbf{K}_{\mathbf{x}\mathbf{x}} = \sigma^2$$

since $\mathbf{K}_{\mathbf{x}\mathbf{x}} - \mathbf{K}_{\mathbf{x}S} \mathbf{K}_{SS}^{-1} \mathbf{K}_{S\mathbf{x}} \geq 0$. \square

Proof of Lemma D.4. Let $B \subseteq \mathcal{S}$ be the set of size k generated by Lemma D.7 to satisfy $\text{Var}[f_{\mathbf{x}'} \mid \mathbf{y}_B] \leq 2\tilde{\sigma}^2 \gamma_k/k$ for all $\mathbf{x}' \in \mathcal{S}$. We have for any $\mathbf{x} \in \mathcal{X}$,

$$\begin{aligned} \text{Var}[f_{\mathbf{x}} \mid \mathcal{D}_n, \mathbf{y}_B] &\stackrel{(i)}{\leq} \text{Var}[f_{\mathbf{x}} \mid \mathbf{y}_B] \\ &\stackrel{(ii)}{\leq} \text{Var}[f_{\mathbf{x}} \mid \mathbf{f}_S] + \epsilon \end{aligned}$$

where (i) follows from monotonicity of variance; and (ii) follows from Lemma D.8; using $|\mathcal{S}| < \infty$ and the condition on k . \square

We remark that Lemma D.7 provides an algorithm (just “undirected” **ITL**!) to compute an approximate Markov boundary, and the set B returned by this algorithm is a valid approximate Markov boundary for all $\mathbf{x} \in \mathcal{X}$. One can simply swap-in **ITL** with target space $\{\mathbf{x}\}$ for “undirected” **ITL** to obtain tighter (but instance-dependent) bounds on the size of the approximate Markov boundary.

D.4. Proof of Theorem 3.3

We first formalize the assumptions of Theorem 3.3:

Assumption D.9 (Regularity of f^*). We assume that f^* is in a reproducing kernel Hilbert space $\mathcal{H}_k(\mathcal{X})$ associated with a kernel k and has bounded norm, that is, $\|f\|_k \leq B$ for some finite $B \in \mathbb{R}$.

Assumption D.10 (Sub-Gaussian noise). We further assume that each ϵ_n from the noise sequence $\{\epsilon_n\}_{n=1}^\infty$ is conditionally zero-mean $\rho(\mathbf{x}_n)$ -sub-Gaussian with known constants $\rho(\mathbf{x}) > 0$ for all $\mathbf{x} \in \mathcal{X}$. Concretely,

$$\forall n \geq 1, \lambda \in \mathbb{R} : \mathbb{E}[e^{\lambda \epsilon_n} \mid \mathcal{F}_{n-1}] \leq \exp\left(\frac{\lambda^2 \rho^2(\mathbf{x}_n)}{2}\right)$$

where \mathcal{F}_{n-1} denotes the σ -algebra generated by the random variables $\{\mathbf{x}_i, \epsilon_i\}_{i=1}^{n-1}$ and \mathbf{x}_n .

We make use of the following foundational result, showing that under the above two assumptions the (misspecified) Gaussian process model from Section 3.1 is an all-time well-calibrated model of f^* :

Lemma D.11 (Well-calibrated confidence intervals; [Abbasí-Yadkori \(2013\)](#); [Chowdhury & Gopalan \(2017\)](#)). *Pick $\delta \in (0, 1)$ and let Assumptions D.9 and D.10 hold. Let*

$$\beta_n(\delta) = \beta_n(\delta) = \|f^*\|_k + \rho \sqrt{2(\gamma_n + 1 + \log(1/\delta))}$$

where $\rho = \max_{\mathbf{x} \in \mathcal{X}} \rho(\mathbf{x})$.¹⁸ Then, for all $\mathbf{x} \in \mathcal{X}$ and $n \geq 0$ jointly with probability at least $1 - \delta$,

$$|f^*(\mathbf{x}) - \mu_n(\mathbf{x})| \leq \beta_n(\delta) \cdot \sigma_n(\mathbf{x})$$

where $\mu_n(\mathbf{x})$ and $\sigma_n^2(\mathbf{x})$ are mean and variance (as defined in Appendix A.2) of the GP posterior of $f(\mathbf{x})$ conditional on the observations \mathcal{D}_n , pretending that ϵ_i is Gaussian with variance $\rho^2(\mathbf{x}_i)$.

The proof of Theorem 3.3 is a straightforward application of Lemma D.11 and Theorem 3.2:

Proof of Theorem 3.3. By Theorem 3.2, we have that for all $\mathbf{x} \in \mathcal{A}$,

$$\sigma_n(\mathbf{x}) \leq \sqrt{\eta^2(\mathbf{x}; \mathcal{S}) + \nu_{n, \epsilon^2}^2 + \epsilon^2} \leq \eta(\mathbf{x}; \mathcal{S}) + \nu_{n, \epsilon^2} + \epsilon.$$

The result then follows by application of Lemma D.11. \square

D.5. Proof of Theorem 5.1

In this section, we derive our main result on Safe BO. In Appendix D.5.1, we give the definition of the reachable safe set \mathcal{R} and derive the conditions under which convergence to the reachable safe set is guaranteed. Then, in Appendix D.5.2, we prove Theorem 5.1.

Notation In the agnostic setting from Section 3.2 (i.e., under Assumptions D.9 and D.10), Lemma D.11 provides us with the following $(1 - \delta)$ -confidence intervals (CIs)

$$\mathcal{C}_n(\mathbf{x}) \stackrel{\text{def}}{=} \mathcal{C}_{n-1}(\mathbf{x}) \cap [\mu_n(\mathbf{x}) \pm \beta_n(\delta) \cdot \sigma_n(\mathbf{x})] \quad (26)$$

where $\mathcal{C}_{-1}(\mathbf{x}) = \mathbb{R}$. We write $u_n(\mathbf{x}) \stackrel{\text{def}}{=} \max \mathcal{C}_n(\mathbf{x})$, $l_n(\mathbf{x}) \stackrel{\text{def}}{=} \min \mathcal{C}_n(\mathbf{x})$, and $w_n(\mathbf{x}) \stackrel{\text{def}}{=} u_n(\mathbf{x}) - l_n(\mathbf{x})$ for its upper bound, lower bound, and width, respectively.

We learn separate statistical models f and $\{g_1, \dots, g_q\}$ for the ground truth objective f^* and ground truth constraints $\{g_1^*, \dots, g_q^*\}$. We write $\mathcal{I} \stackrel{\text{def}}{=} \{f, 1, \dots, q\}$ and collect the constraints in $\mathcal{I}_s \stackrel{\text{def}}{=} \{1, \dots, q\}$. Without loss of generality,

¹⁸ $\beta_n(\delta)$ can be tightened adaptively ([Emmenegger et al., 2023](#)).

we assume that the confidence intervals include the ground truths with probability at least $1 - \delta$ jointly for all $i \in \mathcal{I}$.¹⁹ For $i \in \mathcal{I}$, denote by $u_{n,i}, l_{n,i}, w_{n,i}, \eta_i, \beta_{n,i}$ the respective quantities. In the following, we do not explicitly denote the dependence of β_n on δ .

To improve clarity, we will refer to the set of potential maximizers defined in Equation (8) as \mathcal{M}_n and denote by \mathcal{A}_n an arbitrary target space.

We point out the following corollary:

Corollary D.12 (Safety). *With high probability, jointly for any $n \geq 0$ and any $i \in \mathcal{I}_s$,*

$$\forall \mathbf{x} \in \mathcal{S}_n : g_i^*(\mathbf{x}) \geq 0. \quad (27)$$

D.5.1. CONVERGENCE TO REACHABLE SAFE SET

Definition D.13 (Reachable safe set). Given any pessimistic safe set $\mathcal{S} \subseteq \mathcal{X}$ and any $\epsilon \geq 0$ and $\beta \geq 0$, we define the *reachable safe set* up to (ϵ, β) -slack and its closure as

$$\begin{aligned} \mathcal{R}_{\epsilon, \beta}(\mathcal{S}) &\stackrel{\text{def}}{=} \mathcal{S} \cup \{\mathbf{x} \in \mathcal{X} \setminus \mathcal{S} \mid \\ &\quad g_i^*(\mathbf{x}) - \beta(\eta_i(\mathbf{x}; \mathcal{S}) + \epsilon) \geq 0 \text{ for all } i \in \mathcal{I}_s\} \\ \bar{\mathcal{R}}_{\epsilon, \beta}(\mathcal{S}) &\stackrel{\text{def}}{=} \lim_{n \rightarrow \infty} (\mathcal{R}_{\epsilon, \beta})^n(\mathcal{S}) \end{aligned}$$

where $(\mathcal{R}_{\epsilon, \beta})^n$ denotes the n -th composition of $\mathcal{R}_{\epsilon, \beta}$ with itself.

We denote by \mathcal{S}_0 the initial pessimistic safe set induced by the (prior) statistical model g (cf. Section 5) and write $\bar{\mathcal{R}}_{\epsilon, \beta} \stackrel{\text{def}}{=} \bar{\mathcal{R}}_{\epsilon, \beta}(\mathcal{S}_0)$.

Lemma D.14 (Properties of the reachable safe set). *For all $\mathcal{S}, \mathcal{S}' \subseteq \mathcal{X}$, $\epsilon \geq 0$, and $\beta \geq 0$:*

- (i) $\mathcal{S}' \subseteq \mathcal{S} \implies \mathcal{R}_{\epsilon, \beta}(\mathcal{S}') \subseteq \mathcal{R}_{\epsilon, \beta}(\mathcal{S})$,
- (ii) $\mathcal{R}_{\epsilon, \beta}(\mathcal{S}) \subseteq \mathcal{S} \implies \bar{\mathcal{R}}_{\epsilon, \beta}(\mathcal{S}) \subseteq \mathcal{S}$, and
- (iii) $\mathcal{R}_{0,0}(\emptyset) = \bar{\mathcal{R}}_{0,0} = \mathcal{S}^*$.

Proof (adapted from lemma 7.1 of Berkenkamp et al. (2021)).

1. Let $\mathbf{x} \in \mathcal{R}_{\epsilon, \beta}(\mathcal{S}')$. If $\mathbf{x} \in \mathcal{S}$ then $\mathbf{x} \in \mathcal{R}_{\epsilon, \beta}(\mathcal{S})$, so let $\mathbf{x} \notin \mathcal{S}$. Then, by definition, for all $i \in \mathcal{I}_s$, $f_i^*(\mathbf{x}) - \beta\eta_i(\mathbf{x}; \mathcal{S}') - \epsilon \geq 0$. By the monotonicity of variance, $\eta_i(\mathbf{x}; \mathcal{S}') \geq \eta_i(\mathbf{x}; \mathcal{S})$ for all $i \in \mathcal{I}_s$, and hence $f_i^*(\mathbf{x}) - \beta\eta_i(\mathbf{x}; \mathcal{S}) - \epsilon \geq 0$ for all $i \in \mathcal{I}_s$. It follows that $\mathbf{x} \in \mathcal{R}_{\epsilon, \beta}(\mathcal{S})$.
2. By the monotonicity of variance, $\eta_i(\mathbf{x}; \mathcal{R}_{\epsilon, \beta}(\mathcal{S})) \geq \eta_i(\mathbf{x}; \mathcal{S})$ for all $\mathbf{x} \in \mathcal{X}$ and $i \in \mathcal{I}$. Thus, by definition of the safe region, we have that $\mathcal{R}_{\epsilon, \beta}(\mathcal{R}_{\epsilon, \beta}(\mathcal{S})) \subseteq \mathcal{S}$. The result follows by taking the limit.

¹⁹This can be achieved by taking a union bound and rescaling δ .

3. The result follows directly from the definition of the true safe set \mathcal{S}^* (cf. Equation (7)). \square

Clearly, we cannot expand the safe set beyond $\bar{\mathcal{R}}_{0,0}$. The following is our main intermediate result, showing that either we expand the safe set at some point or the uncertainty converges to the irreducible uncertainty.

Lemma D.15. *Given any $n_0 \geq 0$, $\epsilon > 0$, let n' be the smallest integer such that $\nu_{n', \tilde{\epsilon}^2} \leq \tilde{\epsilon}$ where $\tilde{\epsilon} = \epsilon/2$. Let $\beta_{n_0+n'} = \max_{i \in \mathcal{I}_s} \beta_{n_0+n', i}$. Assume that the sequence of target spaces is monotonically decreasing, i.e., $\mathcal{A}_{n+1} \subseteq \mathcal{A}_n$. Then, we have with high probability (at least) one of*

$$\begin{aligned} &\left(\forall \mathbf{x} \in \mathcal{A}_{n_0+n'}, \forall i \in \mathcal{I} : \right. \\ &\quad w_{n_0+n', i}(\mathbf{x}) \leq \beta_{n_0+n'}[\eta_i(\mathbf{x}; \mathcal{S}_{n_0+n'}) + \epsilon] \\ &\quad \text{and} \quad \mathcal{A}_{n_0+n'} \cap \mathcal{R}_{\epsilon, \beta_{n_0+n'}}(\mathcal{S}_{n_0+n'}) \subseteq \mathcal{S}_{n_0+n'} \Big) \\ &\text{or} \quad |\mathcal{S}_{n_0+n'+1}| > |\mathcal{S}_{n_0}|. \end{aligned}$$

Proof. Suppose that $|\mathcal{S}_{n_0+n'+1}| = |\mathcal{S}_{n_0}|$. Then, by Theorem 3.3 (using that the sequence of target spaces is monotonically decreasing), for any $\mathbf{x} \in \mathcal{A}_{n_0+n'}$ and $i \in \mathcal{I}$,

$$w_{n_0+n', i}(\mathbf{x}) \leq \beta_{n_0+n'}[\eta_i(\mathbf{x}; \mathcal{S}_{n_0+n'}) + \epsilon].$$

As $\mathcal{S}_{n_0+n'+1} = \mathcal{S}_{n_0+n'}$ we have for all $\mathbf{x} \in \mathcal{A}_{n_0+n'} \setminus \mathcal{S}_{n_0+n'}$ and $i \in \mathcal{I}_s$, with high probability that

$$\begin{aligned} 0 > l_{n_0+n', i}(\mathbf{x}) &\geq g_i^*(\mathbf{x}) - w_{n_0+n', i}(\mathbf{x}) \\ &\geq g_i^*(\mathbf{x}) - \beta_{n_0+n'}[\eta_i(\mathbf{x}; \mathcal{S}_{n_0+n'}) + \epsilon]. \end{aligned}$$

It follows that $\mathcal{A}_{n_0+n'} \cap \mathcal{R}_{\epsilon, \beta_{n_0+n'}}(\mathcal{S}_{n_0+n'}) \subseteq \mathcal{S}_{n_0+n'}$. \square

To gather more intuition about the above lemma, consider the target space

$$\mathcal{E}_n \stackrel{\text{def}}{=} \hat{\mathcal{S}}_n \setminus \mathcal{S}_n. \quad (28)$$

We call \mathcal{E}_n the *potential expanders* since it contains all points which might be safe, but are not yet known to be safe. Under this target space, the above lemma simplifies slightly:

Lemma D.16. *For any $n \geq 0$ and $\epsilon, \beta \geq 0$, if $\mathcal{E}_n \subseteq \mathcal{A}_n$ then with high probability,*

$$\mathcal{S}_n \cup (\mathcal{A}_n \cap \mathcal{R}_{\epsilon, \beta}(\mathcal{S}_n)) = \mathcal{R}_{\epsilon, \beta}(\mathcal{S}_n).$$

Proof. With high probability, $\mathcal{R}_{\epsilon, \beta}(\mathcal{S}_n) \subseteq \hat{\mathcal{S}}_n = \mathcal{S}_n \cup \mathcal{E}_n$. The lemma is a direct consequence. \square

The above lemmas can be combined to yield our main result of this subsection, establishing the convergence of **ITL** to the reachable safe set.

Theorem D.17 (Convergence to reachable safe set). *For any $\epsilon > 0$, let n' be the smallest integer satisfying the condition of Lemma D.15, and define $n^* \stackrel{\text{def}}{=} (|\mathcal{S}^*| + 1)n'$. Let $\bar{\beta}_{n^*} \geq \beta_{n,i}$ for all $n \leq n^*, i \in \mathcal{I}_s$. Assume that the sequence of target spaces is monotonically decreasing, i.e., $\mathcal{A}_{n+1} \subseteq \mathcal{A}_n$. Then, the following inequalities hold jointly with probability at least $1 - \delta$:*

$$(i) \forall n \geq 0, \forall i \in \mathcal{I}_s : g_i^*(\mathbf{x}_n) \geq 0,$$

safety

$$(ii) \mathcal{A}_{n^*} \cap \bar{\mathcal{R}}_{\epsilon, \bar{\beta}_{n^*}} \subseteq \mathcal{S}_{n^*} \subseteq \bar{\mathcal{R}}_{0,0} = \mathcal{S}^*,$$

convergence to safe region

$$(iii) \forall \mathbf{x} \in \mathcal{A}_{n^*}, \forall i \in \mathcal{I} : w_{n^*,i}(\mathbf{x}) \leq \bar{\beta}_{n^*} \eta_i(\mathbf{x}; \bar{\mathcal{R}}_{\epsilon, \bar{\beta}_{n^*}}) + \epsilon$$

convergence of width

$$(iv) \forall \mathbf{x} \in \bar{\mathcal{R}}_{\epsilon, \bar{\beta}_{n^*}}, \forall i \in \mathcal{I} : \eta_i(\mathbf{x}; \bar{\mathcal{R}}_{\epsilon, \bar{\beta}_{n^*}}) = 0.$$

convergence of width within safe region

Proof. (i) is a direct consequence of Corollary D.12. $\mathcal{S}_{n^*} \subseteq \mathcal{S}^*$ follows directly from the pessimistic safe set \mathcal{S}_{n^*} from (ii) being a subset of the true safe set \mathcal{S}^* . (iv) follows directly from the definition of irreducible uncertainty. Thus, it remains to establish $\mathcal{A}_{n^*} \cap \bar{\mathcal{R}}_{\epsilon, \bar{\beta}_{n^*}} \subseteq \mathcal{S}_{n^*}$ and (iii).

Recall that with high probability $|\mathcal{S}_n| \in [0, |\mathcal{S}^*|]$ for all $n \geq 0$. Thus, the size of the pessimistic safe set can increase at most $|\mathcal{S}^*|$ many times. By Lemma D.15, using the assumption on n' , the size of the pessimistic safe set increases at least once every n' iterations, or else:

$$\forall \mathbf{x} \in \mathcal{A}_{n_0+n'}, \forall i \in \mathcal{I} :$$

$$w_{n_0+n',i}(\mathbf{x}) \leq \beta_{n_0+n'}[\eta_i(\mathbf{x}; \mathcal{S}_{n_0+n'}) + \epsilon] \quad (29)$$

$$\text{and } \mathcal{A}_{n_0+n'} \cap \mathcal{R}_{\epsilon, \beta_{n_0+n'}}(\mathcal{S}_{n_0+n'}) \subseteq \mathcal{S}_{n_0+n'}.$$

Because the safe set can expand at most $|\mathcal{S}^*|$ many times, Equation (29) occurs eventually for some $n_0 \leq |\mathcal{S}^*|n'$. In this case, since $\bar{\beta}_{n^*} \geq \beta_{n_0+n'}$ and $\mathcal{A}_{n^*} \subseteq \mathcal{A}_{n_0+n'}$ (as $n_0 + n' \leq n^*$) we have that

$$\begin{aligned} \mathcal{A}_{n^*} \cap \mathcal{R}_{\epsilon, \bar{\beta}_{n^*}}(\mathcal{S}_{n_0+n'}) &\subseteq \mathcal{A}_{n_0+n'} \cap \mathcal{R}_{\epsilon, \beta_{n_0+n'}}(\mathcal{S}_{n_0+n'}) \\ &\subseteq \mathcal{S}_{n_0+n'}. \end{aligned}$$

By Lemma D.14(ii), this implies

$$\mathcal{A}_{n^*} \cap \bar{\mathcal{R}}_{\epsilon, \bar{\beta}_{n^*}} \subseteq \mathcal{S}_{n_0+n'} \subseteq \mathcal{S}_{n^*}.$$

□

We emphasize that Theorem D.17 holds for arbitrary target spaces \mathcal{A}_n . If additionally, $\mathcal{E}_n \subseteq \mathcal{A}_n$ for all $n \geq 0$ then by Lemma D.16, Theorem D.17(ii) strengthens to

$\bar{\mathcal{R}}_{\epsilon, \bar{\beta}_{n^*}} \subseteq \mathcal{S}_{n^*}$. Intuitively, $\mathcal{E}_n \subseteq \mathcal{A}_n$ ensures that one aims to expand the safe set in *all* directions. Conversely, if $\mathcal{E}_n \not\subseteq \mathcal{A}_n$ then one aims only to expand the safe set in the direction of \mathcal{A}_n (or not at all if $\mathcal{A}_n \subseteq \mathcal{S}_n$).

“Free” convergence guarantees in many applications

Theorem D.17 can be specialized to yield convergence guarantees in various settings by choosing an appropriate target space \mathcal{A}_n . Straightforward application of Theorem D.17 (informally) requires that the sequence of target spaces is monotonically decreasing (i.e., $\mathcal{A}_{n+1} \subseteq \mathcal{A}_n$), and that each target space \mathcal{A}_n is an “over-approximation” of the actual set of targeted points (such as the set of optimas in the Bayesian optimization setting). We discuss two such applications in the following.

1. *Pure expansion*: For example, for the target space \mathcal{E}_n , Theorem D.17 bounds the convergence of the safe set to the reachable safe set. In this case, the transductive active learning problem corresponds to the “pure expansion” setting, also addressed by the ISE baseline discussed in Section 5. The ISE baseline, however, does not establish convergence guarantees of the kind of Theorem D.17. Note that \mathcal{E}_n satisfies the (informal) requirements laid out previously, since it is monotonically decreasing by definition, and with high probability, any point $\mathbf{x} \in \mathcal{S}^*$ that is not in \mathcal{S}_n is contained within \mathcal{E}_n .

2. *Level set estimation*: Given any $\tau \in \mathbb{R}$, we denote the (safe) τ -level set of f^* by $\mathcal{L}^\tau \stackrel{\text{def}}{=} \{\mathbf{x} \in \mathcal{S}^* \mid f^*(\mathbf{x}) = \tau\}$. We define the *potential level set* as

$$\mathcal{L}_n^\tau \stackrel{\text{def}}{=} \{\mathbf{x} \in \hat{\mathcal{S}}_n \mid l_n^f(\mathbf{x}) \leq \tau \leq u_n^f(\mathbf{x})\}. \quad (30)$$

That is, \mathcal{L}_n^τ is the subset of the optimistic safe set $\hat{\mathcal{S}}_n$ where the τ -level set of f^* may be located. Analogously to the potential expanders, it is straightforward to show that \mathcal{L}_n^τ over-approximates the true τ -level set and is monotonically decreasing.

We remark that our guarantees from this section also apply to the standard (“unsafe”) setting where $\mathcal{S}^* = \mathcal{S}_0 = \mathcal{X}$.

D.5.2. CONVERGENCE TO OPTIMUM

In this section, we specialize Theorem D.17 for the case that the target space contains the potential maximizers \mathcal{M}_n (cf. Equation (8)). It is straightforward to see that the sequence \mathcal{M}_n is monotonically decreasing (i.e., $\mathcal{M}_{n+1} \subseteq \mathcal{M}_n$). The following lemma shows that the potential maximizers over-approximate the set of safe maxima $\mathcal{X}^* \stackrel{\text{def}}{=} \arg \max_{\mathbf{x} \in \mathcal{S}^*} f^*(\mathbf{x})$.

Lemma D.18 (Potential maximizers over-approximate safe maxima). *For all $n \geq 0$ and with probability at least $1 - \delta$,*

(i) $\mathbf{x} \in \mathcal{X}^*$ implies $\mathbf{x} \in \mathcal{M}_n$ and

(ii) $\mathbf{x} \notin \mathcal{M}_n$ implies $\mathbf{x} \notin \mathcal{X}^*$.

Proof. If $\mathbf{x} \notin \mathcal{M}_n$ then

$$u_{n,f}(\mathbf{x}) < \max_{\mathbf{x}' \in \mathcal{S}_n} l_{n,f}(\mathbf{x}') \leq \max_{\mathbf{x}' \in \mathcal{S}^*} l_{n,f}(\mathbf{x}')$$

where we used $\mathcal{S}_n \subseteq \mathcal{S}^*$ with high probability, which directly implies with high probability that $\mathbf{x} \notin \mathcal{X}^*$.

For the other direction, if $\mathbf{x} \in \mathcal{X}^*$ then

$$u_{n,f}(\mathbf{x}) \geq \max_{\mathbf{x}' \in \mathcal{S}^*} l_{n,f}(\mathbf{x}') \geq \max_{\mathbf{x}' \in \mathcal{S}_n} l_{n,f}(\mathbf{x}')$$

with high probability. \square

We denote the set of optimal actions which are safe up to (ϵ, β) -slack by

$$\mathcal{X}_{\epsilon,\beta}^* \stackrel{\text{def}}{=} \arg \max_{\mathbf{x} \in \bar{\mathcal{R}}_{\epsilon,\beta}} f^*(\mathbf{x}),$$

and by $f_{\epsilon,\beta}^*$ the maximum value attained by f^* at any of the points in $\mathcal{X}_{\epsilon,\beta}^*$. The regret can be expressed as

$$r_n(\bar{\mathcal{R}}_{\epsilon,\beta}) = f_{\epsilon,\beta}^* - f^*(\hat{\mathbf{x}}_n)$$

Proof of Theorem 5.1. Let $\bar{\beta}_{n^*} \geq \beta_{n,i}$ for all $n \leq n^*, i \in \mathcal{I}_s$. We prove convergence within the reachable safe set $\bar{\mathcal{R}}_{\epsilon,\bar{\beta}_{n^*}}$ (cf. Definition D.13).

Fix any $\mathbf{x}^* \in \mathcal{X}_{\epsilon,\bar{\beta}_{n^*}}^* \subseteq \bar{\mathcal{R}}_{\epsilon,\bar{\beta}_{n^*}}$. Assume w.l.o.g. that $\mathbf{x}^* \in \mathcal{M}_{n^*}$.²⁰ Then, with high probability,

$$\begin{aligned} f_{\epsilon,\bar{\beta}_{n^*}}^* &= f^*(\mathbf{x}^*) \leq u_{n^*,f}(\mathbf{x}^*) \\ &= l_{n^*,f}(\mathbf{x}^*) + w_{n^*,f}(\mathbf{x}^*) \\ &\stackrel{(i)}{\leq} l_{n^*,f}(\hat{\mathbf{x}}_{n^*}) + w_{n^*,f}(\mathbf{x}^*) \\ &\leq f^*(\hat{\mathbf{x}}_{n^*}) + w_{n^*,f}(\mathbf{x}^*) \\ &\stackrel{(ii)}{\leq} f^*(\hat{\mathbf{x}}_{n^*}) + \epsilon \end{aligned}$$

where (i) follows from the definition of $\hat{\mathbf{x}}_n$; and (ii) follows from Theorem D.17 and noting that $\mathbf{x}^* \in \mathcal{M}_{n^*} \cap \bar{\mathcal{R}}_{\epsilon,\bar{\beta}_{n^*}}$.

We have shown that $f^*(\hat{\mathbf{x}}_{n^*}) \geq f_{\epsilon,\bar{\beta}_{n^*}}^* - \epsilon$, which implies $r_{n^*}(\bar{\mathcal{R}}_{\epsilon,\bar{\beta}_{n^*}}) \leq \epsilon$. Since the upper- and lower-confidence bounds are monotonically decreasing / increasing, respectively, we have that for all $n \geq n^*$, $r_n(\bar{\mathcal{R}}_{\epsilon,\bar{\beta}_{n^*}}) \leq \epsilon$. \square

²⁰Otherwise, with high probability, $f^*(\hat{\mathbf{x}}_{n^*}) > f_{\epsilon,\bar{\beta}_{n^*}}^*$.

D.6. Useful Facts and Inequalities

We denote by \preceq the Loewner partial ordering of symmetric matrices.

Lemma D.19. Let $\mathbf{A} \in \mathbb{R}^{n \times n}$ be a positive definite matrix with diagonal \mathbf{D} . Then, $\mathbf{A} \preceq n\mathbf{D}$.

Proof. Equivalently, one can show $n\mathbf{D} - \mathbf{A} \succeq \mathbf{0}$. We write $\mathbf{A} \stackrel{\text{def}}{=} \mathbf{D}^{1/2} \mathbf{Q} \mathbf{D}^{1/2}$, and thus, $\mathbf{Q} = \mathbf{D}^{-1/2} \mathbf{A} \mathbf{D}^{-1/2}$ is a positive definite symmetric matrix with all diagonal elements equal to 1. It remains to show that

$$n\mathbf{D} - \mathbf{A} = \mathbf{D}^{1/2} (n\mathbf{I} - \mathbf{Q}) \mathbf{D}^{1/2} \succeq \mathbf{0}.$$

Note that $\sum_{i=1}^n \lambda_i(\mathbf{Q}) = \text{tr } \mathbf{Q} = n$, and hence, all eigenvalues of \mathbf{Q} belong to $(0, n)$. \square

Lemma D.20. If $a, b \in (0, M]$ for some $M > 0$ and $b \geq a$ then

$$b - a \leq M \cdot \log\left(\frac{b}{a}\right). \quad (31)$$

If additionally, $a \geq M'$ for some $M' > 0$ then

$$b - a \geq M' \cdot \log\left(\frac{b}{a}\right). \quad (32)$$

Proof. Let $f(x) \stackrel{\text{def}}{=} \log x$. By the mean value theorem, there exists $c \in (a, b)$ such that

$$\frac{1}{c} = f'(c) = \frac{f(b) - f(a)}{b - a} = \frac{\log b - \log a}{b - a} = \frac{\log(\frac{b}{a})}{b - a}.$$

Thus,

$$b - a = c \cdot \log\left(\frac{b}{a}\right) < M \cdot \log\left(\frac{b}{a}\right).$$

Under the additional condition that $a \geq M'$, we obtain

$$b - a = c \cdot \log\left(\frac{b}{a}\right) > M' \cdot \log\left(\frac{b}{a}\right). \quad \square$$

E. Interpretations & Approximations of Principle (†)

We give a brief overview of interpretations and approximations of **ITL**, as well as alternative decision rules adhering to the fundamental principle (†).

The discussed interpretations of (†) differ mainly in how they quantify the “uncertainty” about \mathcal{A} . In the GP setting, this “uncertainty” is captured by the covariance matrix Σ of $f_{\mathcal{A}}$, and we consider two main ways of “scalarizing” Σ :

1. the total (marginal) variance $\text{tr } \Sigma$, and
2. the “generalized variance” $|\Sigma|$.

The generalized variance — which was originally suggested by Wilks (1932) as a generalization of variance to multiple dimensions — takes into account correlations. In contrast, the total variance discards all correlations between points in \mathcal{A} .

E.1. Interpretations of ITL

We briefly discuss three interpretations of ITL .

Minimizing generalized variance In the GP setting, ITL can be equivalently characterized as minimizing generalized posterior variance:

$$\mathbf{x}_n = \arg \min_{\mathbf{x} \in \mathcal{S}} |\text{Var}[\mathbf{f}_{\mathcal{A}} \mid \mathcal{D}_{n-1}, y_{\mathbf{x}}]|. \quad (33)$$

Maximizing relevance and minimizing redundancy An alternative interpretation of ITL is

$$I(\mathbf{f}_{\mathcal{A}}; y_{\mathbf{x}} \mid \mathcal{D}_n) = \underbrace{I(\mathbf{f}_{\mathcal{A}}; y_{\mathbf{x}})}_{\text{relevance}} - \underbrace{I(\mathbf{f}_{\mathcal{A}}; y_{\mathbf{x}}; \mathcal{D}_n)}_{\text{redundancy}} \quad (34)$$

where $I(\mathbf{f}_{\mathcal{A}}; y_{\mathbf{x}}; \mathcal{D}_n) = I(\mathbf{f}_{\mathcal{A}}; y_{\mathbf{x}}) - I(\mathbf{f}_{\mathcal{A}}; y_{\mathbf{x}} \mid \mathcal{D}_n)$ denotes the *multivariate information gain* (cf. Appendix A). In this way, ITL can be seen as maximizing observation relevance while minimizing observation redundancy. This interpretation is common in the literature on feature selection (Peng et al., 2005; Vergara & Estévez, 2014; Beraha et al., 2019).

Steepest descent in measure spaces ITL can be seen as performing steepest descent in the space of probability measures over $\mathbf{f}_{\mathcal{A}}$, with the KL divergence as metric:

$$I(\mathbf{f}_{\mathcal{A}}; y_{\mathbf{x}} \mid \mathcal{D}_n) = \mathbb{E}_{y_{\mathbf{x}}} [\text{KL}(p(\mathbf{f}_{\mathcal{A}} \mid \mathcal{D}_n, y_{\mathbf{x}}) \parallel p(\mathbf{f}_{\mathcal{A}} \mid \mathcal{D}_n))].$$

That is, ITL finds the observation yielding the “largest update” to the current density.

E.2. Variance-based Transductive Learning

Quantifying the uncertainty about $\mathbf{f}_{\mathcal{A}}$ by the marginal variance of points in \mathcal{A} rather than entropy (or generalized variance), principle (†) leads to the decision rule

$$\mathbf{x}_n = \arg \min_{\mathbf{x} \in \mathcal{S}} \text{tr } \text{Var}[\mathbf{f}_{\mathcal{A}} \mid \mathcal{D}_{n-1}, y_{\mathbf{x}}] \quad (35)$$

where we suppose for ease of notation that we are in the GP setting (i.e., Assumptions A.1 and A.2 hold) to ensure that the posterior variance is independent of the value of $y_{\mathbf{x}}$ and only depends on the location \mathbf{x} .²¹ We call this decision rule

²¹Otherwise, one can take the expectation over values $y_{\mathbf{x}}$.

VTL, short for *variance-based transductive learning*. Note that if $|\mathcal{A}| = 1$, then **VTL** is equivalent to **ITL**.

Unlike the similar, but more technical, TRUVAR algorithm proposed by Bogunovic et al. (2016), **VTL** does not require truncated variances, and hence, **VTL** can be applied to constrained settings (where $\mathcal{A} \not\subseteq \mathcal{S}$) as well.

Convergence of uncertainty We derive a convergence guarantee of **VTL** which is analogous to the guarantee for **ITL** from Theorem 3.1. In the following, we denote the marginal reduction in variance during round n by

$$\tilde{\Gamma}_n \stackrel{\text{def}}{=} \text{tr } \text{Var}[\mathbf{f}_{\mathcal{A}} \mid \mathcal{D}_n] - \min_{\mathbf{x} \in \mathcal{S}} \text{tr } \text{Var}[\mathbf{f}_{\mathcal{A}} \mid \mathcal{D}_n, y_{\mathbf{x}}]. \quad (36)$$

Theorem E.1 (Convergence of uncertainty reduction in terms of $\tilde{\Gamma}_n$) *Assume that Assumptions A.1 and A.2 are satisfied. Then for any $n \geq 1$, if $\tilde{\Gamma}_0 \geq \dots \geq \tilde{\Gamma}_{n-1}$ and the sequence $\{\mathbf{x}_i\}_{i=1}^n$ is generated by **VTL**, then*

$$\tilde{\Gamma}_{n-1} \leq \frac{2\sigma^2}{n} \sum_{\mathbf{x}' \in \mathcal{A}} \gamma_n(\{\mathbf{x}'\}; \mathcal{S}). \quad (37)$$

The monotonicity assumption on the sequence $\{\tilde{\Gamma}_n\}_n$ corresponds to a submodularity assumption on the total variance which has been used previously, e.g., in Bogunovic et al. (2016), and which is analogous to the case where the task complexity (cf. Definition 2.3) is upper-bounded by 1. The above result can be generalized analogously to Theorem 3.1 by considering an instance-dependent complexity measure akin to the task complexity.

Proof of Theorem E.1. We have

$$\begin{aligned} \tilde{\Gamma}_{n-1} &= \frac{1}{n} \sum_{i=0}^{n-1} \tilde{\Gamma}_{n-1} \\ &\stackrel{(i)}{\leq} \frac{1}{n} \sum_{i=0}^{n-1} \tilde{\Gamma}_i \\ &= \frac{1}{n} \sum_{i=0}^{n-1} \left[\text{tr } \text{Var}[\mathbf{f}_{\mathcal{A}} \mid \mathcal{D}_i] \right. \\ &\quad \left. - \min_{\mathbf{x} \in \mathcal{S}} \text{tr } \text{Var}[\mathbf{f}_{\mathcal{A}} \mid \mathcal{D}_i, y_{\mathbf{x}}] \right] \\ &\stackrel{(ii)}{=} \frac{1}{n} \sum_{i=0}^{n-1} \left[\text{tr } \text{Var}[\mathbf{f}_{\mathcal{A}} \mid \mathcal{D}_i] - \text{tr } \text{Var}[\mathbf{f}_{\mathcal{A}} \mid \mathcal{D}_{i+1}] \right] \\ &\stackrel{(iii)}{\leq} \frac{\sigma^2}{n} \sum_{\mathbf{x}' \in \mathcal{A}} \sum_{i=0}^{n-1} \log \left(\frac{\text{Var}[\mathbf{f}_{\mathbf{x}'} \mid \mathcal{D}_n]}{\text{Var}[\mathbf{f}_{\mathbf{x}'} \mid \mathcal{D}_{n+1}]} \right) \\ &= \frac{2\sigma^2}{n} \sum_{\mathbf{x}' \in \mathcal{A}} \sum_{i=0}^{n-1} I(\mathbf{f}_{\mathbf{x}'}; y_{\mathbf{x}_{n+1}} \mid \mathcal{D}_n) \\ &\stackrel{(iv)}{=} \frac{2\sigma^2}{n} \sum_{\mathbf{x}' \in \mathcal{A}} I(\mathbf{f}_{\mathbf{x}'}; \mathcal{D}_n) \end{aligned}$$

$$\begin{aligned} &\leq \frac{2\sigma^2}{n} \sum_{\mathbf{x}' \in \mathcal{A}} \max_{\substack{X \subseteq \mathcal{S} \\ |\mathcal{X}|=n}} I(f_{\mathbf{x}'}; \mathbf{y}_X) \\ &= \frac{2\sigma^2}{n} \sum_{\mathbf{x}' \in \mathcal{A}} \gamma_n(\{\mathbf{x}'\}; \mathcal{S}) \end{aligned}$$

where (i) follows by assumption; (ii) follows from the **VTL** decision rule; (iii) follows from Lemma D.20 and monotonicity of variance; and (iv) uses the chain rule of mutual information. The remainder of the proof is analogous to the proof of Theorem 3.1 (cf. Appendix D.1). \square

Theorem E.1 can be seen as an analogous statement to Theorem 3.1 for **VTL**, where $\tilde{\Gamma}_n$ quantifies the reduction in ‘‘uncertainty’’ in terms of the total marginal variance (whereas Γ_n quantifies this reduction in terms of entropy). The following result shows that the marginal variances can be bounded uniformly in terms of $\tilde{\Gamma}_n$, which is analogous to Theorem 3.2 (which bounded them in terms of Γ_n).

To this end, we define

$$\tilde{\alpha}'_{n,\epsilon} \stackrel{\text{def}}{=} \frac{\text{Var}[f_{\mathbf{x}} \mid \mathcal{D}_n] - \text{Var}[f_{\mathbf{x}} \mid \mathbf{y}_{B_{n,\epsilon}(\mathbf{x})}, \mathcal{D}_n]}{\sum_{\tilde{\mathbf{x}} \in B_{n,\epsilon}(\mathbf{x})} (\text{Var}[f_{\mathbf{x}} \mid \mathcal{D}_n] - \text{Var}[f_{\mathbf{x}} \mid \mathbf{y}_{\tilde{\mathbf{x}}}, \mathcal{D}_n])}$$

which analogously to $\tilde{\alpha}_{n,\epsilon}$ from Theorem 3.2 can be interpreted as a measure of the synergies between points in $B_{n,\epsilon}(\mathbf{x})$.

Theorem E.2 (Uniform convergence of marginal variance in terms of $\tilde{\Gamma}_n$). *Under the assumptions of Theorem E.1 and if $|\mathcal{S}| < \infty$, then for any $n \geq 0, \epsilon > 0$, and $\mathbf{x} \in \mathcal{A}$, there exists a constant \tilde{C}_ϵ independent of n such that*

$$\sigma_n^2(\mathbf{x}) \leq \underbrace{\eta^2(\mathbf{x}; \mathcal{S})}_{\text{irreducible}} + \underbrace{\tilde{\nu}_{n,\epsilon}^2}_{\text{reducible}} + \epsilon \quad (38)$$

where $\tilde{\nu}_{n,\epsilon}^2 \stackrel{\text{def}}{=} \tilde{C}_\epsilon \tilde{\Gamma}_n \tilde{\alpha}'_{n,\epsilon}$ denotes the reducible uncertainty.

Proof. Analogously to Lemma D.5, we have

$$\begin{aligned} \sigma_n^2(\mathbf{x}) &= \text{Var}[f_{\mathbf{x}} \mid \mathcal{D}_n] - \eta^2(\mathbf{x}; \mathcal{S}) + \eta^2(\mathbf{x}; \mathcal{S}) \\ &\stackrel{(i)}{\leq} \text{Var}[f_{\mathbf{x}} \mid \mathcal{D}_n] - \text{Var}[f_{\mathbf{x}} \mid \mathbf{y}_{B_{n,\epsilon}(\mathbf{x})}, \mathcal{D}_n] \\ &\quad + \eta^2(\mathbf{x}; \mathcal{S}) + \epsilon \end{aligned}$$

where (i) follows from the defining property of an ϵ -approximate Markov boundary (cf. Equation (18)). Further, we have

$$\begin{aligned} &\text{Var}[f_{\mathbf{x}} \mid \mathcal{D}_n] - \text{Var}[f_{\mathbf{x}} \mid \mathbf{y}_{B_{n,\epsilon}(\mathbf{x})}, \mathcal{D}_n] \\ &\stackrel{(i)}{=} \tilde{\alpha}'_{n,\epsilon} \sum_{\tilde{\mathbf{x}} \in B_{n,\epsilon}(\mathbf{x})} (\text{Var}[f_{\mathbf{x}} \mid \mathcal{D}_n] - \text{Var}[f_{\mathbf{x}} \mid \mathbf{y}_{\tilde{\mathbf{x}}}, \mathcal{D}_n]) \\ &\stackrel{(ii)}{\leq} \tilde{\alpha}'_{n,\epsilon} b_\epsilon \tilde{\Gamma}_n \end{aligned}$$

where (i) follows from the definition of $\tilde{\alpha}'_{n,\epsilon}$; and (ii) follows from the definition of $\tilde{\Gamma}_n$ and Lemma D.4. \square

Experiments We observe empirically in our synthetic experiments on GPs (cf. Appendix H) and our experiments on Safe BO Appendix J that **VTL** reduces the marginal variance of points in \mathcal{A} faster than **ITL**, while **ITL** reduces the entropy of $f_{\mathcal{A}}$ faster than **VTL**.

E.3. Correlation-based Transductive Learning

We will briefly look at the decision rule

$$\mathbf{x}_n = \arg \max_{\mathbf{x} \in \mathcal{S}} \sum_{\mathbf{x}' \in \mathcal{A}} \text{Cor}[f_{\mathbf{x}}, f_{\mathbf{x}'} \mid \mathcal{D}_{n-1}] \quad (39)$$

which as we will see can be thought of as an approximation to both **VTL** and **ITL**, and sheds light on the differences between the two. We refer to this decision rule as **CTL**, short for *correlation-based transductive learning*.

Once more, we consider the GP setting, i.e., Assumptions A.1 and A.2 hold.

Approximation of VTL Observe that the following decision rule is equivalent to **VTL**:

$$\mathbf{x}_n = \arg \max_{\mathbf{x} \in \mathcal{S}} \text{tr} \text{Var}[f_{\mathcal{A}} \mid \mathcal{D}_{n-1}] - \text{tr} \text{Var}[f_{\mathcal{A}} \mid \mathcal{D}_{n-1}, \mathbf{y}_{\mathbf{x}}].$$

By Lemma D.20, for any $\mathbf{x} \in \mathcal{S}$, this objective value can be tightly lower- and upper-bounded (up to constant-factors) by

$$\begin{aligned} &\sum_{\mathbf{x}' \in \mathcal{A}} \log \left(\frac{\text{Var}[f_{\mathbf{x}'} \mid \mathcal{D}_{n-1}]}{\text{Var}[f_{\mathbf{x}'} \mid \mathcal{D}_{n-1}, \mathbf{y}_{\mathbf{x}}]} \right) \\ &= 2 \sum_{\mathbf{x}' \in \mathcal{A}} I(f_{\mathbf{x}'}; \mathbf{y}_{\mathbf{x}} \mid \mathcal{D}_{n-1}) \\ &\stackrel{(i)}{=} - \sum_{\mathbf{x}' \in \mathcal{A}} \log \left(1 - \text{Cor}[f_{\mathbf{x}'}, \mathbf{y}_{\mathbf{x}} \mid \mathcal{D}_{n-1}]^2 \right) \end{aligned}$$

where (i) is detailed in example 8.5.1 of (Cover, 1999). It is therefore not surprising that we observe a similar performance of **VTL** and **CTL** in all our experiments.

Approximation of ITL In contrast, the **ITL** objective can be shown to be lower bounded by

$$\begin{aligned} &I(f_{\mathcal{A}}; \mathbf{y}_{\mathbf{x}} \mid \mathcal{D}_{n-1}) \\ &\stackrel{(i)}{\geq} \frac{1}{|\mathcal{A}|} \sum_{\mathbf{x}' \in \mathcal{A}} I(f_{\mathbf{x}'}; \mathbf{y}_{\mathbf{x}} \mid \mathcal{D}_{n-1}) \\ &\stackrel{(ii)}{=} - \frac{1}{2|\mathcal{A}|} \sum_{\mathbf{x}' \in \mathcal{A}} \log \left(1 - \text{Cor}[f_{\mathbf{x}'}, \mathbf{y}_{\mathbf{x}} \mid \mathcal{D}_{n-1}]^2 \right) \\ &\stackrel{(iii)}{\gtrsim} \sum_{\mathbf{x}' \in \mathcal{A}} \text{Cor}[f_{\mathbf{x}'}, \mathbf{y}_{\mathbf{x}} \mid \mathcal{D}_{n-1}]^2 + \text{const} \end{aligned}$$

where (ii) is detailed in example 8.5.1 of (Cover, 1999); and (iii) follows from Jensen’s inequality and exponentiating. (i) is a loose approximation which highlights that **ITL** takes into account the correlations *between* points in \mathcal{A} while **CTL** does not.

F. Subsampling Target Spaces

When the target space \mathcal{A} is large, it may be computationally infeasible to compute the exact objective. A natural approach to address this issue is to approximate the target space by a smaller set of size K .

One possibility is to select the K “most explanatory” points within \mathcal{A} . This selection problem is similar to the batch selection problem in active learning (Holzmüller et al., 2023) and can be tackled using, e.g., the *greedy max determinant* or *greedy max kernel distance* strategies. In the remainder of this section, we study an alternative approach which is based on sampling points from \mathcal{A} according to some probability distribution $\mathcal{P}_{\mathcal{A}}$ supported on \mathcal{A} .

F.1. Stochastic Target Spaces

Concretely, in iteration n , a subset \mathcal{A}'_n of K points is sampled independently from \mathcal{A} according to the distribution $\mathcal{P}_{\mathcal{A}}$ and the objective is computed on this subset.

It is straightforward to extend the convergence guarantees to the setting of stochastic target spaces. Intuitively, after sufficiently many iterations, each $\mathbf{x} \in \mathcal{A}$ will have been sampled roughly as often as its “weight” (i.e., probability) suggests.

Lemma F.1. *Consider the stochastic target space setting. For any $n \geq 0$, $K \geq 1$, and $\mathbf{x} \in \mathcal{A}$, with probability at least $1 - \exp(-n\nu/8)$ where $\nu = 1 - (1 - \mathcal{P}_{\mathcal{A}}(\mathbf{x}))^K$, we have that after at most n iterations \mathbf{x} was within the subsampled target space in at least $n\nu/2$ iterations.*

Proof. Let $Y_i \sim \text{Binom}(K, \mathcal{P}_{\mathcal{A}}(\mathbf{x}))$ denote the random variable counting the number of occurrences of \mathbf{x} in \mathcal{A}'_i . Moreover, we write $X_i \stackrel{\text{def}}{=} \mathbb{1}\{\mathbf{x} \in \mathcal{A}'_i\}$. Note that

$$\begin{aligned} \nu_i &\stackrel{\text{def}}{=} \mathbb{E}X_i = \mathbb{P}(\mathbf{x} \in \mathcal{A}'_i) \\ &= 1 - \mathbb{P}(Y_i = 0) \\ &= 1 - (1 - \mathcal{P}_{\mathcal{A}}(\mathbf{x}))^K \\ &= \nu. \end{aligned}$$

Let $X \stackrel{\text{def}}{=} \sum_{i=1}^n X_i$ with $\mathbb{E}X = n\nu$. By Chernoff’s bound,

$$\mathbb{P}\left(X \leq \frac{n\nu}{2}\right) \leq \exp\left(-\frac{n\nu}{8}\right).$$

□

With this result, the previously derived convergence guarantees follow also for the stochastic target space setting. We leave a tighter analysis of stochastic target spaces to future work.

G. Computational Complexity

Evaluating the acquisition function of **ITL** in round n requires computing for each $\mathbf{x} \in \mathcal{S}$,

$$\begin{aligned} &I(\mathbf{f}_{\mathcal{A}}; \mathbf{y}_{\mathbf{x}} \mid \mathcal{D}_n) \\ &= \frac{1}{2} \log\left(\frac{|\text{Var}[\mathbf{f}_{\mathcal{A}} \mid \mathcal{D}_n]|}{|\text{Var}[\mathbf{f}_{\mathcal{A}} \mid \mathbf{y}_{\mathbf{x}}, \mathcal{D}_n]|}\right) \quad (\text{forward}) \\ &= \frac{1}{2} \log\left(\frac{\text{Var}[\mathbf{y}_{\mathbf{x}} \mid \mathcal{D}_n]}{\text{Var}[\mathbf{y}_{\mathbf{x}} \mid \mathbf{f}_{\mathcal{A}}, \mathcal{D}_n]}\right) \quad (\text{backward}). \end{aligned}$$

Let $|\mathcal{S}| = m$ and $|\mathcal{A}| = k$. Then, the forward method has complexity $\mathcal{O}(m \cdot k^3)$. For the backward method, observe that the variances are scalar and the covariance matrix $\text{Var}[\mathbf{f}_{\mathcal{A}} \mid \mathcal{D}_n]$ only has to be inverted once for all points \mathbf{x} . Thus, the backward method has complexity $\mathcal{O}(k^3 + m)$.

When the size m of \mathcal{S} is relatively small (and hence, all points in \mathcal{S} can be considered during each iteration of the algorithm), GP inference corresponds simply to computing conditional distributions of a multivariate Gaussian. The performance can therefore be improved by keeping track of the full posterior distribution over $\mathbf{f}_{\mathcal{S}}$ of size $\mathcal{O}(m^2)$ and conditioning on the latest observation during each iteration of the algorithm. In this case, after each observation the posterior can be updated at a cost of $\mathcal{O}(m^2)$ which does not grow with the time n , unlike classical GP inference.

Overall, when m is small, the computational complexity of **ITL** is $\mathcal{O}(k^3 + m^2)$. When m is large (or possibly infinite) and a subset of \tilde{m} points is considered in a given iteration, the computational complexity of **ITL** is $\mathcal{O}(k^3 + \tilde{m} \cdot n^3)$, neglecting the complexity of selecting the \tilde{m} candidate points. In the latter case, the computational cost of **ITL** is dominated by the cost of GP inference.

Khanna et al. (2017) discuss distributed and stochastic approximations of greedy algorithms to (weakly) submodular problems that are also applicable to **ITL**.

H. Additional GP Experiments & Details

We use homoscedastic Gaussian noise with standard deviation $\rho = 0.1$ and a discretization of $\mathcal{X} = [-3, 3]^2$ of size 2500. Uncertainty bands correspond to one standard error over 10 random seeds.

Additional experiments Figure 5 includes the following additional experiments:

1. *Marginal Variance*: Average marginal standard deviation within \mathcal{A} in the top experiment from Figure 2 (B) under the Gaussian kernel. As one would expect, **ITL** reduces the entropy fastest whereas the variance-based algorithms such as **VTL** and **CTL** are faster to reduce the average standard deviation.

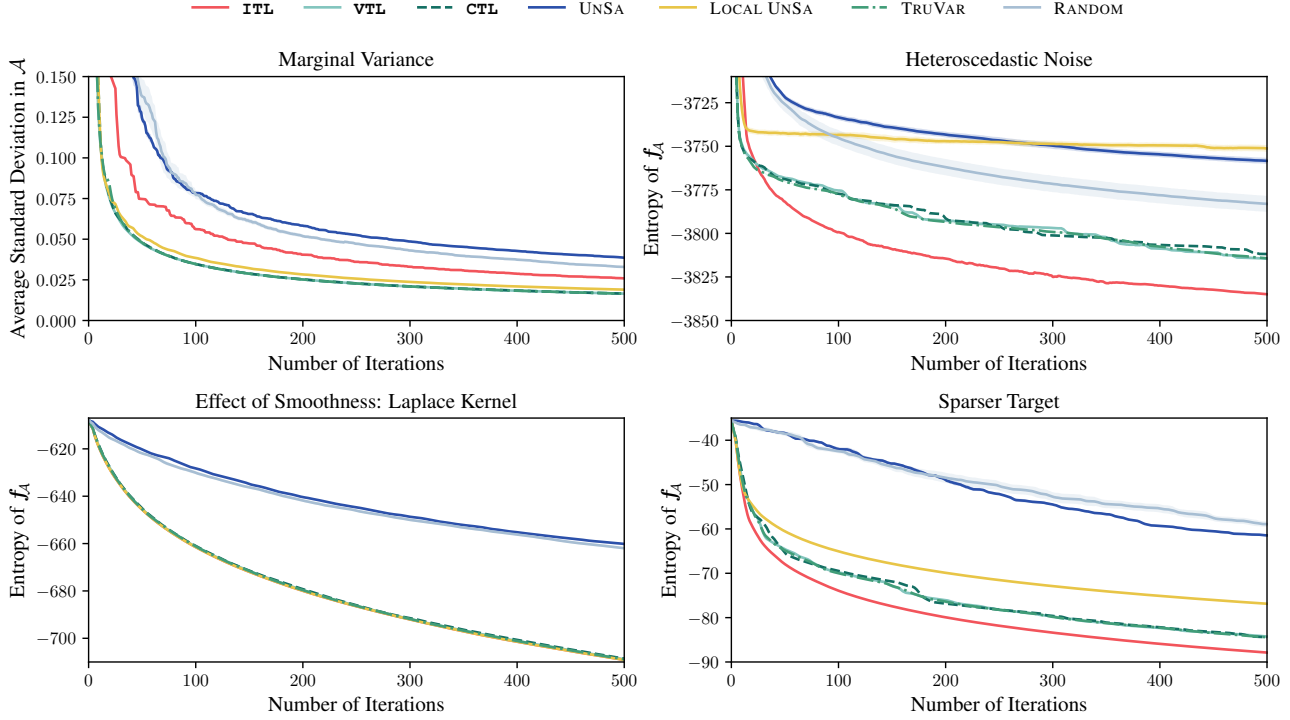


Figure 5. Additional GP experiments

2. *Heteroscedastic Noise*: Top experiment from Figure 2 (B) under the Gaussian kernel with heteroscedastic Gaussian noise

$$\rho(x) = \begin{cases} 1 & \text{if } x \in [-\frac{1}{2}, \frac{1}{2}]^2 \\ 0.1 & \text{otherwise} \end{cases}.$$

If observation noise is heteroscedastic, in considering *posterior* rather than *prior* uncertainty, **ITL** avoids points with high aleatoric uncertainty, which accelerates learning.

3. *Effect of Smoothness*: Top experiment from Figure 2 (B) under the Laplace kernel. All algorithms except for US and RANDOM perform equally well. This validates our claims from Section 3.3: in the extreme non-smooth case of a Laplace kernel and $\mathcal{A} \subseteq \mathcal{S}$, points outside \mathcal{A} do not provide any additional information, and **ITL** and “local” UNSA coincide.

4. *Sparser Target*: Top experiment from Figure 2 (B) under the Gaussian kernel, but with domain extended to $\mathcal{X} = [-10, 10]^2$.

Hyperparameters of TRUVAR As suggested by Bozovic et al. (2016), we use $\tilde{\eta}_{(1)}^2 = 1$, $r = 0.1$, and $\delta = 0$ (even though the theory only holds for $\delta > 0$).

Smoothing to reduce numerical noise Applied running average with window 5 to entropy curves of Figures 2 and 5 to smoothen out numerical noise.

I. Additional NN Experiments & Details

We outline the few-shot training of NNs in Algorithm 1.

Algorithm 1 Few-shot training of NNs

Given: initialized or pre-trained model f , *small* sample $A \sim \mathcal{P}_A$
initialize dataset $\mathcal{D} = \emptyset$
repeat
 sample $S \sim \mathcal{P}_S$
 subsample target space $A' \stackrel{\text{u.a.r.}}{\sim} A$
 initialize batch $B = \emptyset$
 compute kernel matrix \mathbf{K} over domain $[S, A']$
repeat b **times**
 compute acquisition function w.r.t. A' , based on \mathbf{K}
 add maximizer $x \in S$ of acquisition function to B
 update conditional kernel matrix \mathbf{K}
 obtain labels for B and add to dataset \mathcal{D}
 update f using data \mathcal{D}

In Appendix I.1, we detail metrics and hyperparameters. We describe in Appendices I.2 and I.3 how to compute the (initial) conditional kernel matrix \mathbf{K} , and in Appendix I.4

Table 1. Hyperparameter summary of NN experiments. (*) we train until convergence on oracle validation accuracy.

	MNIST	CIFAR-100
ρ	0.01	1
M	30	100
m	3	10
k	1 000	1 000
batch size b	1	10
# of epochs	(*)	5
learning rate	0.001	0.001

how to update this matrix \mathbf{K} to obtain conditional embeddings for batch selection.

In Appendix I.5, we show that **ITL** and **CTL** significantly outperform a wide selection of commonly used heuristics. In Appendices I.6 and I.7, we conduct additional experiments and ablations.

Hübotter et al. (2024) discusses additional motivation and related work that has previously studied few-shot fine-tuning, but which has largely focused on the training algorithm rather than data selection.

I.1. Experiment Details

We evaluate the accuracy with respect to \mathcal{P}_A using a Monte Carlo approximation with out-of-sample data:

$$\text{accuracy}(\hat{\theta}) \approx \mathbb{E}_{(\mathbf{x}, y) \sim \mathcal{P}_A} \mathbb{1}\{y = \arg \max_i f_i(\mathbf{x}; \hat{\theta})\}.$$

We provide an overview of the hyperparameters used in our NN experiments in Table 1. The effect of noise standard deviation ρ is small for all tested $\rho \in [1, 100]$ (cf. ablation study in Table 2).²² M denotes the size of the sample $A \sim \mathcal{P}_A$. In each iteration, we select the target space $\mathcal{A} \leftarrow A'$ as a random subset of m points from A .²³ We provide an ablation over m in Appendix I.6.

During each iteration, we select the batch B according to the decision rule from a random sample from \mathcal{P}_S of size k .²⁴

Since we train the MNIST model from scratch, we train from random initialization until convergence on oracle

²²We use a larger noise standard deviation ρ in CIFAR-100 to stabilize the numerics of batch selection via conditional embeddings (cf. Table 2).

²³This appears to improve the training, likely because it prevents overfitting to peculiarities in the finite sample A (cf. Figure 13).

²⁴In large-scale problems, the work of Coleman et al. (2022) suggests to use an (approximate) nearest neighbor search to select the (large) candidate set rather than sampling u.a.r. from \mathcal{P}_S . This can be a viable alternative to simply increasing k and suggests future work.

validation accuracy.²⁵ We do this to stabilize the learning curves, and provide the least biased (due to the training algorithm) results. For CIFAR-100, we train for 5 epochs (starting from the previous iterations' model) which we found to be sufficient to obtain good performance.

We use the ADAM optimizer (Kingma & Ba, 2014). In our CIFAR-100 experiments, we use a pre-trained EfficientNet-B0 (Tan & Le, 2019), and fine-tune the final and penultimate layers. We freeze earlier layers to prevent overfitting to the few-shot training data.

To prevent numerical inaccuracies when computing the **ITL** objective, we optimize

$$I(\mathbf{y}_A; \mathbf{y}_x \mid \mathcal{D}_{n-1}) = \frac{1}{2} \log \left(\frac{\text{Var}[y_x \mid \mathcal{D}_{n-1}]}{\text{Var}[y_x \mid \mathbf{y}_A, \mathcal{D}_{n-1}]} \right) \quad (40)$$

instead of Equation (1), which amounts to adding ρ^2 to the diagonal of the covariance matrix before inversion. This appears to improve numerical stability, especially when using gradient embeddings.²⁶

I.2. Embeddings and Kernels

Using a neural network to parameterize f , we evaluate the canonical approximations of f by a stochastic process in the following.

An embedding $\phi(\mathbf{x})$ is a latent representation of an input \mathbf{x} . Collecting the embeddings as rows in the design matrix Φ of a set of inputs X , one can approximate the network by the linear function $\mathbf{f}_X = \Phi\beta$ with weights β . Approximating the weights by $\beta \sim \mathcal{N}(\mu, \Sigma)$ implies that $\mathbf{f}_X \sim \mathcal{N}(\Phi\mu, \Phi\Sigma\Phi^\top)$. The covariance matrix $\mathbf{K}_{XX} = \Phi\Sigma\Phi^\top$ can be succinctly represented in terms of its associated kernel $k(\mathbf{x}, \mathbf{x}') = \phi(\mathbf{x})^\top \Sigma \phi(\mathbf{x}')$. Here,

- $\phi(\mathbf{x})$ is the latent representation of \mathbf{x} , and
- Σ captures the dependencies in the latent space.

While any choice of embedding ϕ is possible, the following are common choices:

1. *Last-Layer*: A common choice for $\phi(\mathbf{x})$ is the representation of \mathbf{x} from the penultimate layer of the neural network (Holzmüller et al., 2023). Interpreting the early layers as a feature encoder, this uses the low-dimensional feature map akin to random feature methods (Rahimi & Recht, 2007).

²⁵That is, to stop training as soon as accuracy on a validation set from \mathcal{P}_A decreases in an epoch.

²⁶In our experiments, we observe that the effect of various choices of ρ on this slight adaptation of the **ITL** decision rule has negligible impact on performance. The more prominent effect of ρ appears to arise from the batch selection via conditional embeddings (cf. Table 2).

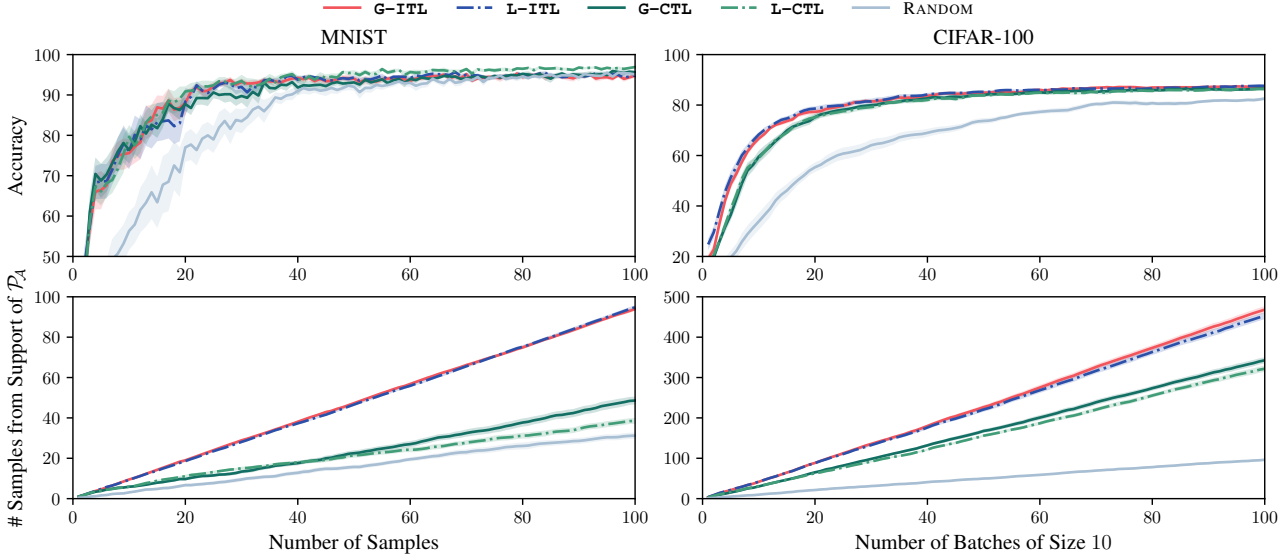


Figure 6. Comparison of loss gradient (“G-”) and last-layer embeddings (“L-”).

2. *Output Gradients (eNTK)*: Another common choice is $\phi(\mathbf{x}) = \nabla_{\theta} f(\mathbf{x}; \theta)$ where θ are the network parameters (Holzmüller et al., 2023). Its associated kernel is known as the *empirical neural tangent kernel* (eNTK) and the posterior mean of this GP approximates ultra-wide NNs trained with gradient descent (Jacot et al., 2018; Arora et al., 2019; Lee et al., 2019; Khan et al., 2019; He et al., 2020; Malladi et al., 2023). Kassraie & Krause (2022) derive bounds of γ_n under this kernel. If θ is restricted to the weights of the final linear layer, then this embedding is simply the last-layer embedding.

3. *Loss Gradients*: Another possible choice is

$$\phi(\mathbf{x}) = \nabla_{\theta} \ell(f(\mathbf{x}; \theta), \hat{y}(\mathbf{x}))|_{\theta=\hat{\theta}}$$

where ℓ is a loss function, $\hat{y}(\mathbf{x})$ is the predicted label, and $\hat{\theta}$ are the current parameter estimates Ash et al. (2020).

4. *Outputs (eNNGP)*: Another possible choice is $\phi(\mathbf{x}) = f(\mathbf{x})$, i.e., the output of the network. Its associated kernel is known as the *empirical neural network Gaussian process* (eNNGP) kernel (Lee et al., 2018).

In the additional experiments from this appendix we use last-layer embeddings unless noted otherwise. We compare the performance of last-layer and the loss gradient embedding

$$\phi(\mathbf{x}) = \nabla_{\theta'} \ell_{\text{CE}}(f(\mathbf{x}; \theta), \hat{y}(\mathbf{x}))|_{\theta=\hat{\theta}} \quad (41)$$

where θ' are the parameters of the final output layer, $\hat{\theta}$ are the current parameter estimates, $\hat{y}(\mathbf{x}) = \arg \max_i f_i(\mathbf{x}; \hat{\theta})$

are the associated predicted labels, and ℓ_{CE} denotes the cross-entropy loss. This gradient embedding captures the potential update direction upon observing a new point (Ash et al., 2020). Moreover, Ash et al. (2020) show that for most neural networks, the norm of these gradient embeddings are a conservative lower bound to the norm assumed by taking any other proxy label $\hat{y}(\mathbf{x})$. In Figure 6, we observe only negligible differences in performance between this and the last-layer embedding.

I.3. Towards Uncertainty Quantification in Latent Space

A straightforward and common approximation of the uncertainty about NN weights is given by $\Sigma = \mathbf{I}$, and we use this approximation throughout our experiments.

The poor performance of UNSA (cf. Appendix I.5) with this approximation suggests that with more sophisticated approximations, the performance of **ITL** and **CTL** can be further improved. Further research is needed to study the effect of more sophisticated approximations of “uncertainty” in the latent space. For example, with parameter gradient embeddings, the latent space is the network parameter space where various approximations of Σ based on Laplace approximation (Daxberger et al., 2021; Antorán et al., 2022), variational inference (Blundell et al., 2015), or Markov chain Monte Carlo (Maddox et al., 2019) have been studied. We also evaluate Laplace approximation (LA, Daxberger et al. (2021)) for estimating Σ but see no improvement (cf. Figure 7). Nevertheless, we believe that uncertainty quantification is a promising direction for future work, with the potential to improve performance of **ITL** and its variations substantially.

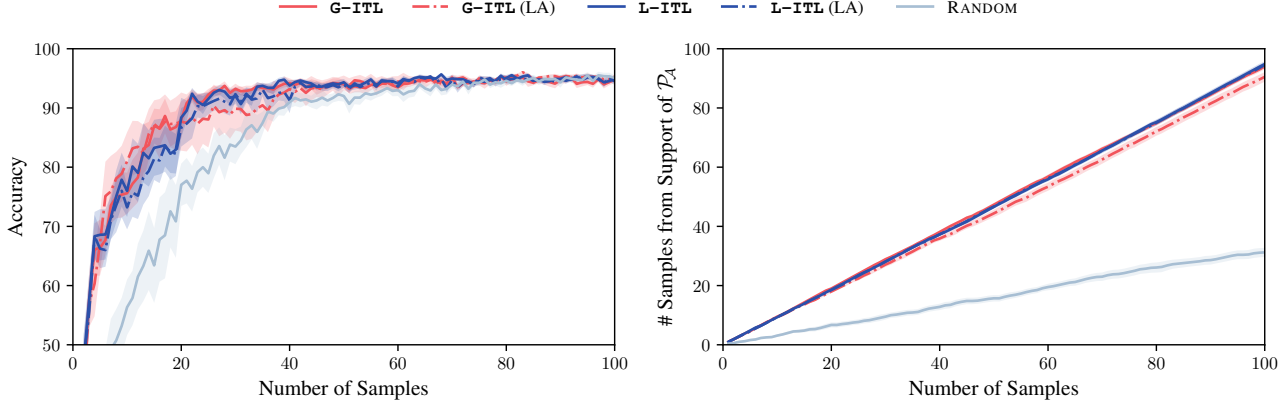


Figure 7. Uncertainty quantification (i.e., estimation of Σ) via a Laplace approximation (LA, Daxberger et al. (2021)) over last-layer weights using a Kronecker factored log-likelihood Hessian approximation (Martens & Grosse, 2015) and the loss gradient embeddings from Equation (41). The results are shown for the MNIST experiment. We do not observe a performance improvement beyond the trivial approximation $\Sigma = \mathbf{I}$.

I.4. Batch Selection via Conditional Embeddings

We will refer to Equation (6) as BACE, short for *batch selection via conditional embeddings*. BACE can be implemented efficiently using the Gaussian approximation of f_X from Appendix I.2 by iteratively conditioning on the previously selected points $\mathbf{x}_{n,1:i-1}$, and updating the kernel matrix \mathbf{K}_{XX} using the closed-form formula for the variance of conditional Gaussians:

$$\mathbf{K}_{XX} \leftarrow \mathbf{K}_{XX} - \frac{1}{\mathbf{K}_{\mathbf{x}_j \mathbf{x}_j} + \rho^2} \mathbf{K}_{X \mathbf{x}_j} \mathbf{K}_{\mathbf{x}_j X} \quad (42)$$

where j denotes the index of the selected $\mathbf{x}_{n,i}$ within X and ρ^2 is the noise variance. Note that $\mathbf{K}_{\mathbf{x}_j \mathbf{x}_j}$ is a scalar and $\mathbf{K}_{X \mathbf{x}_j}$ is a row vector, and hence, this iterative update can be implemented efficiently.

We remark that Equations (5) and (6) are natural extensions of previous non-adaptive active learning methods, which typically maximize some notion of “distance” between points in the batch, to the “directed” setting (Ash et al., 2020; Zanette et al., 2021; Holzmüller et al., 2023; Pacchiano et al., 2024). BACE simultaneously maximizes “distance” between points in a batch and minimizes “distance” to points in \mathcal{A} .

The efficiency of BACE Equation (5), and therefore also Equation (6), yields diverse batches by design. In Figure 8, we compare BACE to selecting the top- b points according to the decision rule (which does *not* yield diverse batches). We observe a significant improvement in accuracy and data retrieval when using BACE. We expect the gap between both approaches to widen further with larger batch sizes.

I.5. Baselines

In the following, we briefly describe the most commonly used “undirected” decision rules.

Denote the softmax distribution over labels i at inputs \mathbf{x} by

$$p_i(\mathbf{x}; \hat{\boldsymbol{\theta}}) \propto \exp(f_i(\mathbf{x}; \hat{\boldsymbol{\theta}})).$$

The following heuristics computed based on the softmax distribution aim to quantify the “uncertainty” about a particular input \mathbf{x} :

- MAXENTROPY (Settles & Craven, 2008):

$$\mathbf{x}_n = \arg \max_{\mathbf{x} \in \mathcal{S}} H[p(\mathbf{x}; \hat{\boldsymbol{\theta}}_{n-1})].$$

- MAXMARGIN (Scheffer et al., 2001; Settles & Craven, 2008):

$$\mathbf{x}_n = \arg \min_{\mathbf{x} \in \mathcal{S}} p_1(\mathbf{x}; \hat{\boldsymbol{\theta}}_{n-1}) - p_2(\mathbf{x}; \hat{\boldsymbol{\theta}}_{n-1})$$

where p_1 and p_2 are the two largest class probabilities.

- LEASTCONFIDENCE (Lewis & Gale, 1994; Settles & Craven, 2008; Hendrycks & Gimpel, 2017; Tamkin et al., 2022):

$$\mathbf{x}_n = \arg \min_{\mathbf{x} \in \mathcal{S}} p_1(\mathbf{x}; \hat{\boldsymbol{\theta}}_{n-1})$$

where p_1 is the largest class probability.

An alternative class of decision rules aims to select diverse batches by maximizing the distances between points. Embeddings $\phi(\mathbf{x})$ induce the (Euclidean) embedding distance

$$d_\phi(\mathbf{x}, \mathbf{x}') \stackrel{\text{def}}{=} \|\phi(\mathbf{x}) - \phi(\mathbf{x}')\|_2.$$

Similarly, a kernel k induces the kernel distance

$$d_k(\mathbf{x}, \mathbf{x}') \stackrel{\text{def}}{=} \sqrt{k(\mathbf{x}, \mathbf{x}) + k(\mathbf{x}', \mathbf{x}') - 2k(\mathbf{x}, \mathbf{x}')}$$

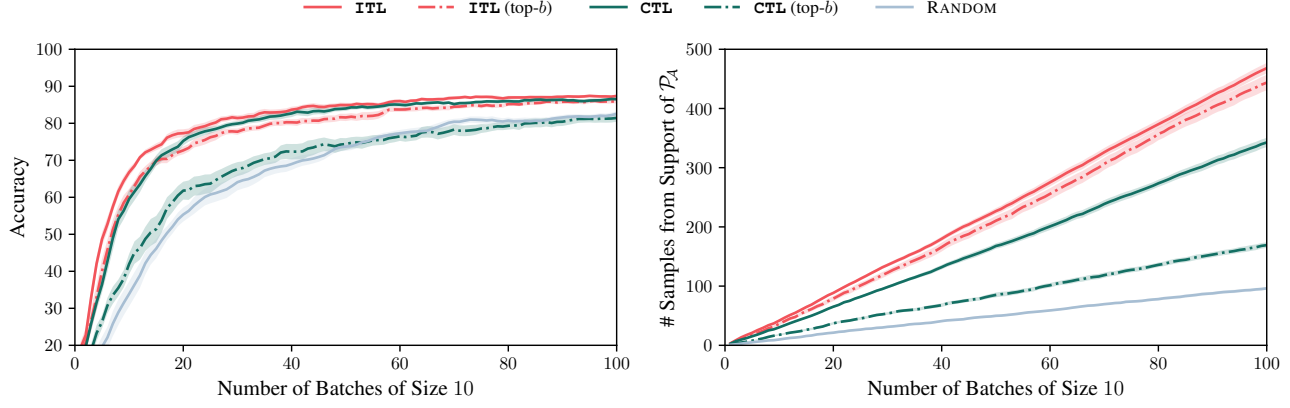


Figure 8. Advantage of batch selection via conditional embeddings over top- b selection in the CIFAR-100 experiment.

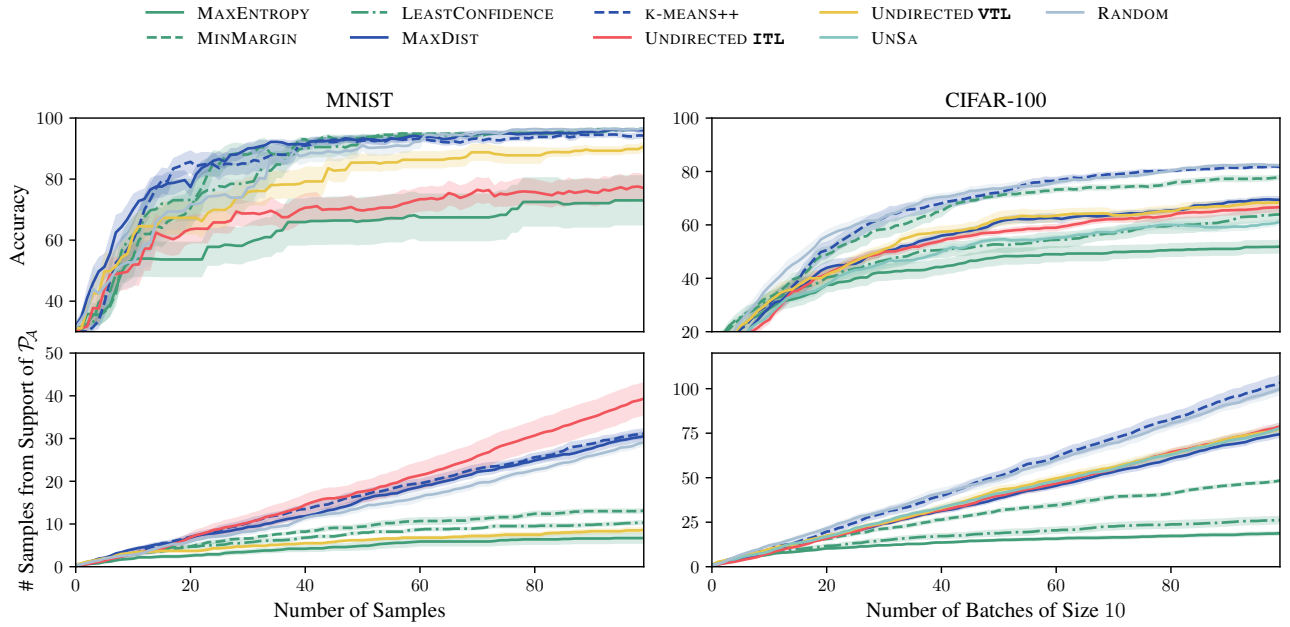


Figure 9. Comparison of “undirected” baselines for the experiment of Figure 3. In the MNIST experiment, UNSA and UNDIRECTED ITL coincide, and we therefore only plot the latter.

It is straightforward to see that if $k(\mathbf{x}, \mathbf{x}') = \phi(\mathbf{x})^\top \phi(\mathbf{x}')$, then embedding and kernel distances coincide, i.e., $d_\phi(\mathbf{x}, \mathbf{x}') = d_k(\mathbf{x}, \mathbf{x}')$.

- MAXDIST (Holzmüller et al., 2023; Yu & Kim, 2010; Sener & Savarese, 2017; Geifman & El-Yaniv, 2017) constructs the batch by choosing the point with the maximum distance to the nearest previously selected point:

$$\mathbf{x}_n = \arg \max_{\mathbf{x} \in \mathcal{S}} \min_{i < n} d(\mathbf{x}, \mathbf{x}_i)$$

- Similarly, K-MEANS++ (Holzmüller et al., 2023) selects the batch via K-MEANS++ seeding (Arthur et al., 2007; Ostrovsky et al., 2013). That is, the first centroid \mathbf{x}_1 is chosen uniformly at random and the subsequent centroids are chosen with a probability proportional to the square of the distance to the nearest previously selected centroid:

$$\mathbb{P}(\mathbf{x}_n = \mathbf{x}) \propto \min_{i < n} d(\mathbf{x}, \mathbf{x}_i)^2.$$

When using the loss gradient embeddings from Equation (41), this decision rule is known as BADGE (Ash et al., 2020).

Finally, we summarize common kernel-based decision rules.

- UNDIRECTED **ITL** chooses

$$\begin{aligned} \mathbf{x}_n &= \arg \max_{\mathbf{x} \in \mathcal{S}} I(f_{\mathcal{S}}; y_{\mathbf{x}} \mid \mathcal{D}_{n-1}) \\ &= \arg \max_{\mathbf{x} \in \mathcal{S}} I(f_{\mathbf{x}}; y_{\mathbf{x}} \mid \mathcal{D}_{n-1}). \end{aligned}$$

This can be shown to be equivalent to MAXDET (Holzmüller et al., 2023) which selects

$$\mathbf{x}_n = \arg \max_{\mathbf{x} \in \mathcal{S}} |\mathbf{K}_{\mathbf{x}} + \sigma^2 \mathbf{I}|$$

where $\mathbf{K}_{\mathbf{x}}$ denotes the kernel matrix over $\mathbf{x}_{1:n-1} \cup \{\mathbf{x}\}$, conditioned on the prior observations \mathcal{D}_{n-1} .

- UNSA (Lewis & Catlett, 1994) which with embeddings ϕ_{n-1} after round $n-1$ corresponds to:

$$\mathbf{x}_n = \arg \max_{\mathbf{x} \in \mathcal{S}} \sigma_{n-1}^2(\mathbf{x}) = \arg \max_{\mathbf{x} \in \mathcal{S}} \|\phi_{n-1}(\mathbf{x})\|_2^2.$$

With batch size $b = 1$, UNSA coincides with UNDIRECTED **ITL**. When evaluated with gradient embeddings, this acquisition function is similar to previously used “embedding length” or “gradient length” heuristics (Settles & Craven, 2008).

- UNDIRECTED **VTL** (Cohn, 1993) is the special case of **VTL** without specified prediction targets (i.e., $\mathcal{A} = \mathcal{S}$). In the literature, this decision rule is also known as BAIT (Ash et al., 2021).

We compare to the abovementioned decision rules and summarize the results in Figure 9. We observe that most “undirected” decision rules perform worse (and often significantly so) than RANDOM. This is likely due to frequently selecting points from the support of $\mathcal{P}_{\mathcal{S}}$ which are not in the support of $\mathcal{P}_{\mathcal{A}}$ since the points are “adversarial examples” that the model $\hat{\theta}$ is not trained to perform well on. In the case of MNIST, the poor performance can also partially be attributed to the well-known “cold-start problem” (Gao et al., 2020).

In Figure 3, we also compare to the following “directed” decision rules:

- COSINESIMILARITY (Settles & Craven, 2008) selects $\mathbf{x}_n = \arg \max_{\mathbf{x} \in \mathcal{S}} \angle_{\phi_{n-1}}(\mathbf{x}, \mathcal{A})$ where

$$\angle_{\phi}(\mathbf{x}, \mathcal{A}) \stackrel{\text{def}}{=} \frac{1}{|\mathcal{A}|} \sum_{\mathbf{x}' \in \mathcal{A}} \frac{\phi(\mathbf{x})^\top \phi(\mathbf{x}')}{\|\phi(\mathbf{x})\|_2 \|\phi(\mathbf{x}')\|_2}.$$

- INFORMATIONDENSITY (Settles & Craven, 2008) is defined as the multiplicative combination of MAXENTROPY and COSINESIMILARITY:

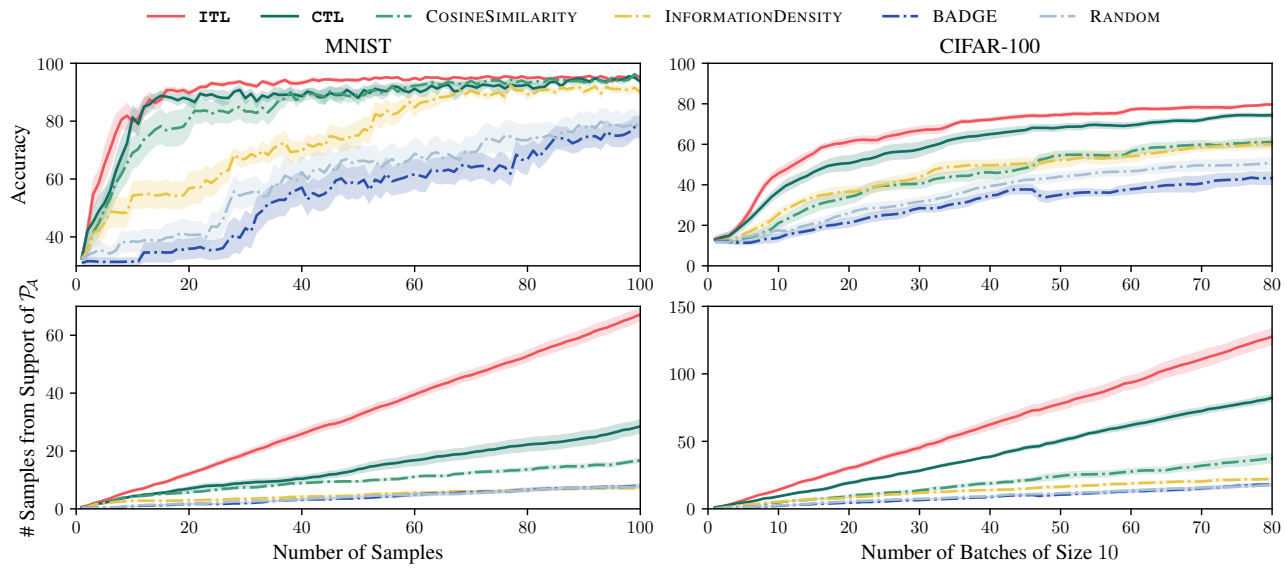
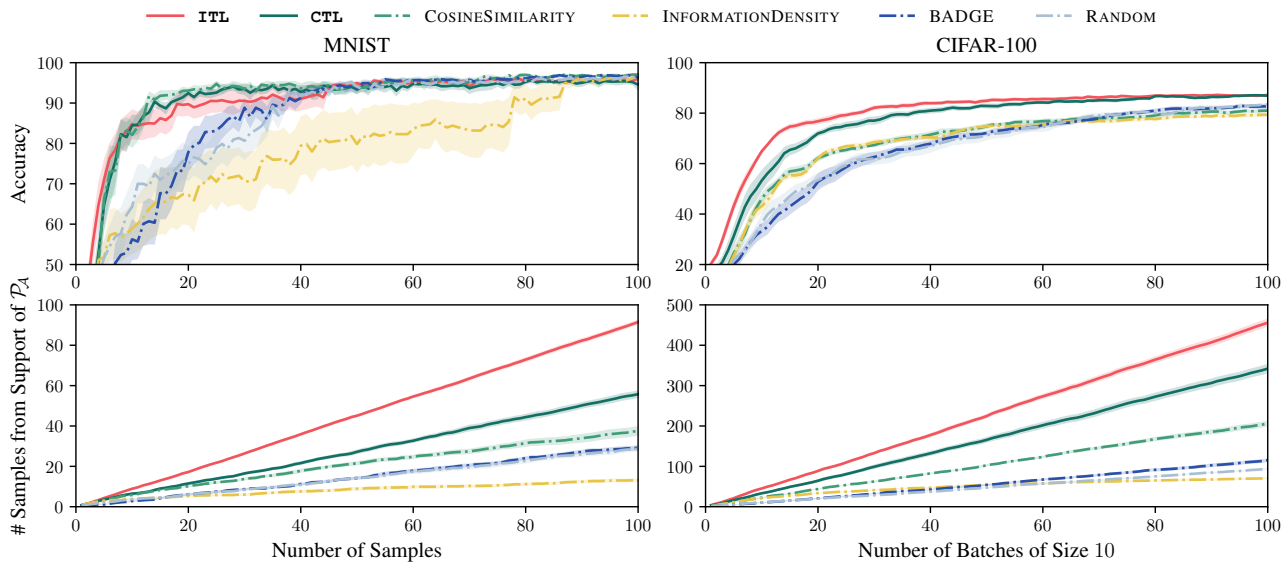
$$\mathbf{x}_n = \arg \max_{\mathbf{x} \in \mathcal{S}} H[p(\mathbf{x}; \hat{\theta}_{n-1})] \cdot \left(\angle_{\phi_{n-1}}(\mathbf{x}, \mathcal{A}) \right)^\beta$$

where $\beta > 0$ controls the relative importance of both terms. We set $\beta = 1$ in our experiments.

I.6. Additional experiments

We conduct the following additional experiments:

1. *Imbalanced $\mathcal{P}_{\mathcal{S}}$* (Figure 10): We artificially remove 80% of the support of $\mathcal{P}_{\mathcal{A}}$ from $\mathcal{P}_{\mathcal{S}}$. For example, in case of MNIST, we remove 80% of the images with labels 3, 6, and 9 from $\mathcal{P}_{\mathcal{S}}$. This makes the learning task more difficult, as $\mathcal{P}_{\mathcal{A}}$ is less represented in $\mathcal{P}_{\mathcal{S}}$, meaning that the “targets” are more sparse. The trend of **ITL** outperforming **CTL** which outperforms RANDOM is even more pronounced in this setting.
2. *Imbalanced $A \sim \mathcal{P}_{\mathcal{A}}$* (Figure 11): We artificially remove 50% of part of the support of $\mathcal{P}_{\mathcal{A}}$ while generating $A \sim \mathcal{P}_{\mathcal{A}}$ to evaluate the robustness of **ITL** and **CTL** in presence of an imbalanced target space \mathcal{A} . Concretely, in case of MNIST, we remove 50% of the images with labels 3 and 6 from A . In case of CIFAR-100, we remove 50% of the images with labels $\{0, \dots, 4\}$ from A . We still observe the same trends as in the other experiments.


 Figure 10. Imbalanced \mathcal{P}_S experiment.

 Figure 11. Imbalanced $A \sim \mathcal{P}_A$ experiment.

3. **VTL & choice of k** (Figure 12): We observe that **VTL** performs almost as well as **ITL**. Additionally, we evaluate the effect of the number of points k at which the decision rule is evaluated. Not surprisingly, we observe that the performance of **ITL**, **VTL**, and **CTL** improves with larger k .
4. **Choice of m** (Figure 13): Next, we evaluate the choice of m , i.e., the size of the target space \mathcal{A} relative to the number M of candidate points $A \sim \mathcal{P}_{\mathcal{A}}$. We write $p = m/M$. We generally observe that a larger p leads to better performance (with $p = 1$ being the best choice). However, it appears that a smaller p can be beneficial with respect to accuracy when a large number of batches are selected. We believe that this may be because a smaller p improves the diversity between selected batches.
5. **Choice of M** (Figure 14): Finally, we evaluate the choice of M , i.e., the size of $A \sim \mathcal{P}_{\mathcal{A}}$. Not surprisingly, we observe that the performance of **ITL** improves with larger M .

I.7. Ablation study of noise standard deviation ρ

In Table 2, we evaluate the CIFAR-100 experiment with different noise standard deviations ρ . We observe that the performance of batch selection via conditional embeddings drops (mostly for the less numerically stable gradient embeddings) if ρ is too small, since this leads to numerical inaccuracies when computing the conditional embeddings. Apart from this, the effect of ρ is negligible.

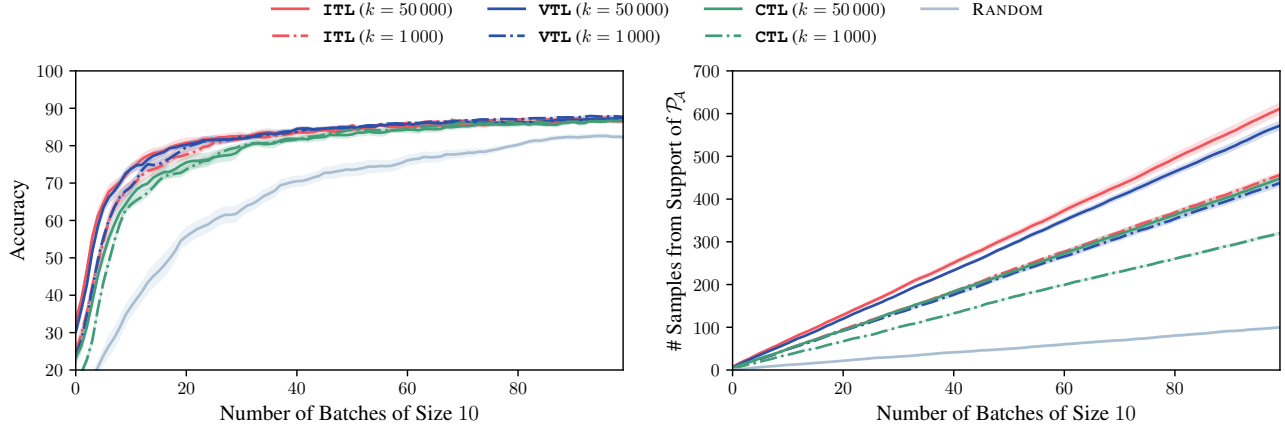
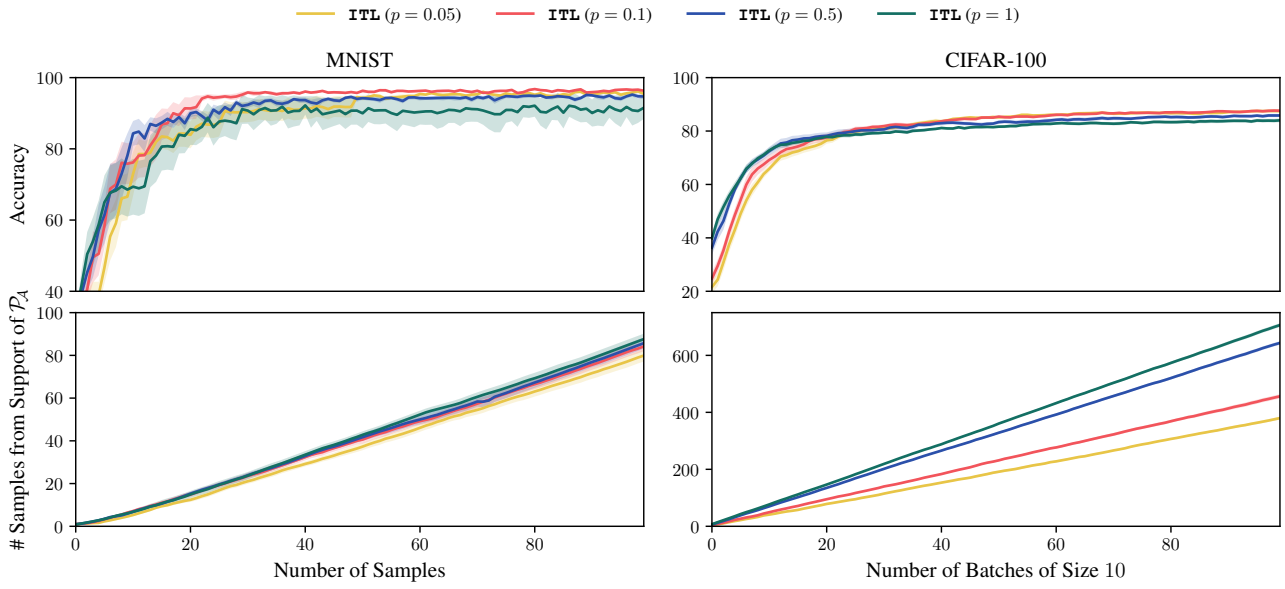
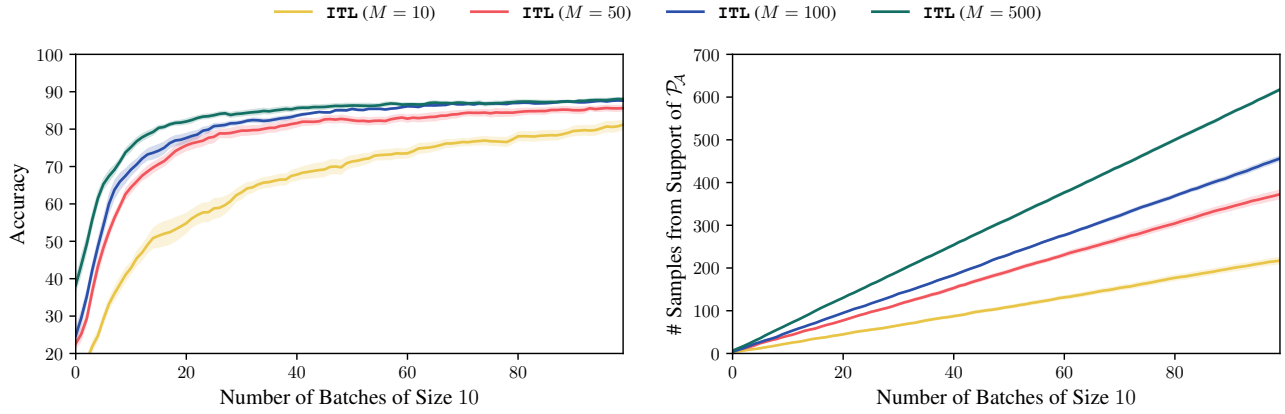

 Figure 12. Performance of **VTL** & choice of k in the CIFAR-100 experiment.

 Figure 13. Evaluation of the choice of m relative to the size M of $A \sim P_A$. Here, $p = m/M$.

 Figure 14. Evaluation of the choice of M , i.e., the size of $A \sim P_A$, in the CIFAR-100 experiment.

Table 2. Ablation study of noise standard deviation ρ in the CIFAR-100 experiment. We list the accuracy after 100 rounds per decision rule, with its standard error over 10 random seeds. “(top- b)” denotes variants where batches are selected by taking the top- b points according to the decision rule rather than using batch selection via conditional embeddings. Shown in **bold** are the best performing decision rules, and shown in *italics* are results due to numerical instability.

ρ	0.0001	0.01	1	100
G-ITL	<i>78.26 ± 1.40</i>	<i>79.12 ± 1.19</i>	87.16 ± 0.29	87.18 ± 0.28
L-ITL	87.52 ± 0.48	87.52 ± 0.41	87.53 ± 0.35	86.47 ± 0.22
G-CTL	<i>58.68 ± 2.11</i>	<i>81.44 ± 1.04</i>	86.52 ± 0.44	86.92 ± 0.56
L-CTL	86.40 ± 0.71	86.38 ± 0.75	86.00 ± 0.69	84.78 ± 0.39
G-ITL (top- b)	85.84 ± 0.54	85.92 ± 0.52	85.84 ± 0.54	85.55 ± 0.46
L-ITL (top- b)	85.44 ± 0.58	85.46 ± 0.54	85.44 ± 0.59	85.29 ± 0.36
G-CTL (top- b)	82.27 ± 0.67	82.27 ± 0.67	82.27 ± 0.67	82.27 ± 0.67
L-CTL (top- b)	80.73 ± 0.68	80.73 ± 0.68	80.73 ± 0.68	80.73 ± 0.68
BADGE	83.24 ± 0.60	83.24 ± 0.60	83.24 ± 0.60	83.24 ± 0.60
INFORMATIONDENSITY	79.24 ± 0.51	79.24 ± 0.51	79.24 ± 0.51	79.24 ± 0.51
RANDOM	82.49 ± 0.66	82.49 ± 0.66	82.49 ± 0.66	82.49 ± 0.66

J. Additional Safe BO Experiments & Details

In Appendix J.1, we discuss the use of stochastic target spaces in the safe BO setting. We provide a comprehensive overview of prior works in Appendix J.2 and an additional experiment highlighting that **ITL**, unlike **SAFEOPT**, is able to “jump past local barriers” in Appendix J.3. In Appendix J.4, we provide details on the experiments from Figure 4.

J.1. Subsampling \mathcal{A} via Thompson Sampling

We discuss in the following one possible approach of “sub-sampling” \mathcal{A}_n in the context of Bayesian optimization. To this end, we consider the stochastic target space $\mathcal{P}_{\mathcal{A}_n}$ from Equation (9):

$$\mathcal{P}_{\mathcal{A}_n}(\cdot) = \mathbb{P}(\arg \max_{\mathbf{x} \in \mathcal{X}: g(\mathbf{x}) \geq 0} f(\mathbf{x}) = \cdot \mid \mathcal{D}_n).$$

Observe that $\mathcal{P}_{\mathcal{A}_n}$ is supported precisely on the set of potential maximizers \mathcal{A}_n . We provide a formal analysis of stochastic target spaces in Appendix F.

Note that performing **ITL** with this target space is analogous to output-space entropy search (Wang & Jegelka, 2017). Samples from $\mathcal{P}_{\mathcal{A}_n}$ can be obtained via Thompson sampling (Russo et al., 2018). That is, in iteration $n+1$, we sample $K \in \mathbb{N}$ independent functions $f^{(j)} \sim f \mid \mathcal{D}_n$ from the posterior distribution and select K points $\mathbf{x}^{(1)}, \dots, \mathbf{x}^{(K)}$ which are a safe maximum of $f^{(1)}, \dots, f^{(K)}$, respectively.

Experiments In Figure 15, we contrast the performance of **ITL** with $\mathcal{P}_{\mathcal{A}_n}$ to the performance of **ITL** with the exact target space \mathcal{A}_n . We observe that their relative performance is instance dependent: in tasks that require more difficult expansion, **ITL** with \mathcal{A}_n converges faster, whereas in simpler tasks (such as the 2d experiment), **ITL** with $\mathcal{P}_{\mathcal{A}_n}$ converges faster. We compare against the **GOOSE** algorithm (Turchetta et al., 2019) which is a heuristic extension of **SAFEOPT** that explores more greedily in directions of (assumed) high reward (cf. Appendix J.2.3). **GOOSE** suffers from the same limitations as **SAFEOPT**, which were highlighted in Section 5, and additionally is limited by its heuristic approach to expansion which fails in the 1d task and safe controller tuning task. Analogously to our experiments with **SAFEOPT**, we also compare against **ORACLE GOOSE** which has oracle knowledge of the true Lipschitz constants.

The different behaviors of **ITL** with \mathcal{A}_n and $\mathcal{P}_{\mathcal{A}_n}$, respectively, as well as **SAFEOPT** and **GOOSE** are illustrated in Figure 16. We observe that **ITL** with \mathcal{A}_n and **SAFEOPT** expand the safe set more “uniformly” since the set of potential maximizers encircles the true safe set.²⁷ Intuitively, this is because the set of potential maximizers *conservatively*

²⁷This is because typically, there will always remain points in $\widehat{\mathcal{S}}_n \setminus \mathcal{S}_n$ of which the safety cannot be fully determined, and since,

captures might points might be safe and optimal. In contrast, **ITL** with $\mathcal{P}_{\mathcal{A}_n}$ and **GOOSE** focus exploration and expansion in those regions where the objective is likely to be high.

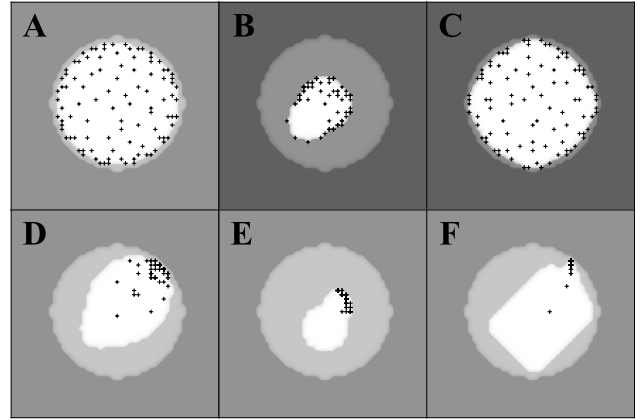


Figure 16. The first 100 samples of (A) **ITL** with \mathcal{A}_n , (B) **SAFEOPT**, (C) **ORACLE SAFEOPT**, (D) **ITL** with $\mathcal{P}_{\mathcal{A}_n}$, (E) **GOOSE**, (F) **ORACLE GOOSE**. The white region denotes the pessimistic safe set \mathcal{S}_{100} , the light gray region denotes the true safe set \mathcal{S}^* (i.e., the “island”), and the darker gray regions denotes unsafe points (i.e., the “ocean”).

J.2. Detailed Comparison with Prior Works

J.2.1. **SAFEOPT**

SAFEOPT (Sui et al., 2015; Berkenkamp et al., 2021) is a well-known algorithm for Safe BO.

Lipschitz-based expansion **SAFEOPT** expands the set of known-to-be safe points by assuming knowledge of an upper bound L_i to the Lipschitz constant of the unknown constraints g_i^* .²⁸ In each iteration, the (pessimistic) safe set \mathcal{S}_n is updated to include all points which can be reached safely (with respect to the Lipschitz continuity) from a known-to-be-safe point $\mathbf{x} \in \mathcal{S}_n$. Formally,

$$\mathcal{S}_n^{\text{SAFEOPT}} \stackrel{\text{def}}{=} \bigcup_{\mathbf{x} \in \mathcal{S}_{n-1}^{\text{SAFEOPT}}} \{\mathbf{x}' \in \mathcal{X} \mid l_{n,i}(\mathbf{x}) - L_i \|\mathbf{x} - \mathbf{x}'\|_2 \geq 0 \text{ for all } i \in \mathcal{I}_s\}. \quad (43)$$

The expansion of the safe set is illustrated in Figure 17.

We remark two main limitations of this approach. First, the Lipschitz constant is an additional safety critical hyperparameter of the algorithm, which is typically not known. The RKHS assumption (cf. Assumption D.9)

they cannot be observed, it can also not be ruled out that they have high objective value.

²⁸Recall that due to the assumption that $\|g_i^*\|_k < \infty$, g_i^* is indeed Lipschitz continuous.

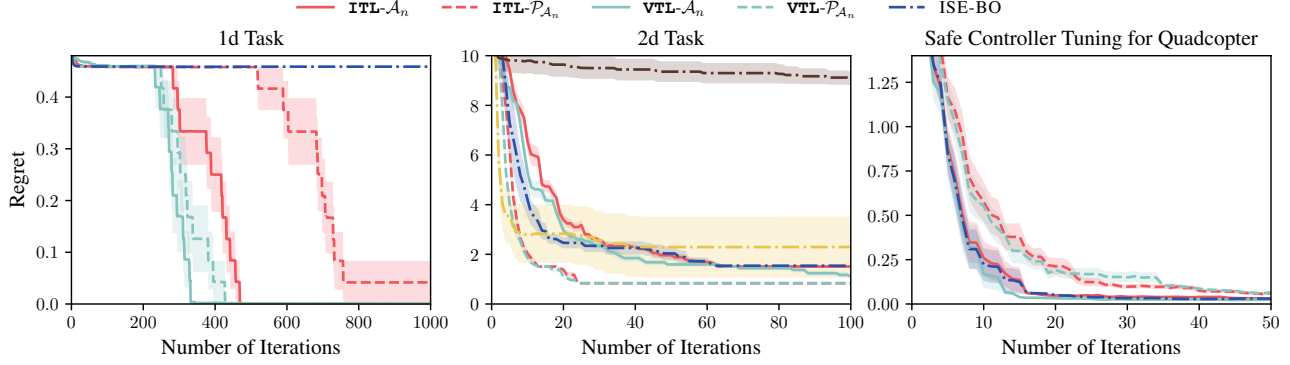


Figure 15. We perform the tasks of Figure 4 using Thompson sampling to evaluate the stochastic target space \mathcal{P}_{A_n} . We additionally compare to GoOSE (cf. Appendix J.2.3) and ISE-BO (cf. Appendix J.2.4).

induces an assumption on the Lipschitz continuity, however, the worst-case a-priori Lipschitz constant is typically very large, and prohibitive for expansion. Second, the Lipschitz constant is global property of the unknown function, meaning that it does not adapt to the local smoothness. For example, a constraint may be “flat” in one direction (permitting straightforward expansion) and “steep” in another direction (requiring slow expansion). Furthermore, the Lipschitz constant is constant over time, whereas **ITL** is able to adapt to the local smoothness and reduce the (induced) Lipschitz constant over time.

Undirected expansion **SAFEOPT** addresses the trade-off between expansion and exploration by focusing learning on two different sets. First, the set of *maximizers*

$$\mathcal{M}_n^{\text{SAFEOPT}} \stackrel{\text{def}}{=} \{x \in \mathcal{S}_n^{\text{SAFEOPT}} \mid u_{n,f}(x) \geq \max_{x' \in \mathcal{S}_n^{\text{SAFEOPT}}} l_{n,f}(x)\}$$

which contains all *known-to-be-safe* points which are potentially optimal. Note that if $\mathcal{S}_n^{\text{SAFEOPT}} = \mathcal{S}_n$ then $\mathcal{M}_n^{\text{SAFEOPT}} \subseteq \mathcal{A}_n$ since \mathcal{A}_n contains points which are potentially optimal and potentially safe *but possibly unsafe*.

To facilitate expansion, for each point $x \in \mathcal{S}_n$, the algorithm considers a set of *expanding points*

$$\mathcal{F}_n^{\text{SAFEOPT}}(x) \stackrel{\text{def}}{=} \{x' \in \mathcal{X} \setminus \mathcal{S}_n^{\text{SAFEOPT}} \mid u_{n,i}(x) - L_i \|x - x'\|_2 \geq 0 \text{ for all } i \in \mathcal{I}_s\}$$

A point is expanding if it is unsafe initially and can be (optimistically) deduced as safe by observing x . The set of *expanders* corresponds to all known-to-be-safe points which optimistically lead to expansion of the safe set:

$$\mathcal{G}_n^{\text{SAFEOPT}} \stackrel{\text{def}}{=} \{x \in \mathcal{S}_n \mid |\mathcal{F}_n(x)| > 0\}.$$

That is, an expander is a safe point x which is “close” to at least one expanding point x' . Observe that here, we start with a safe x and then find a close and potentially safe

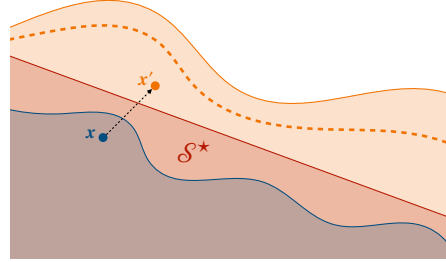


Figure 17. Illustration of the expansion of the safe set à la **SAFEOPT**. Here, the blue region denotes the pessimistic safe set \mathcal{S} , the red region denotes the true safe set \mathcal{S}^* , and the orange region denotes the optimistic safe set $\hat{\mathcal{S}}$. Whereas **ITL** learns about the point x' *directly*, **SAFEOPT** expands the safe set using the reduction of uncertainty at x , and then extrapolating using the Lipschitz constant (cf. Equation (43)). The dashed orange line denotes the expanding points of **SAFEOPT** which under-approximate the optimistic safe set of **ITL** (cf. Lemma J.1). Thus, **ITL** may even learn about points in $\hat{\mathcal{S}}$ which are “out of reach” for **SAFEOPT**.

x' using the Lipschitz-property of the constraint function. Thus, the set of expanding points is inherently limited by the assumed Lipschitzness (cf. Figure 17), and generally a subset of the potential expanders \mathcal{E}_n (cf. Equation (28)):

Lemma J.1. *For any $n \geq 0$, if $\mathcal{S}_n^{\text{SAFEOPT}} = \mathcal{S}_n$ then*

$$\bigcup_{x \in \mathcal{S}_n} \mathcal{F}_n^{\text{SAFEOPT}}(x) \subseteq \mathcal{E}_n.$$

Proof. Without loss of generality, we consider the case where $\mathcal{I}_s = \{i\}$. We have

$$\mathcal{E}_n = \hat{\mathcal{S}}_n \setminus \mathcal{S}_n = \{x \in \mathcal{X} \setminus \mathcal{S}_n \mid u_{n,i}(x) \geq 0\}.$$

The result follows directly by observing that $L_i \|x - x'\|_2 \geq 0$. \square

SAFEOPT then selects \mathbf{x}_{n+1} according to uncertainty sampling *within* the maximizers and expanders: $\mathcal{M}_n^{\text{SAFEOPT}} \cup \mathcal{G}_n^{\text{SAFEOPT}}$. We remark that due to the separate handling of expansion and exploration, SAFEOPt expands the safe set in *all* directions — even those that are known to be suboptimal. In contrast, **ITL** only expands the safe set in directions that are potentially optimal by balancing expansion and exploration through the single set of potential maximizers \mathcal{A}_n .

Based on uncertainty sampling As mentioned in the previous paragraph, SAFEOPt selects as next point the maximizer/expander with the largest prior uncertainty.²⁹ In contrast, **ITL** selects the point within \mathcal{S}_n which minimizes the posterior uncertainty within \mathcal{A}_n . Note that the two approaches are not identical as typically $\mathcal{M}_n^{\text{SAFEOPT}} \cup \mathcal{G}_n^{\text{SAFEOPT}} \subset \mathcal{S}_n^{\text{SAFEOPT}}$ and $\mathcal{A}_n \not\supseteq \mathcal{S}_n$.

We show empirically in Section 3.3 that depending on the kernel choice (i.e., the smoothness assumptions), uncertainty sampling within a given target space neglects higher-order information that can be attained by sampling outside the set. This can be seen even more clearly when considering linear functions, in which case points outside the maximizers and expanders can be equally informative as points inside.

Finally, note that the set of expanders is constructed “greedily”, i.e., only considering *single-step* expansion. This is necessitated as the inference of safety is based on single reference points. Instead, **ITL** directly quantifies the information gained towards the points of interest without considering intermediate reference points.

Requires homoscedastic noise SAFEOPt imposes a homoscedasticity assumption on the noise which is an artifact of the analysis of uncertainty sampling. It is well known that in the presence of heteroscedastic noise, one has to distinguish epistemic and aleatoric uncertainty. Uncertainty sampling fails because it may continuously sample a high variance point where the variance is dominated by aleatoric uncertainty, potentially missing out on reducing epistemic uncertainty at points with small aleatoric uncertainty. In contrast, maximizing mutual information naturally takes into account the two sources of uncertainty, preferring those points where epistemic uncertainty is large and aleatoric uncertainty is small (cf. Appendix D.2).

Suboptimal reachable safe set Sui et al. (2015) and Berkenkamp et al. (2021) show that SAFEOPt converges to the optimum within the closure $\bar{\mathcal{R}}_{\epsilon}^{\text{SAFEOPT}}(\mathcal{S}_0)$ of

$$\mathcal{R}_{\epsilon}^{\text{SAFEOPT}}(\mathcal{S}) \stackrel{\text{def}}{=} \mathcal{S} \cup \{\mathbf{x} \in \mathcal{X} \mid \exists \mathbf{x}' \in \mathcal{S} \text{ such that } f_i^*(\mathbf{x}') - (L_i \|\mathbf{x} - \mathbf{x}'\|_2 + \epsilon) \geq 0 \text{ for all } i \in \mathcal{I}_s\}.$$

²⁹The use of uncertainty sampling for safe sequential decision-making goes back to Schreiter et al. (2015) and Sui et al. (2015).

Note that analogously to the expansion of the safe set, the “expansion” of the reachable safe set is based on “inferring safety” through a reference point in \mathcal{S} and using Lipschitz continuity. This is opposed to the reachable safe set of **ITL** (cf. Definition D.13).

We remark that under the additional assumption that a Lipschitz constant is known, **ITL** can easily be extended to expand its safe set based on the kernel *and* the Lipschitz constant, resulting in a strictly larger reachable safe set than SAFEOPt. We leave the concrete formalization of this extension to future work. Moreover, we do not evaluate this extension in our experiments, as we observe that even without the additional assumption of a Lipschitz constant, **ITL** outperforms SAFEOPt in practice.

J.2.2. HEURISTIC SAFEOPt

Berkenkamp et al. (2016) also implement a heuristic variant of SAFEOPt which does not assume a known Lipschitz constant. This heuristic variant uses the same (pessimistic) safe sets \mathcal{S}_n as **ITL**. The set of maximizers is identical to SAFEOPt. As expanders, the heuristic variant considers all safe points $\mathbf{x} \in \mathcal{S}_n$ that if \mathbf{x} were to be observed next with value $\mathbf{u}_n(\mathbf{x})$ lead to $|\mathcal{S}_{n+1}| > |\mathcal{S}_n|$. We refer to this set as $\mathcal{G}_n^{\text{H-SAFEOPt}}$. The next point is then selected by uncertainty sampling within $\mathcal{M}_n^{\text{SAFEOPT}} \cup \mathcal{G}_n^{\text{H-SAFEOPt}}$.

The heuristic variant shares some properties with SAFEOPt, such that it is based on uncertainty sampling, not adapting to heteroscedastic noise, and separate notions of maximizers and expanders (leading to an “undirected” expansion of the safe set). Note that there are no known convergence guarantees for heuristic SAFEOPt. Importantly, note that similar to SAFEOPt the set of expanders is constructed “greedily”, and in particular, does only take into account *single-step* expansion. In contrast, an objective such as **ITL** which quantifies the “information gained towards expansion” also actively seeks out *multi-step* expansion.

J.2.3. GOOSE

To address the “undirected” expansion of SAFEOPt discussed in the previous section, Turchetta et al. (2019) proposed *goal-oriented safe exploration* (GOOSE). GOOSE extends any unsafe BO algorithm (which we subsequently call an oracle) to the safe setting. In our experiments, we evaluate GOOSE-UCB which uses UCB as oracle and which is also the variant studied by Turchetta et al. (2019). In the following, we assume for ease of notation that $\mathcal{I}_s = \{c\}$.

Given the oracle proposal \mathbf{x}^* , GOOSE first determines whether \mathbf{x}^* is safe. If \mathbf{x}^* is safe, \mathbf{x}^* is queried next. Otherwise, GOOSE first learns about the safety of \mathbf{x}^* by querying “expansionist” points until the oracle’s proposal

is determined to be either safe or unsafe.

GOOSE expands the safe set identically to SAFEOPT according to Equation (43). In the context of GOOSE, $\mathcal{S}_n^{\text{SAFEOPT}}$ is called the *pessimistic safe set*. To determine that a point cannot be deduced as safe, GOOSE also keeps track of a Lipschitz-based *optimistic safe set*:

$$\widehat{\mathcal{S}}_{n,\epsilon}^{\text{GOOSE}} \stackrel{\text{def}}{=} \bigcup_{\mathbf{x} \in \mathcal{S}_{n-1}^{\text{SAFEOPT}}} \{ \mathbf{x}' \in \mathcal{X} \mid u_{n,c}(\mathbf{x}) - L_c \|\mathbf{x} - \mathbf{x}'\|_2 - \epsilon \geq 0 \}.$$

We summarize the algorithm in Algorithm 2 where we denote by $\mathcal{O}(\mathcal{X})$ the oracle proposal over the domain \mathcal{X} .

Algorithm 2 GOOSE

Given: Lipschitz constant L_c , prior model $\{f, g_c\}$, oracle \mathcal{O} , and precision ϵ
 Set initial safe set $\mathcal{S}_0^{\text{SAFEOPT}}$ based on prior
 $\widehat{\mathcal{S}}_{n,\epsilon}^{\text{GOOSE}} \leftarrow \mathcal{X}$
 $n \leftarrow 0$
for k from 1 to ∞ **do**
 $\mathbf{x}_k^* \leftarrow \mathcal{O}(\widehat{\mathcal{S}}_{n,\epsilon}^{\text{GOOSE}})$
while $\mathbf{x}_k^* \notin \mathcal{S}_n^{\text{SAFEOPT}}$ **do**
 Observe “expansionist” point \mathbf{x}_{n+1} , set $n \leftarrow n + 1$, and update model and safe sets
end while
 Observe \mathbf{x}_k^* , set $n \leftarrow n + 1$, and update model and safe sets
end for

It remains to discuss the heuristic used to select the “expansionist” points. GOOSE considers all points $\mathbf{x} \in \mathcal{S}_n^{\text{SAFEOPT}}$ with confidence bands of size larger than the accuracy ϵ , i.e.,

$$\mathcal{W}_{n,\epsilon}^{\text{GOOSE}} \stackrel{\text{def}}{=} \{ \mathbf{x} \in \mathcal{S}_n^{\text{SAFEOPT}} \mid u_{n,c}(\mathbf{x}) - l_{n,c}(\mathbf{x}) > \epsilon \}.$$

Which of the points in this set is evaluated depends on a set of learning targets $\mathcal{A}_{n,\epsilon}^{\text{GOOSE}} \stackrel{\text{def}}{=} \widehat{\mathcal{S}}_{n,\epsilon}^{\text{GOOSE}} \setminus \mathcal{S}_n^{\text{SAFEOPT}}$ akin to the “potential expanders” \mathcal{E}_n (cf. Equation (28)), to each of which we assign a priority $h(\mathbf{x})$. When $h(\mathbf{x})$ is large, this indicates that the algorithm is prioritizing to determine whether \mathbf{x} is safe. We use as heuristic the negative ℓ_1 -distance between \mathbf{x} and \mathbf{x}^* . GOOSE then considers the set of *potential immediate expanders*

$$\mathcal{G}_{n,\epsilon}^{\text{GOOSE}}(\alpha) \stackrel{\text{def}}{=} \{ \mathbf{x} \in \mathcal{W}_{n,\epsilon}^{\text{GOOSE}} \mid \exists \mathbf{x}' \in \mathcal{A}_{n,\epsilon}^{\text{GOOSE}} \text{ with} \\ \text{priority } \alpha \text{ such that } u_{n,c}(\mathbf{x}) - L_c \|\mathbf{x} - \mathbf{x}'\|_2 \geq 0 \}.$$

The “expansionist” point selected by GOOSE is then any point in $\mathcal{G}_{n,\epsilon}^{\text{GOOSE}}(\alpha^*)$ where α^* denotes the largest priority such that $|\mathcal{G}_{n,\epsilon}^{\text{GOOSE}}(\alpha^*)| > 0$.

We observe empirically that the sample complexity of GOOSE is not always better than that of SAFEOPT.

Notably, the expansion of the safe set is based on a “greedy” heuristic. Moreover, determining whether a single oracle proposal \mathbf{x}^* is safe may take significant time. Consider the (realistic) example where the prior is uniform, and UCB proposes a point which is far away from the safe set and suboptimal. GOOSE will typically attempt to derive the safety of the proposed point until the uncertainty at *all* points within $\mathcal{S}_0^{\text{SAFEOPT}}$ is reduced to ϵ .³⁰ Thus, GOOSE can “waste” a significant number of samples, aiming to expand the safe set towards a known-to-be suboptimal point. In larger state spaces, due to the greedy nature of the expansion strategy, this can lead to GOOSE being effectively stuck at a suboptimal point for a significant number of rounds.

J.2.4. ISE AND ISE-BO

Recently, Bottero et al. (2022) proposed an information-theoretic approach to efficiently expand the safe set which they call *information-theoretic safe exploration* (ISE). Specifically, they choose the next action \mathbf{x}_n by approximating

$$\arg \max_{\mathbf{x} \in \mathcal{S}_{n-1}} \max_{\mathbf{x}' \in \mathcal{X}} \underbrace{\mathbb{I}\{\mathbf{g}_{\mathbf{x}'} \geq 0\}; \mathbf{y}_{\mathbf{x}} \mid \mathcal{D}_{n-1}}_{\alpha^{\text{ISE}}(\mathbf{x})}. \quad (\text{ISE})$$

In a parallel independent work, Bottero et al. (2024) extended ISE to the Safe BO problem where they propose to choose \mathbf{x}_n according to

$$\arg \max_{\mathbf{x} \in \mathcal{S}_{n-1}} \max \{ \alpha^{\text{ISE}}(\mathbf{x}), \alpha^{\text{MES}}(\mathbf{x}) \} \quad (\text{ISE-BO})$$

where α^{MES} denotes the acquisition function of max-value entropy search (Wang & Jegelka, 2017). Similarly to SAFEOPT, ISE-BO treats expansion and exploration separately, which leads to “undirected” expansion of the safe set. That is, the safe set is expanded in all directions, even those that are known to be suboptimal. In contrast, **ITL** balances expansion and exploration through the single set of potential maximizers \mathcal{A}_n . With a stochastic target space, **ITL** generalizes max-value entropy search (cf. Appendix J.1).

We evaluate ISE-BO in Figure 15 and observe that it does not outperform **ITL** and **VTL** in any of the tasks, while performing poorly in the 1d task and suboptimally in the 2d task.

J.3. Jumping Past Local Barriers

In this additional experiment we demonstrate that **ITL** is able to extrapolate safety beyond local unsafe “barriers”, which is a fundamental limitation of Lipschitz-based methods such as SAFEOPT. We consider the ground truth

³⁰This is because the proposed point typically remains in the optimistic safe set when it is sufficiently far away from the pessimistic safe set.

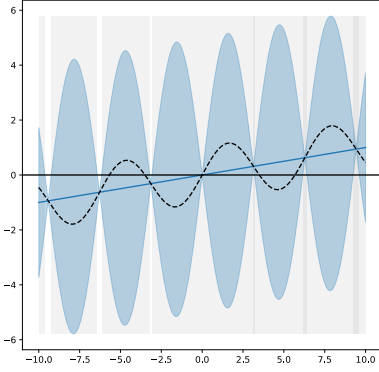


Figure 18. The ground truth f^* is shown as the dashed black line. The solid black line denotes the constraint boundary. The GP prior is given by a linear kernel with sin-transform and mean $0.1x$. The light gray region denotes the initial optimistic safe set $\hat{\mathcal{S}}_0$ and the dark gray region denotes the initial pessimistic safe set \mathcal{S}_0 .

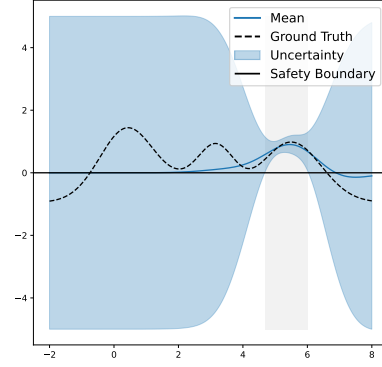


Figure 20. Ground truth and prior well-calibrated model in 1d synthetic experiment. The function serves simultaneously as objective and as constraint. The light gray region denotes the initial safe set \mathcal{S}_0 .

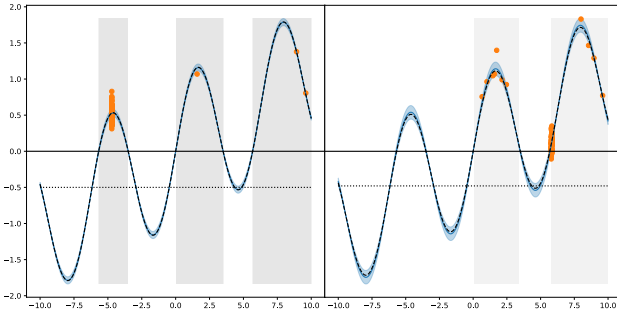


Figure 19. First 100 samples of **ITL** using the potential expanders \mathcal{E}_n (cf. Equation (28)) as target space (left) and **SAFEOPT** sampling only from the set of expanders $\mathcal{G}_n^{\text{SAFEOPT}}$ (right).

function and prior statistical model shown in Figure 18. Note that initially, there are three disjoint safe “regions” known to the algorithm corresponding to two of the three safe “bumps” of the ground truth function. In this experiment, the main challenge is to “jump past” the local barrier separating the leftmost and initially unknown safe “bump”.

Figure 19 shows the sampled points during the first 100 iterations of **SAFEOPT** and **ITL**. Clearly, **SAFEOPT** does not discover the third safe “bump” while **ITL** does. Indeed, it is a fundamental limitation of Lipschitz-based methods that they can never “jump past local barriers”, even if the oracle Lipschitz constant were to be known and tight (i.e., locally accurate) around the barrier. This is because Lipschitz-based methods expand to the point x based on a reference point x' , and by definition, if x is added to the safe set so are all points on the line segment between x and x' . Hence, if there is a single point on this line segment which is unsafe (i.e., a “barrier”), the algorithm will *never* expand past it. This limitation does not exist for kernel-based algorithms as expansion occurs in function space.

Moreover, note that for a non-stationary kernel such as in this example, **ITL** samples the “closest points” in function space rather than Euclidean space. We observe that **SAFEOPT** still samples “locally at the boundary” whereas **ITL** samples the most informative point which in this case is the local maximum of the sinusoidal function. In other words, **ITL** adapts to the geometry of the function. This generally leads us to believe that **ITL** is more capable to exploit (non-stationary) prior knowledge than distance-based methods such as **SAFEOPT**.

J.4. Experiment Details

J.4.1. SYNTHETIC EXPERIMENTS

1d task Figure 20 shows the objective and constraint function, as well as the prior. We discretize using 500 points. The main difficulty in this experiment lies in sufficiently expanding the safe set to discover the global maximum. Figure 21 plots the size of the safe set \mathcal{S}_n for the compared algorithms, which in this experiment matches the achieved regret closely.

2d task We model our constraint in the form of a spherical “island” where the goal is to get a good view of the coral reef located to the north-east of the island while staying in the interior of the island during exploration (cf. Figure 22). The precise objective and constraint functions are unknown to the agent. Hence, the agent has to gradually and safely update its belief about boundaries of the “island” and the location of the coral reef. The prior is obtained by a single observation within the center of the island $[-0.5, 0.5]^2$. We discretize using 2 500 points.

J.4.2. SAFE CONTROLLER TUNING FOR QUADCOPTER

Modeling the real-world dynamics We learn a feedback policy (i.e., “control gains”) to compensate for inaccuracies

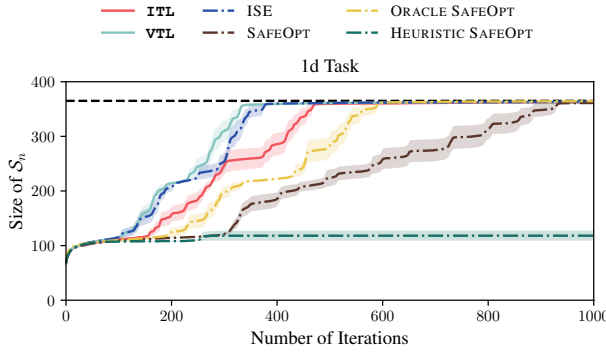


Figure 21. Size of S_n in 1d synthetic experiment. The dashed black line denotes the size of S^* . In this task, “discovering” the optimum is closely linked to expansion of the safe set, and HEURISTIC SAFEOPT fails since it does not expand the safe set sufficiently.

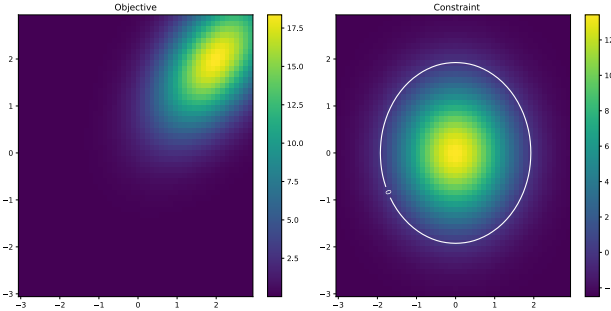


Figure 22. Ground truth in 2d synthetic experiment.

in the initial controller. In our experiment, we model the real world dynamics and the adjusted model using the PD control feedback (Widmer et al., 2023),

$$\delta_t(\mathbf{x}) \stackrel{\text{def}}{=} (\mathbf{x}^* - \mathbf{x})[(\mathbf{s}^* - \mathbf{s}_t)(\dot{\mathbf{s}}^* - \dot{\mathbf{s}}_t)], \quad (44)$$

where \mathbf{x}^* are the *unknown* ground truth disturbance parameters, and \mathbf{s}^* and $\dot{\mathbf{s}}^*$ are the desired state and state derivative, respectively. This yields the following ground truth dynamics:

$$\mathbf{s}_{t+1}(\mathbf{x}) = \mathbf{T}(\mathbf{s}_t, \mathbf{u}_t + \delta_t(\mathbf{x})). \quad (45)$$

The feedback parameters $\mathbf{x} = [\mathbf{x}_p \ \mathbf{x}_d]^\top$ can be split into \mathbf{x}_p tuning the state difference which are called *proportional parameters* and \mathbf{x}_d tuning the state derivative difference which are called *derivative parameters*. We use the “critical damping” heuristic to relate the proportional and derivative parameters: $\mathbf{x}_d = 2\sqrt{\mathbf{x}_p}$. We thus consider the restricted domain $\mathcal{X} = [0, 20]^4$ where each dimension corresponds to the proportional feedback to one of the four rotors.

Ground truth disturbance parameters are sampled from a chi-squared distribution with one degree of freedom (i.e., the square of a standard normal distribution), $\mathbf{x}_p^* \sim \chi_1^2$, and \mathbf{x}_d^* is determined according to the critical damping heuristic.

The learning problem The goal of our learning problem is to move the quadcopter from its initial position $\mathbf{s}(0) = [1 \ 1 \ 1]^\top$ (in Euclidean space with meter as unit) to position $\mathbf{s}^* = [0 \ 0 \ 2]^\top$. Moreover, we aim to stabilize the quadcopter at the goal position, and therefore regularize the control signal towards an action \mathbf{u}^* which results in hovering (approximately) without any disturbances. We formalize these goals with the following objective function:

$$f^*(\mathbf{x}) \stackrel{\text{def}}{=} -\sigma \left(\sum_{t=0}^T \|\mathbf{s}^* - \mathbf{s}_t(\mathbf{x})\|_Q^2 + \|\mathbf{u}^* - \mathbf{u}_t(\mathbf{x})\|_R^2 \right) \quad (46)$$

where $\sigma(v) \stackrel{\text{def}}{=} \tanh((v - 100)/100)$ is used to smoothen the objective function and ensure that its range is $[-1, 1]$. The non-smoothed control objective in Equation (46) is known as a *linear-quadratic regulator* (LQR) which we solve exactly for the undisturbed system using ILQR (Tu et al., 2023). Finally, we want to ensure at all times that the quadcopter is at least 0.5 meter above the ground, that is,

$$g^*(\mathbf{x}) \stackrel{\text{def}}{=} \min_{t \in [T]} \mathbf{s}_t^z(\mathbf{x}) - 0.5 \quad (47)$$

where we denote by \mathbf{s}_t^z the z-coordinate of state \mathbf{s}_t .

We use a time horizon of $T = 3$ seconds which we discretize using 100 steps. The objective is modeled by a zero-mean GP with a Matérn($\nu = 5/2$) kernel with lengthscale 0.1, and the constraint is modeled by a GP with mean -0.5 and a Matérn($\nu = 5/2$) kernel with lengthscale 0.1. The prior is obtained by a single observation of the “safe seed” $[0 \ 0 \ 0 \ 10]^\top$.

Adaptive discretization We discretize the domain \mathcal{X} adaptively using coordinate LINEBO (Kirschner et al., 2019). That is, in each iteration, one of the four control dimensions is selected uniformly at random, and the active learning oracle is executed on the corresponding one-dimensional subspace.

Safety Using the (unsafe) constrained BO algorithm EIC (Gardner et al., 2014) leads constraint violation,³¹ while **ITL** and **VTL** do not violate the constraints during learning for any of the random seeds.

Hyperparameters The observation noise is Gaussian with standard deviation $\rho = 0.1$. We let $\beta = 10$. The control target is $\mathbf{u}^* = [1.766 \ 0 \ 0 \ 0]^\top$.

The state space is 12-dimensional where the first three states correspond to the velocity of the quadcopter, the next three states correspond to its acceleration, the following three states correspond to its angular velocity, and the last three states correspond to its angular velocity in local frame. The LQR parameters are given by

$$\mathbf{Q} = \text{diag}\{1, 1, 1, 1, 1, 1, 0.1, 0.1, 0.1, 0.1, 0.1, 0.1\} \quad \text{and}$$

³¹On average, 1.6 iterations of the first 50 violate the constraints.

$$\mathbf{R} = 0.01 \cdot \text{diag}\{5, 0.8, 0.8, 0.3\}.$$

The quadcopter simulation was adapted from [Chandra \(2023\)](#).

Each one-dimensional subspace is discretized using 2 000 points.

Random seeds We repeat the experiment for 25 different seeds where the randomness is over the ground truth disturbance, observation noise, and the randomness in the algorithm.

Table 3. Magnitudes of γ_n for common kernels. The magnitudes hold under the assumption that \mathcal{X} is compact. Here, B_ν is the modified Bessel function. We take the magnitudes from Theorem 5 of Srinivas et al. (2009) and Remark 2 of Vakili et al. (2021). The notation $\tilde{\mathcal{O}}(\cdot)$ subsumes log-factors. For $\nu = 1/2$, the Matérn kernel is equivalent to the Laplace kernel. For $\nu \rightarrow \infty$, the Matérn kernel is equivalent to the Gaussian kernel. The functions sampled from a Matérn kernel are $\lceil \nu \rceil - 1$ mean square differentiable.

Kernel	$k(\mathbf{x}, \mathbf{x}')$	γ_n
Linear	$\mathbf{x}^\top \mathbf{x}'$	$\mathcal{O}(d \log(n))$
Gaussian	$\exp\left(-\frac{\ \mathbf{x} - \mathbf{x}'\ _2^2}{2h^2}\right)$	$\tilde{\mathcal{O}}\left(\log^{d+1}(n)\right)$
Laplace	$\exp\left(-\frac{\ \mathbf{x} - \mathbf{x}'\ _1}{h}\right)$	$\tilde{\mathcal{O}}\left(n^{\frac{d}{1+d}} \log^{\frac{1}{1+d}}(n)\right)$
Matérn	$\frac{2^{1-\nu}}{\Gamma(\nu)} \left(\frac{\sqrt{2\nu} \ \mathbf{x} - \mathbf{x}'\ _2}{h}\right)^\nu B_\nu\left(\frac{\sqrt{2\nu} \ \mathbf{x} - \mathbf{x}'\ _2}{h}\right)$	$\tilde{\mathcal{O}}\left(n^{\frac{d}{2\nu+d}} \log^{\frac{2\nu}{2\nu+d}}(n)\right)$